2016

An Investigation of Environmentally Persistent Free Radical (EPFR) Formation in Contaminated Soils Using Surrogate-Based Model Systems

Ugwumsinachi Godwin Nwosu
Louisiana State University and Agricultural and Mechanical College, unwosu2@lsu.edu

AN INVESTIGATION OF ENVIRONMENTALLY PERSISTENT FREE RADICAL (EPFR) FORMATION IN CONTAMINATED SOILS USING SURROGATE-BASED MODEL SYSTEMS

A Dissertation

Submitted to the Graduate Faculty of the
Louisiana State University and
Agricultural and Mechanical College
in partial fulfillment of the
requirements for the degree of
Doctor of Philosophy

in

The Department of Chemistry

by

Ugwumsinachi Godwin Nwosu
B.Sc., Federal University of Technology Owerri (FUTO), 2007
December 2016

To the Almighty God for his mercies, love and kindness. For his grace that has been sufficient for me

To my lovely Mum whose prayers and encouragement I cannot do without. I love you

To my Uncles who has always been there for me at all times and their unwavering support

To my lovely wife Lynn Nwosu for her immense support encouragement steadfast love.

To my brother Franklin Nwaubani who has been a true brother since childhood and has consistently showed me unswerving support.

ACKNOWLEDGEMENTS

I would like to first thank the Almighty God for seeing me thorough this Ph.D. program. He has shown me favor, kindness, mercy, and his grace has been abundant towards me.

I am truly grateful to the following people for their immense support and role they have played in my academic life and career:

Professor Robert Cook, my Ph.D. advisor for his support, timely advice, guidance, and encouragement throughout my time at LSU. You certainly have helped me increase my independent thinking skills. These skills have guided and shaped me into a better researcher. Thank you for the opportunity to work with you. I will cherish it forever.

To my doctoral committee members: Prof. Graca Vicente, Prof. Bin Chen and Prof. Jun Xu, thank you for your support and guidance throughout my time here. Your helpful suggestions and constructive advice during my general exam and beyond guided me through my research path. I also dedicate this work to Prof. Dellinger whose blessed memory and passion for a cleaner environment encouraged me greatly.

To my LSU family: LSU Department of Chemistry and LSU Superfund research center, LSU graduate school and LSU CAMD. I am grateful for your support. Thank you for providing a warm environment in which one can learn, research, and juggle ideas. Your love and friendliness is second to none. I will forever be indebted to this community. I would want to especially thank Dr. Amitava Roy, whose down-to-earth attitude and approach is one to which none can rival. This research would not have been achieved without your continued assistance with your expertize guiding me through the use of XANES and EXAFS.

To my Alma Marta FUTO: From the first day I was admitted, you challenged me through countless opportunities and possibilities. I am indebted to you. I am especially grateful for my undergraduate advisor Dr. Gerald Onyedika. I want to thank you for inspiring me and giving me

all the support humanly possible (can this be rephrased). I am forever indebted to you. Also to Dr. Alofoje Unuigboje, your continuous inspiration and encouragement to continue pursuing my dreams and goals is highly appreciated. Without such encouragement I would not be here today.

To my family, my beloved uncles Philip, Sabinus, Martin and Eugene Nwosu, I do not know what the journey would have been like without all of you. Especially to my Uncle Herbert O. Nwosu, you were for me in rough and good times. I am forever indebted to you! To my sister Sorochi, you mean the world to me.

To my friends: Ifeanyi Okafor my best friend, words cannot express how much our friendship means to me. I draw inspiration from our conversations and the knowledge that you've been there for me for 10 years and counting. You are a true friend. Also to Chinenyeze Nwankwoala, you have also been a true friend. Also to my brother Franklin Nwaubani, your piece of advice that often come in form of conversation are priceless. I would not be here today without you; I am forever indebted to you.

To my lovely Mum, words cannot begin to express how much you mean to me. You encourage and pray for me all the time. I do not know what the journey would have been like without your prayers and support. I am a product of your answered prayers. You mean more than the world to me. This dissertation work is dedicated to you.

To my lovely wife Lynn, thank you for your persistent support, your love, and encouragement. I love you. You mean so much to me.

Finally, this dissertation will not be complete without acknowledging the entire science community. The hope of a better environment would not exist without you.

TABLE OF CONTENTS

LIST OF TABLES

LIST OF FIGURES

LIST OF ABBREVIATIONS

$\Delta H_{p\text{-}p}$	Peak-to-Peak Line Width
CaM	Calcium Montmorillonite
CaMMT	Calcium Montmorillonite
CEC	Cation-Exchange Capacity
Cu(II)CaMMT	Copper(II) Cation-Exchanged Montmorillonite Clay
DCB	Dichlorobenzene
DPPH	2,2-diphenyl-1-picrylhydrazyl
EPA	Environmental Protection Agency
EPFR	Environmentally-Persistent Free Radical
EPR	Electron Paramagnetic Resonance Spectroscopy
EXAFS	Extended X-ray absorption fine structure
Fe(III)CaMMT	Iron(III) Cation-Exchanged Montmorillonite Clay
Fe(III)CaM	Iron(III) Cation-Exchanged Montmorillonite Clay
ICPOES	Inductively Coupled Plasma–Optical Emission Spectroscopy
HPLC	High-Performance Liquid Chromatography
FTIR	Fourier Transform Infrared
MCP	2-Monochlorophenol
PM	Particulate Matter
POP	Persistent Organic Pollutant
PPP_Cu(II)CaMMT	Copper-Loaded Poly-*p*-phenylene Montmorillonite
RO	Reverse Osmosis
ROS	Reactive Oxygen Species
SOM	Soil Organic Matter
XANES	X-ray absorption near edge structure

XPS	X-Ray Photoelectron Spectroscopy
XRD	X-Ray Diffraction

ABSTRACT

Our previous studies on Environmentally persistent free radicals (EPFRs)-contaminated Superfund soil sites utilized a “top-down” approach to reduce the soil matrix into its constituting components in order to determine which soil component was associated with the majority of the formed EPFRs. However, due to the inherent complexity associated with this method, no real mechanistic information was obtained from these studies. To overcome this limitation, the work presented in this dissertation was carried out using a “bottom-up” approach, which utilized surrogate systems to individually investigate the component(s) of the soil which are involved in the formation and stabilization of EPFRs in the Superfund soil.

The first part of this work (chapter 2), utilized Fe(III)-loaded montmorillonite as a surrogate system the clay/mineral component of the soil and phenol as the organic pollutant to mimic the polluted, EPFR-containing Superfund soil. This approach allowed, for a molecular level understanding of the mechanism of EPFR formation occurring in the clay/mineral component system of the soil and was accomplished by a combination of FT-IR, EPR, ICP-OES and XANES analyses. It revealed that, once sorbed, the phenol transfers an electron to Fe(III), forming Fe(II) and an organic EPFR.

In chapter 3, the work was extended to a bi-component clay/humin surrogate soil system, utilizing Cu(II)-loaded as well as poly-*p*-phenylene (PPP)-grafted Cu(II)-loaded montmorillonite clay surrogate soil systems. Both individually and in combination, the effects of the make-up of the surrogate soil system on the EPFR formation were compared in terms of EPFR concentrations, lifetimes, and their potential to generate reactive oxygen species (ROS).

The effects of soil pH and other environmental conditions, such as humidity and solar irradiation, on EPFR formation were probed in chapter 4 of this dissertation and EPFRs were shown to be affected by these environmental factors.

Finally, insight into the naturally (non-pollution) occurring EPFRs was obtained by comparing three different natural organic matter (NOM) samples sourced from the Humic Substance Society (IHSS), and revealed that NOM contains EPFRs with very similar characteristics to those detected in Superfund samples, but at much lower levels. This research reveals that EPFRs are ubiquitous in the environment.

CHAPTER 1
INTRODUCTION

1.1 Background

Soil contamination and its adverse effects to living organisms have become a major concern in recent years, primarily due to the potential risk of human exposure through wind-blown dust or through ingestion. Over the decades, a wide spectrum of polycyclic aromatic hydrocarbons (PAHs), chlorinated hydrocarbons (CHCs), and other organic pollutants in soil and sediments has been investigated.[1-4] PAHs were found to be the parent compounds to a large range of important, environmentally toxic compounds, such as polychlorinated dibenzodioxins (PCDDs), polychlorinated dibenzofurans (PCDFs), 2,3,7,8-tetrachlorodibenzo-*p*-dioxin (TCDD) and polychlorinated biphenyls (PCBs)[1-4], which are known to be mutagenic and carcinogenic to humans.[5-6] Some well-known processes leading to the formation of dioxins and their parent compounds, such as PCDDs, its congers, and chlorinated products include the photochemical degradation of antimicrobial compounds, pesticide release from chemical industries, waste water and sewage sludge release, forest fires and metal smelting.[1-4,7] Among all these sources, dioxins formed from chlorophenol precursors, like pentachlorophenol (PCP), appear more dominant in the environment, especially in the soil. This effect is due to a number of processes that can transform chlorophenol precursors to dioxins in the environment. For instance, studies have shown that PCDDs can be formed from white rot fungi through chlorophenol degradation pathways involving peroxidase and oxidase enzymes or, alternatively, from chlorinated anicyl compounds.[7-11] Similarly, chlorophenols, the basic precursors to PCPs, OCDD (octachlorodibenzodioxin) and PCDDs, have been reported to have formed through natural halogenation of phenols via nonspecific chloroperoxidase (CPO) enzymes.[12-14] Large deposits of OCDD have been found in the soil that had been leached of their soluble precursor, PCP.[3,11] Chlorophenols have also been introduced to the environment through human activities, or

instance from spills at wood treating sites, where chlorophenols—due to their antifungal properties—have been historically used in large amounts. [2-4,11,13]. Despite the large body of literature in regards to the potential toxicity of dioxins formed through PAH and CHC contamination, only very recently have the researchers started to understand that the intermediates in the transformation of parent compounds to dioxins could be not only highly toxic, but even more toxic that the parent or dioxin compounds themselves. This new direction of revealed that a new class of radicals, known as the environmentally persistent free radicals (EPFRs), constitutes an important intermediate product in the transformation of a number dioxin precursor compounds, justifying further investigations into (i) the real identity of these type of toxicants which, over the past decade, have been commonly misidentified as molecular pollutants and dioxins, (ii) the fundamental chemistry that leads to EPFR formation, and, in the long run, (iii) developing EPFR remediation techniques.

1.2 Environmentally Persistent Free Radical

Free radicals in the general sense are a group of highly unstable species, or groups of atoms, with an unpaired electron. Radicals are generally highly reactive and react in a fraction of a second in their quest to achieve stability, stripping off electrons from atoms with which they come in contact, often resulting in a sequence of reaction.[15-16] Environmentally persistent free radicals (EPFRs) are resonance-stabilized surface bound free radicals of semiquinones, phenoxyls, and cyclopentadienyls. These radicals form by the association of aromatic and polychlorinated aromatic hydrocarbon compounds with a redox-active transition metal center.[18] They are more stable and persistent, meaning that they experience much longer lifetimes than most free radicals.[18,19] They were initially shown to form under post-flame conditions during the creation of particulate matter (PM) of fine (PM 2.5-0.1 μm) and ultrafine (PM 0.1 μm and smaller) sizes.[19-20] Post-combustion particulate matter is found to be particularly rich in transition metals, such as copper, iron, nickel, and zinc in their highest oxidation states.[18-20] EPFRs are formed at

transition metal centers that can be easily reduced when an organic compound chemisorbs.[18-20] As depicted schematically in Figure 1.1, EPFRs form by an initial physisorption mechanism, in which the organic molecule engages in a weak bonding with the metal center. Subsequently, an elimination of water or hydrogen chloride results in chemisorption of the organic molecular adsorbate, followed by a single electron transfer from the organic molecule to the transition metal center, resulting in the formation of a metal center-bound free radical. This metal center association, and the subsequent mesomerism, provides stability to the formed organic radical, which manifests itself as resistance to oxidation, recombination, and degradation over a period of time.[18-23] The organic radicals produced from this process, thanks to resonance, lead to the possible formation either oxygen-centered or carbon-centered EPFRs which, in turn, determines the EPFRs' exact environmental and biological activity. Initially, EPFRs were thought to have formed direct surface-bound radicals with the primary associating organic molecule precursors; however, present research has shown the formation of reactive oxygen species (ROS) of hydrogen peroxide (H_2O_2), superoxide ($O_2^{-}\bullet$) and hydroxyl radicals(•OH) through the synergistic interaction of EPFRs with the associated reduced metal oxides.[17,18,23-24] ROS have been found to induce oxidative stress, which can then result in a myriad of harmful effects, such as DNA damage, pulmonary dysfunction, cardiovascular diseases, and cell death. [17,18,23-24] EPFRs are known to promote active oxygen species formation in aqueous media, with the particle-associated EPFRs acting essentially as free radicals from the chemical and biological perspective. [17,18,23-24]

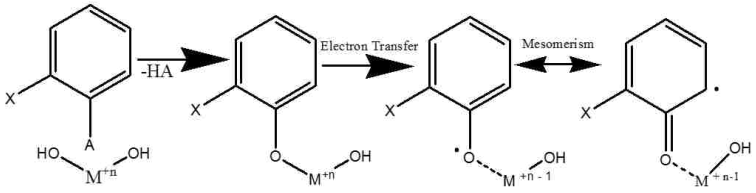

Figure 1.1 Simplified model mechanism of surface-associated EPFR formation from a substituted aromatic molecule via physisorption, chemisorption, and electron transfer.

Previous studies with transition metal oxides, such as Ni(II)O, Cu(II)O, Zn(II)O and $Fe(III)_2O_3$, that have been supported on silica surfaces generated from combustion and thermal processes under post-flame conditions, have demonstrated the formation and stabilization of EPFRs.[20,22,25-26] These model system studies laid foundations for studying EPFR formation in soils, as soils naturally contain significant amounts of transition metals in the form of minerals, including metal oxide species and clays. Thus, soils constitute a reservoir of transition metal centers that are involved in the EPFR formation. In parallel, the use of organic molecular precursors, such as PCPs, in wood preservation and other industrial processes, has led to their presence at elevated levels, in the environment, especially in soils. Similarly, increased levels of PAHs and CHCs from such sources as the on-road emissions from heavy-duty diesel vehicles[27-29] and even deposition of industrial products, such as automobile tires and household plastics[30], have resulted in the heightened presence of aromatic precursors in soils and sediments. Given the research showing that EPFRs can be formed when the appropriate organic precursors and transition metal centers are brought together, and the widespread presence of these components in soils and sediments across the globe, the following question arises: can EPFRs form in soils and are they present in the environment, especially at sites polluted with organic contaminants.

In regards to the presence of EPFRs in soil question, EPFRs have been discovered to have formed at PCP-contaminated Superfund soil sites, which indicates that EPFRs are not confined only to the combustion-generated particles.[31-32] The detection of EPFRs in soil sets the tone for even further research on EPFRs in soil matrices, which are known to serve as a major repository for organic contaminants. Further analysis of the PCP wood treating soils correlated very high concentrations of EPFRs with high metal and PCP concentrations, strongly suggesting the importance of metal centers and the aromatic precursor contaminants in the EPFR formation in the soil. This means that EPFRs can form in soils. After the detection of EPFRs at a PCP-contaminated wood treatment Superfund site, subsequent investigations performed at other

Superfund sites with PCP contamination also indicated the presence of EPFRs. [32] EPFRs have also been detected in soils high in coal and tars.[33-36] This is not surprising, considering that PAHs are also present in soils contaminated with coals.[37-39] These contaminants are known to bind to the metal sites in the sediments, which are abundant in the soil, leading to the formation of natural EPFRs.[31-33,39] For instance, Kiruri et al. detected high concentrations of highly stabilized organic radical in tar balls collected from the Gulf of Mexico shores of Louisiana and Florida after the BP oil spill.[33] Probing the tar balls' EPFRs, it was concluded that the EPFRs were formed from the partial oxidation of crude oil components, that occurred as a result of an interaction between the oxidized aromatics in the crude with metal ion centers. The tar ball EPFRs also had a chemical signature similar to that in the EPFRs detected in Superfund soils and $PM_{2.5}$.

Further efforts have been made to extend the understanding of EPFRs in both the soil and PM2.5, and these efforts have yielded the application of surrogate models in the study of EPFRs. Several recent studies have employed different metals in the study EPFRs using surrogate systems in order to understand the importance of metals to EPFR stability and persistency as well as their reactions with different aromatic precursors. Our group has recently employed two transition metals, Cu(II) and Fe(III), with which a clay soil surrogate was loaded, as well as phenol, as the organic precursor, to mechanistically study EPFR formation. Both the organic precursor and the metal center perspectives were taken into account in teasing out the influence of a number of environmental factors on EPFR stability (a more detailed discussion on these studies is presented in chapters 2 and 3). Recently, Hangzong et al. followed our lead to study the formation and stabilization of EPFRs induced by the interaction of anthracene with Fe(III)-modified clays. [40] Also, it has recently been illustrated in aqueous solution that, under UV irradiation, catechol in the presence of hematite (HMT)-silica leads to the formation of EPFRs, with catechol acting as the organic precursor.[41-42] The results from these works indicate that EPFRs in the surrogate systems were similar in terms of their make-up and stability to EPFRs detected in contaminated soils, thus

showing the promise of the surrogate soil approach. While the research on EPFR formation in soil using surrogate systems has only focused on two metal centers, a good number of other metals have been studied using silica-based nanoparticles.[20-22,25,43] For example, the formation of EPFRs on Ni(II)O, ZnO, TiO_2 and Al_2O_3 has been documented [20,25,43], which all yielding EPFRs with similar properties as EPFRs formed with the Fe and Cu clay systems.

The model mechanistic hypothesis for how EPFRs are formed involves physisorption, chemisorption, and concurrent electron transfer steps, and has been first proposed by Dellinger et al.[19,22] (as seen in Figure 1.1). This model has been shown to be appropriate for all EPFR formation studies to-date. Initial experiments with XANES showed the reduction of Cu(II) to Cu(I), in copper oxide, after exposure to organic precursor pollutants, such as 2-chlorophenols.[44] Sprunger et al a group of Superfund scientists in LSU have conducted an extensive research on the electronic structure of the EPFR forming processes employing ultraviolet photoelectron spectroscopy (UPS), low energy electron diffraction (LEED), and electron energy loss spectroscopy (EELS).[43,45-46] According to their findings, the chemisorption steps in the hypothesized EPFR formation mechanism were confirmed by the observed changes in the photoemission spectrum, which showed features of the chemisorbed phenol involving the phenol HOMO located 1.1 eV above the top of the TiO_2 valence band. [43,45-46] Following the EPFR formation at high temperature, an observed enhancement of the Ti 3*d*-derived “defect” peak and the attenuation of the phenol HOMO and phenol σ orbitals. [43,45-46] Collectively, these effects were interpreted as an indication of a high temperature chemisorption-associated charge transfer from phenol to TiO_2, which serves as evidence of an electron transfer process involved in the EPFR formation. Similar behaviors were also identified in the studies with Al_2O_3, [43,45-46] giving further credence to the electron transfer being subsequent to the chemisorption onto the metal surface step, initially proposed by Dellinger et al.,[19] and corroborates the findings from this work, as presented in Chapters 2 and 3.

1.3 The role of EPFRs in the degradation of organic pollutants

While there is a lot of literature on the toxicity of EPFRs, to-date, very few papers report on the role EPFRs may play beyond their toxicity. In their recent work, Xing et al., studied the degradation of *p*-Nitrophenol (PNP) concentration caused by EPFRs containing biochars.[47] Similarly, EPFRs containing biochars have been observed to enhance the degradation of 2-chlorobiphenyl (2-CB).[48] Although EPFRs in the biochars were responsible for the degradation of both PNP and 2-CB, the degradation mechanism appears to differ between pollutants. For PNP degradation, EPFRs were directly involved through direct radical association.[47] However, with the 2-CB degradation, EPFRs containing biochar generated •OH radicals through hydrogen peroxide (H_2O_2) activation, leading to the degradation of 2-CB by the •OH radicals.[48]

1.4 Toxicity of EPFRs

As stated earlier in section 1.2, EPFRs are known to form ROS through the reduction of molecular oxygen, followed by a disproportionation reaction, which produces hydrogen peroxide in situ. which, in turn, undergoes Fenton reaction with the reduced metal center to produce •OH radical.[17,23] The production of ROS is one of the main reasons for why EPFRs are toxic. [17,23-24] The reduction of the metals to their respective low oxidation states by the aromatic pollutants (phenols and chlorophenols) in the EPFR forming processes is key to ROS generation because of the reduced metal center which is essential for Fenton chemistry. These metal centers, and the matrices they are associated with, are regarded as vehicles for the transport of toxic pollutants into the body via the respiratory system, reaching the lungs, tissues, and other organs, prompting oxidative stress and the consequent tissue damages. While metals and organic pollutants are synergistic in their influence and contributions to the toxicity of EPFRs to humans, toxicological studies have widely correlated EPFR toxicity to the sizes of the EPFR carriers.[49,51] The reasons behind this is not far-fetched; Kiruri et al. have previously reported higher EPFRs concentrations and enhanced stabilization on smaller-sized CuO nanoclusters, compared to large-sized CuO

nanoclusters.[52] Based on their work and other literature, the smaller-sized metal nanoclusters catalyze EPFR formation better due to their larger surface area, thanks to which they can bind to a larger number of aromatic pollutants and hence, form more EPFRs. [51-52] This analogy can also explain the reason for the higher toxicity of $PM_{0.1}$ or $PM_{2.5}$ compared to other larger- sized PM's (PM_{10}).[49-54] Due to the ability of EPFRs to travel through the respiratory system to the lungs and penetrate to other tissues, most of the early combustion work on EPFRs has been largely focused on EPFRs formed on $PM_{2.5}$.Particulate matter sources can range from combustion-generated particles to wind-raised dust from the soil.[29,54-55] They are complex and heterogeneous in nature, making it difficult to attribute their toxicity to a particular component.[18,51] In 2009, Cormier and Dellinger first reported the effect of EPFRs associated with CuO/silica particles (ultrafine surrogates for PM) on human bronchial cells (BEAS-2B).[18] The results revealed that EPFRs containing CuO/silica ultrafine particles caused a myriad of cell damaging effects. Among them was the generation of ROS, which were detected by observing an increased level of 8-epi and PF2α lipid peroxidation products, which are notable oxidative stress markers in patients with respiratory disease.[18] Furthermore, their experiments also showed that BEAS-2B cells exposed to EPFRs containing CuO/silica particles triggered an increased expression of cytokines.[18] The latter effect was the result of an oxidative stress due to the ROS generation, leading to poor regulation of the antigen via oxidant-antioxidant imbalance[18], an activity associated with cell inflammation.[18] In addition, researchers also showed that ROS induced irreversible inhibition and distortion of cytochrome P450 metabolic activities in rat liver microsomes and other living organisms when exposed to two different types of EPFR-containing CuO/silica particles (MCP230 and DCB 230).[55-57] Generally, cytochrome P450s are known to modulate the xenobiotic metabolism in living tissues[55-57] thus their inhibition adversely affects their functions. Over the last five years, more epidemiological evidence has emerged on the toxicity of EPFRs to living organisms with the negative impact resulting in chronic pulmonary diseases, impairment of cardiovascular functions, DNA damage, and eventual cell death.[18,51,55-60] The case of enhanced

influenza disease severity has also been reported following pulmonary oxidative stress caused by EPFR-induced ROS from PM.[61] Fundamentally, these deleterious consequences are all linked to the potential EPFRs have to generate ROS which, in turn, cause oxidative stress. Finally, toxic effects of EPRFs are not only limited to humans. A recent report has revealed that EPFRs in biochar can cause decreased germination rate, damage to plasma membrane, and shoot growth retardation[62] which ultimately inhibits growth in plants as a consequence of oxidative stress.[62]

1.5 Research Scope

EPFRs in the nature of in the form of phenoxyl and semiquinone radicals have been recently found by our center at a 25-years old wood preserving Superfund site contaminated with PCP. [31] Further work revealed that the component of soil which the vast majority of the EPFRs were associated with, was the clay/humin fraction. However, this discovery-based research did not examine the chemical mechanism of in-situ EPFR formation in soils. Given the potential health risks of such EPFRs, it is imperative that the role of the different soil components be determined in an in-situ EPFR formation, whether acting individually and synergistically. Another motivation behind this dissertation research is that the in-situ formation of EPFRs may participate in the relatively slow intermediate stage in which chlorophenol is transformed into potentially more toxic dioxins.

Given the inherent complexity and heterogeneity of soils, the previously [31-32] used “top-down” approach to study the formation of EPFRs at Superfund sites has limitations, especially when one wishes to obtain fundamental mechanistic information essential to devising remediation strategies. Therefore, in this work, a “bottom-up” approach has been taken, as illustrated in Figure 1.2, in which surrogate systems are used and systematically built up in order to introduce the complexity and heterogeneity of real soils.

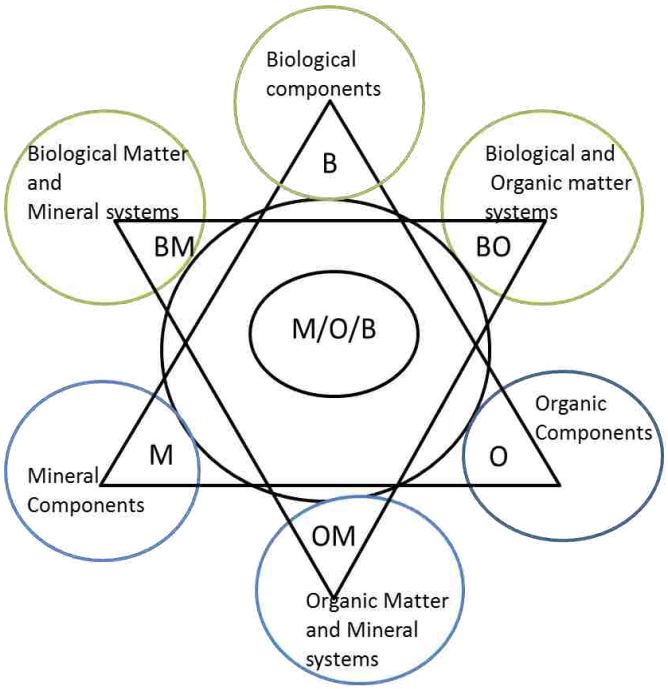

Figure 1.2 Experimental design for bottom – top approach utilizing single component, bi-component and tri-component system (figure from superfund research proposal- project 3)

1.6 Soil components

From the physical perspective, soil can be viewed as being composed of three phases, namely the gaseous, solution, and solid phases. Alternatively, as Figure 1.2 illustrates, soil can be broken down into three major, chemically active components, especially in regards to EPFR formation, namely the mineral, organic, and biological components. The mineral and organic components encompass the clay/humic fraction or the Superfund soils that showed, by far, the highest EPFR concentration of any of the soil components. As discussed in detail below,

1) the mineral phase provides a template for redox active metal centers;

2) the organic component provides a medium in which (i) hydrophobic compounds can be concentrated, (ii) the electrons essential to redox processes can be transported, and (iii) EPFRs can be stabilized due to the delocalization of the unpaired electron over a larger conjugated system; and

3) the biological component provides enzymes, such as laccase and peroxidase, that may allow redox processes at the relatively low soil temperatures that may not be energetically possible by other pathways, such as those facilitated by the high temperatures found in combustion process or the energy input provided by UV/Vis radiation. All of these components are known to play a vital role in the fate and transport of pollutants (PCP) within the soil. [64]

1.6.1 Clay minerals

Clay minerals are known to catalyze organic reactions transforming organic compounds through polymerization.[2,3,4] High levels of PCCD, which has been found in livestocks, meat, fish and baby food and linked to dioxin-containing minerals used in feed stocks, has been associated with PCP contamination of soils and the presence of transition metals within the clay component of the soils. [2,3,4] Active transition metal centers in clay mineral are known to play a key role in the formation and stabilization of the intermediate radicals obtained *en route* to the formation of dioxins. A number of studies have reported the formation of radical cations of 1- and 2-chlorodibenzo-*p*-dioxin as intermediate products on the surface of a Cu(II)-smectite clay.[65-66] Researchers have also used density functional theory to predict, and Fourier transform infrared studies to confirmed that pentachlorophenol radical cation generated on Fe(III)-montmorillonite can initiate octachlorodibenzo-*p*-dioxin formation from PCP.[4] Other studies have also shown that clays can play a role in the CO_2 sorption and the storage of radioactive wastes.[67-68] These works buttress the diverse role the clay component embedded in the soil play as a natural reservoir and in pollutant contamination. Naturally occurring clay minerals are known to contain both transition and non-transition metal cations, with metal smelting activities increasing the transition metal content of the clay components of soils [2,4] In the research contained in this dissertation work, we have used a smectite -montmorillonite clay, that has been exchanged with the commonly found soil, especially in some anthropogenically polluted soils, transition metal cations, namely Cu(II) and Fe(III).

1.6.1.1 Smectite-montmorillonite clay

Smectites are a group of phyllosilicate mineral species that includes saponite, montmorillonite, nontronite, beidellite, and hectorite.[69-70] Montmorillonite is a 2:1 type of smectite clay mineral with an assemblage of a stacked octahedral aluminate layers in between two tetrahedral silicate layers, containing exchangeable interlayer cations, see Figure 1.3. [69,70,71] Smectite clays possess distinct properties, such as high cation exchange capacity, large surface area which is chemically active and remarkable hydration characteristics at the interlamellar surfaces.[69,70] The presence of exchangeable cations, usually alkali and alkaline earth metals (Na, Ca and Mg), in smectites compensates for the variable net negative charge of the clay surface. These net negative surface charges caused by the charge deficiency which is arises during isomorphous substitution of lower charge cations for higher charge cations and this occurs through intercalation between the interlayer sites. These cations constitute the exchangeable ions found in the interlayers of montmorillonite clay, with commercial clay deposits containing greater number of Ca and Mg compared to Na and H.[69,70] These ions can be reversibly exchanged. For instance, during soil mineral leaching process, a Na-containing montmorillonite is usually exchanged by higher valence Ca and Mg. [69]

Montmorillonite clay is regarded as a swelling clay and the extent of swelling is dependent ability for the interlayer cation to form well oriented water layers on the clay interlamellar surfaces. This is also defined by the swelling ratio is which is directly related to the ratio of Na and Ca ions in the interlayer. Among the interlayer cations, Na-containing montmorillonite exhibits a high swelling ratio. Na swelling usually leads to dispersion and the development of colloidal-like properties, such as high natural viscosity.[69] Commercial smectite clay originates from a variety of natural processes, suggesting the reason for its widespread occurrence. One of such natural processes is through the hydrolysis of extrusive volcanic rocks, with minor contributions from intrusive rocks, in environments exposed to surface weathering.[69] Also, during geochemical

processes, smectites can form through the alteration of Si-, Al-, Fe- and Mg-bearing minerals as well as the precipitation of natural elements containing fluids.[69,71] In recent years, smectites have been studied due to their ability to serve as adsorbents for organic pollutants.[72] The large surface area and small particle sizes that characterize smectite clays assist in their sorption of, and the ability to catalyze the transformation of organic molecules.[69-71]

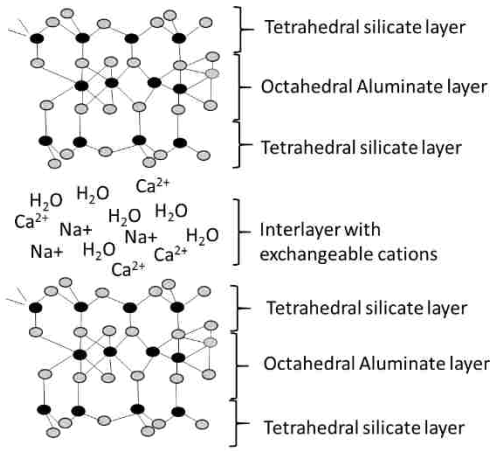

Figure 1.3 A schematic diagram of montmorillonite.

1.6.2 Organic component – soil organic matter (SOM) and humic substances (HSs)

Soil organic matter (SOM) is a class of natural organic matter (NOM), that originates primarily from the degradation of plant materials with a little contribution from animal litter.[73-75] (Ref) Humic substances (HSs), which constitute the major component of SOM, are made up of a weakly associated molecular assemblies of heterogeneous polymer-like moieties, which can be hydrophobic and hydrophilic in nature and are akin to proteins,[31] They have molecular weights that ranges from 100 to 100,000 Da. [73,76] HSs contribute 40-90% of the total organic carbon of the soil and sediments.[74] HSs are composed of three main chemical entities, namely alkyl, O-alkyl, and aryl, which arise from the degradation of long chain aliphatic, cellulose, and lignin parent materials as well as other biomolecules, such as fats, proteins, pectines, and cutines.[39,75,76,77] The core structure of HSs is typically polyphenolic, or/and carbohydrate with polymeric aliphatic

branches and linkers.[78-79] HSs are operationally divided into three different fractions depending on their characteristic solubility in alkaline and acidic media. Fuvic acid represents the fraction soluble at all pH conditions and humic acid (HA) is the fraction that is soluble under alkaline conditions. Humin is the insoluble fraction of humic substances.[77] This variation in solubility of humic substances does not necessarily indicate the presence of three categories of organic molecules. [77,80]

HSs are polyfunctional in nature (i.e., contain carboxylic, phenolic, alcohol, amine, etc functional groups), which enables their effective interactions with both metal ions and organic molecules. These interactions can be as a result of ion exchange, complexation, redox transformations, and hydrophobic associations [77-82] Since HSs can act as redox mediators, their accumulation in the terrestrial and aquatic environments plays a vital role in stimulating the redox biotransformation of organic molecules in the soil. This property has been attributed to the very abundant quinone moieties in humus.[81-86]

1.6.2.1 Humics as electron shuttles

A number of studies have investigated the role of HSs in the remediation of organic pollutants in the soil and the environment. [81-86]It has been shown that HSs act as terminal electron acceptors in microbial degradation and biotransformation of a range of organic pollutants.[86-87] The electron shuttling activities of HSs in the soil cannot be overemphasized in terms of soil redox processes. Previous literature has demonstrated that quinone moieties are responsible for the electron transfer redox mediating role of HSs in the reductive transformation of organic pollutants.[77,81-83] For example, it has been shown that microorganisms, such as halorespiring bacterium, *Desulfitobacterium dehalogenans,* with non-iron-reducing capabilities have exhibited effective iron-reducing capability in the presence of anthraquinone-2,6-disulfonate(AQDS, a HS quinone surrogate), highlighting the electron accepting role of humic substances.[89] The oxidation state of quinone moieties usually varies depending on local environmental conditions, stage of

redox reaction, and the transforming agents involved. The quinone moieties within HSs can be present in three oxidation states, quinone, semiquinone, and hydroquinone, (Figure 1.4, a). [90] The ability of quinone moieties within HSs to exhibit these oxidation states highlights HSs' ability to shuttle electrons back and forth from organic compounds to HS-coated redox centers, including clay minerals, in the soil system. In this case, the degradation of the organic polutants is aided by the electron shuttling capabilities of HSs, with the clay mineral acting as the final electron destination. As an ultimate consequence, EPFRs are formed by, and become associated with, the clay/humin soil fraction. EPFRs resulting from this process can be derived from two sources: 1) direct electron shuttling by HSs from PCP to the transition metal center of clay mineral (Figure 1.4, b) and 2) the shuttling of electrons, with HSs acting as the main redox active centre, induced by the HS-oxidixing microorganism degradation of PCP. The latter effect can easily lead to dechlorination of PCP, with phenol usually being the final product (Figure1.4, c). Futhermore, clay minerals and other redox center-containing minerals may not be required as a source of transition metal centers as HSs can bind transition redox centers due to the inherent presence of phenol and carboxyl groups, and thus, HS-transition metal complexes can act as both electron sink and source in the fate and transport of organic pollutants in the soil.[31]

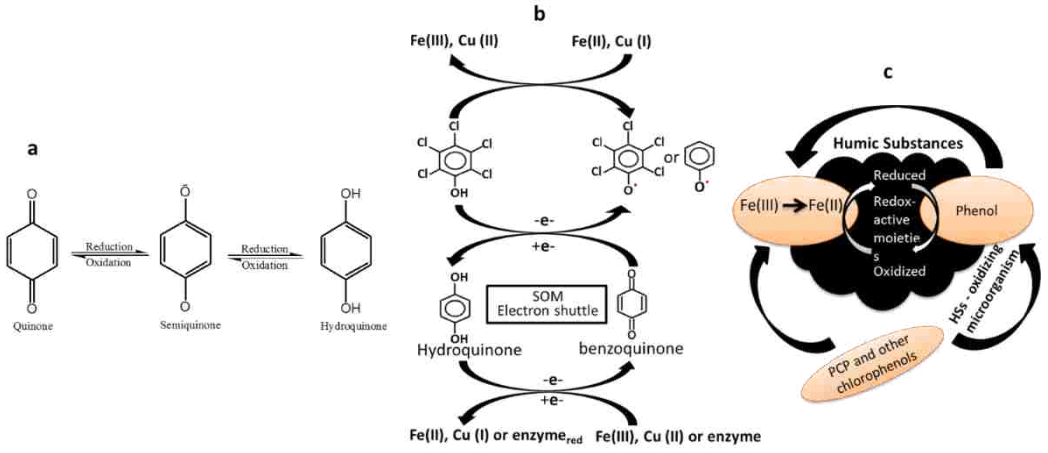

Figure 1.4 (a) Quinone-hydroquinone electron route in SOM. (b) Direct electron shuttling by SOM from PCP to metal center of clay mineral. (c) PCP degradation leading to phenol formation

1.6.3 Biological component

A number of microorganisms have been found to be able to degrade chlorinated phenols, by the chlorinated phenol compound undergoing reductive dechlorination when subjected to anaerobic conditions in the presence of electron donating groups.[81,91-93] Thus, it can be postulated that the biological components of soils may play a major role in the formation EPFRs in soils. Previous studies have shown that microorganisms can anaerobically reduce humic substances in the process leading to the reduction of high valency transition metal-containing mineral.[81] In particular, high Fe(III) metal reducing capacity of NOM was demonstrated when incubated with *S. putrefaciens*.[81] In fact, a large number of microorganisms such as Desulfitobacterium spp, Geobacter spp, Sulfurospirillum spp fall into this category. Furthermore, under anoxic conditions mineralization of organic pollutants to CO_2 can occur in the presence of quinone-reducing microorganisms.[90],[94,95] Similarly, White rot fungi which are usually found on woods and trees produces three ligninolytic enzymes; lignin peroxidase, manganese dependent peroxidase and laccase.[96-98] These enzymes are able to degrade chlorinated phenols, including PCP, through the formation of stabilized phenolic radical intermediate by one-electron oxidation of phenolic compounds. The product of this class of degradation pathway varies sometimes depending on the composition of the reaction. Several studies have reported the formation of chloroquinones and other products of polymerization.[92,93,99] Reduction of oxidized chlorophenol is generally catalyzed by redox enzymes, such as lignin peroxidases or manganese peroxidases (Mn-P), in concert with H_2O_2 in the presence of quinone reductase or glucose, with laccase (a copper containing oxidase) reducing dissolved oxygen to water in this process.[98]

1.7 Techniques

Several analytical techniques were employed in accomplishing the research projects in this dissertation work, including electron paramagnetic resonance (EPR) spectroscopy, X-ray absorption near edge structures (XANES) spectroscopy, extended X-ray absorption fine

structures (EXAFS) spectroscopy, Fourier transform infrared (FTIR) spectroscopy, Raman spectroscopy, X-ray powder diffraction (XRD) spectroscopy, and photoelectron spectroscopy (XPS) will be discussed in detail.

1.7.1 Electron Paramagnetic Resonance Spectroscopy (EPR)

Electron paramagnetic resonance (EPR) was the key technique used to identifying, characterize, and quantify EPFRs in this work. EPR is an electromagnetic radiation absorption based spectroscopic technique, which can be applied to detect paramagnetic species containing one or more unpaired electrons.[100-101] Paramagnetic species can be organic or inorganic in nature. As a result of the intrinsic angular momentum possessed by the free electron, an unpaired electron can be in one of two spin states, namely an α state (+½ low energy electron) and a β state (–½ high energy electron), which mutually are degenerate and randomly oriented in the absence of a magnetic field.[100-102] However, when an external magnetic field is applied, denoted as B_0 , degeneracy is removed and the magnetic ½ moments (μ) of the unpaired electrons are aligned either parallel or anti-parallel to B_0, typically populating electrons into two energy levels due to the Zeeman effect and resulting in the α and β states, respectively.[99-102] Initially, the majority of electrons settle in the lower energy level; however, with the application of microwave radiation, electrons are also promoted to the higher energy level, as shown in Figure 1.5. A point of field resonance is established when the energy of the incident (microwave) radiation frequency, ω_0, corresponds to the energy difference (ΔE) between the α state and β states. At this point of field resonance, microwave absorption occurs and can be detected. [100-103]

The energy difference is expressed with the following equation;

$$\Delta E = h\omega_0 = g\mu_0 B_0 \qquad \text{equation 1.1,}$$

where h is the Planck's constant (h = 6.63 $\times$ 10^{-34} J s), ω (Hz) represents the frequency of the

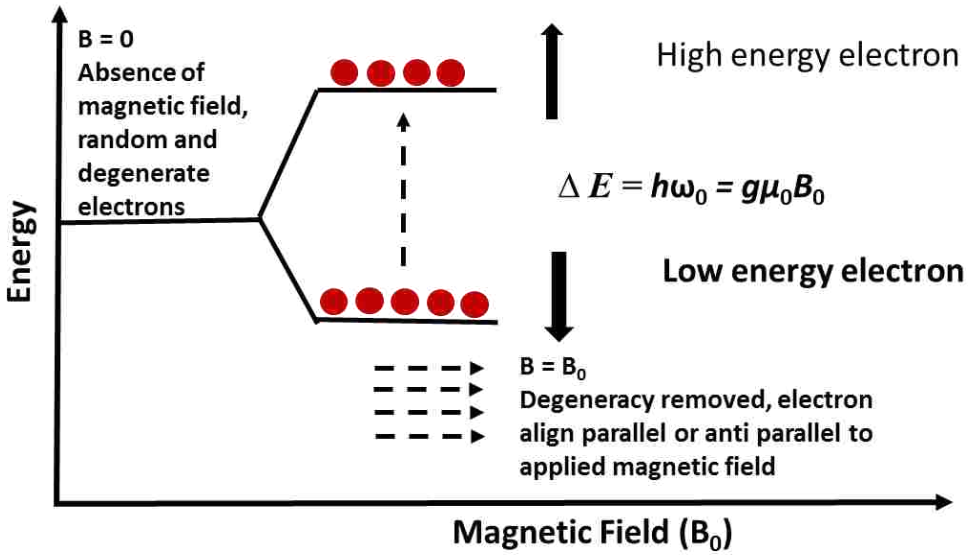

Figure 1.5 Diagram showing the Zeeman effect, with the splitting of the energy level of an electron as a result of applied magnetic field.

incident microwave radiation, B_0 (Tesla) is the applied magnetic field, g is known as the spectroscopic g-factor, and μ_0 is the Bohr magneton conversion constant ($\mu_0 = 9.27 \times 10^{-24}$ J T^{-1}). It can be deduced from equation 1.1 that the measured energy difference is a function of the frequency of the incident radiation and is directly proportional to the magnetic field.[100-103] The resonance frequency, ω_0, is also known as the Larmor frequency[100-103] and can be expressed with the equation:

$$\omega_0 = \gamma_e B_0 \qquad \text{equation 1.2,}$$

where γ_e is the magnetogyric ratio of the electron. The g-factor can be derived by a rearrangement of equation 1.1, as follows:

$$g = h\omega_0 / \mu_0 B_0 \qquad \text{equation 1.3.}$$

The g-factor is a highly insightful EPR parameter, as it is used to determine the chemical identity of the paramagnetic species giving rise to the detected signal .[100-101] The spectroscopic g-factor, denoted as g_e, is the g-factor of a free electron with zero angular momentum and has a value of; ~2.0023. However, the interaction between the ground and excited state electrons

results in an additional amount of orbital angular momentum, which is regarded as the spin-orbit coupling contribution. The *g*-factor is affected by the degree of the spin-orbit coupling contribution from the local environment of neighboring atoms, the magnitude of which is dependent on the size of the nucleus of the paramagnetic species of interest. [100-103] This results in the deviation of the measured *g*-factor from that of the free electron (g_e) For instance, the *g*-factors for paramagnetic metal centers in metal complexes are larger compared to the paramagnetic centers in organic radicals. This this is due to the spin-orbital couple contribution from lighter nucleus atoms (H, O, N, and C) in organic radicals compared to the heavy nucleus paramagnetic metal centers. [100,102] The *g*-factor provides chemical information of not only the immediate atom but also the chemical environment, bonding type, and electronic structures between electron-molecule or electron-atom interactions. [100,102]

An EPR spectrum is plotted as the first derivative, f'(x), of the absorption spectrum, f(x), as shown in Figure 1.6 first derivative is to obtain the *g*-value from the crossover point as the falling inflection point of the first derivative of the absorption curve, i.e., when the function goes

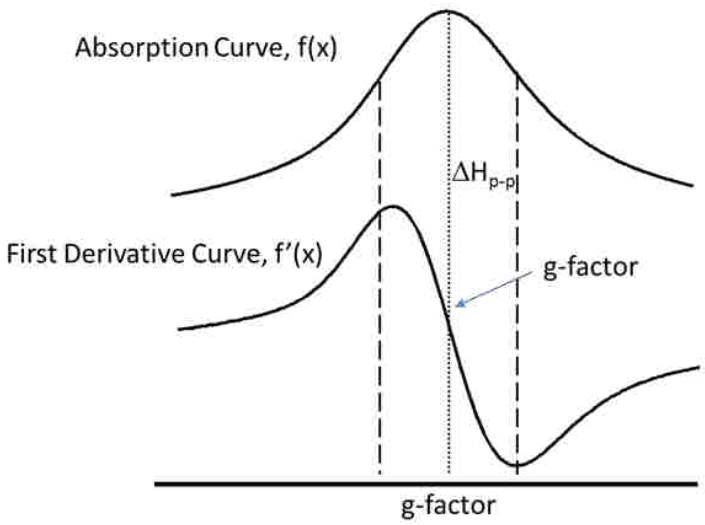

Figure. 1.6 Absorption curve, f(x), and first derivative, f'(x), EPR spectra.

from concave to convex. The *g*-factor is measured by a line drawn through the first derivative spectrum at the peak maxima of the absorption spectrum.[100-102] Another important parameter that defines the nature of the paramagnetic species is the resonance line width, $\Delta H_{p\text{-}p}$, otherwise referred to as the peak-to-peak linewidth, which is determined by measuring the distance between f'(x) at the maximum and the minimum of the first derivative EPR spectrum.[100-101] The narrowness or broadness of EPR spectrum peak-to-peak linewidth is can also be used to determine the local environment of the interacting paramagnetic centers.[100,102]

The interaction that results from the unpaired electrons (electron spins) interacting with the nuclear magnetic moment is defined as the nuclear hyperfine interaction. Nuclear hyperfine interactions are very important in EPR measurements since they can be used to extract information about the interacting unpaired electron and the atomic nuclei. This is usually determined by identifying the splitting patterns that result from these hyperfine interactions with their hyperfine splitting constants, which are characteristic of the neighboring interacting nuclei.[100-102].

The basic components of an EPR spectrometer are presented in Figure 1.7, in which the

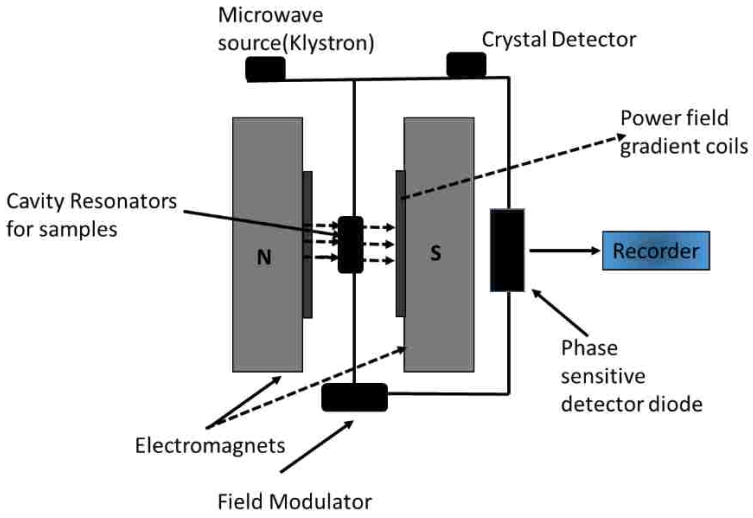

Figure 1.7 Schematic block diagram of an EPR spectrometer.

EPR microwave cavity (sample cavity) or resonator, which serves as a sample holder, is saddled with two magnets that provide the magnetic field following the generation of the high frequency electromagnetic microwave from a klystron source.[100-101] The microwaves generated by the spectrometer are then passed through the sample where the modulated signal is reflected on to the phase-sensitive detector diode. The so generated signal is equivalent to the amount of absorbed microwaves. In the EPR operation, the microwave frequency is kept constant while the magnetic field is varied.[100-102] Typically, most EPR instruments operate with an approximate microwave frequency of 9.5 GHz, which falls within an X-band region of 8-12 GHz. [103] Other EPR spectrometers operate at higher microwave frequencies (similar to higher field NMR spectrometers), including 35 GHz (Q band region EPR) and 95 GHz (W band region EPR).[101-103]

1.7.2 X-ray Absorption Spectroscopy (XAS) Techniques

Two other important techniques used in the work presented in this dissertation, namely XANES and EXAFS, are categorized under X-ray absorption spectroscopy (XAS). XAS techniques are based on the absorption of X-ray lights in the form of a photon by a tightly bound electron at the core level of an atom.[104-105] The absorbed energy causes the ejection of an electron from the core shell, thereby creating a so-called core hole (figure 1.8). The ejected electron is known as the photo electron.[104-105] For these processes to occur, the energy of the incident photon must be greater than the binding energy of the core shell electron.[104] The absorbed energy is characteristic of the binding energy of the electron core. Often, with further absorption, the core edges are promoted to a continuum which, in turn, gives rise to an absorption edge. [104-105] The excess energy from the incident photon is released as a photo-electron.[104]X-ray absorption is often defined with the basic Beer's law equation:

$$I = I_0 e^{-\mu t} \qquad \text{equation 1.4,}$$

where I_0 and I represent the incident and the transmitted X-ray intensities, respectively, while t is the thickness of the absorbing atom. The most important parameter from equation 1.4 is μ, which

is the coefficient of absorption; it is a function of energy and is related to the properties of the absorbing atom[104] and can be expressed as follows:

$$\mu \approx \rho Z^4 / AE^3 \qquad \text{equation 1.5,}$$

where ρ is the sample density, Z is the atomic number, A is the atomic mass number, and E represents the X-ray energy. Equation 1.5 shows an important correlation between the absorption coefficient, μ, the atomic mass number, A, and the X-ray energy, E. The edge energy varies proportionately with twice the atomic number of the target element nuclei in the absorbing species, and usually falls between 5 and 35 keV, allowing most elements to be probed with XAS based methods. 104 In XAS techniques, the energy near and above the core absorption edges of atomic species are measured as a function of their absorption intensities.[104] Since all atomic species have core-level electrons with distinct binding energies, XAS measurements are element specific. [104-106]

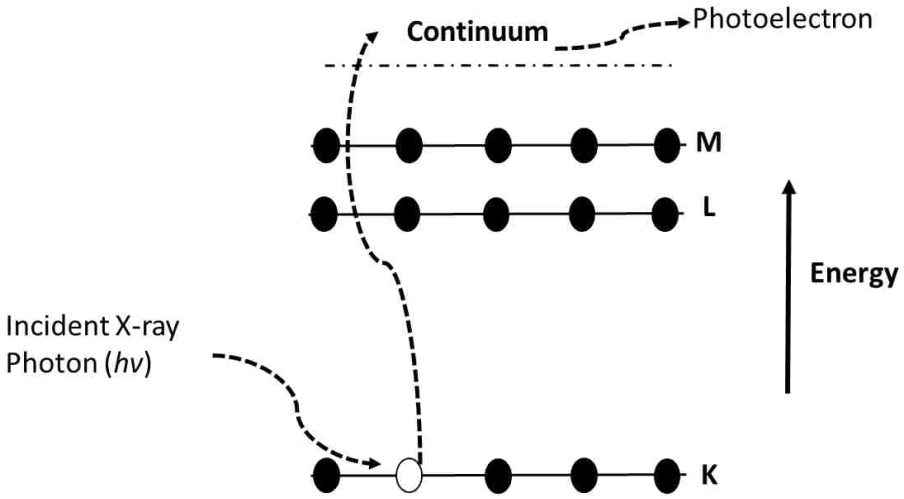

Figure 1.8 Ejection of a photoelectron from a core shell *K* orbital by incident X-ray energy to form a core-hole. (figure redrawn from ref .104)

After the ejection of an electron from a core-edge electron shell, the atom becomes excited with a highly unstable electron core hole, with a lifetime on the order of a few femtoseconds.[104-106] Subsequently, the excited state atom decays, most typically in one of the following two ways:

1) the higher energy shell electron level tends to drop into the core-hole, and an X-ray of a characteristic well defined energy is emitted or 2) the higher energy shell electron level drops into the core-hole, which is then accompanied by an emission of a second electron (known as an Auger electron) into the continuum, see Figure 1.8 and Figure 1.9. As depicted in Figure 1.9, the core hole can be filled in by either an electron from the immediate higher energy shell, *L*, or the penultimate shell, *M*, which will result in the emission of different fluorescent lines.[104] The energy emitted in the first process is known as X-ray fluorescence energy, while the second process is referred to as the Auger electron emission effect.[104] Auger effects are usually encountered in the lower energy X-ray absorption regimes. The energy resulting from both processes are characteristic of specific atomic transitions in an element, thus they can be used to identify different elements as well as quantify their concentrations. [104-106]

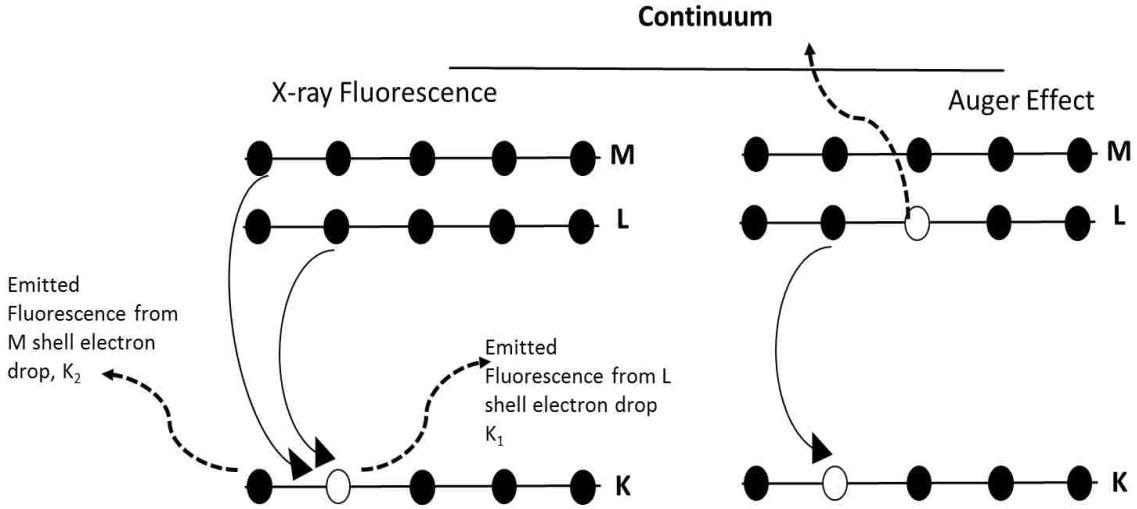

Figure 1.9 Excited state decay via X-ray fluorescence and Auger electron emission processes. (figure redrawn based on ref. 104)

XAS techniques utilize either transmission or emission (fluorescence) modes for detection. For both measurements, experimental signals are determined as their respective energy function of the absorption coefficient and can be derived as follows:

Transmission measurement ……. $\mu(E)=\log(I_0/I)$ equation 1.6

Fluorescence measurement ……. $\mu(E)=\alpha(I_f/I_0)$ equation 1.7

Generally, X-ray absorption spectroscopic data are categorized as: 1) X-ray absorption near edge structures, XANES, or extended X-ray absorption extended fine-structure, EXAFS.[104]

1.7.2.1 X-ray absorption near edge spectroscopy (XANES)

X-ray absorption near edge spectroscopy XANES) is a unique X-ray absorption tool for determining the formal oxidation numbers of elements the local coordination environment around an absorbing atom. It probes the fine structure of the elements in the vicinity of the absorption edge (*K*, *L*, *M*... subshells).[106-109] This is achieved by measuring the photoelectron intensity for photon energies from the absorption edge up to 50 eV beyond the edge energy.[106-108] XANES evaluates unoccupied electronic states by determining the X-ray absorption coefficient, which depends on the photon energy at a fixed angle of illumination. This absorption coefficient decreases with increasing photon energy, which is, in turn, dependent on the atomic number of the absorbing atom. As depicted in Figure 1.10, the XANES region is composed from the pre-edge, the main edge, and the multiple scattering region, the latter being primarily associated with the white line.[104-109] While the pre-edge and the main edge are solely used to extract information about the oxidation numbers, all three regions are responsible for determining the coordination sphere of the absorbing atomic species.[104-109] The XANES spectrum is determined in large part by the symmetry of a local site irrespective of the crystalline order.[104-105, 107] Therefore, it can provide more information about the chemical bonding as well as the site symmetry probed compound.(from both amorphous and crystalline materials) [108-111] The pre-edge region primarily shows the absorption edge features of the absorbing atoms; these features result from the bound state's electronic transitions, with transition probability being typically determined by dipolar selection rules.[107,108,111] In most transition metal oxides, especially those of the first row transition metals, pre-edge changes can depict 1*s* to 3*d* transitions as a result of the presence of the partly filled *d* orbitals. This is made possible due to the hybridization of *d* and *p* orbitals.[107,110] Information

about the oxidation state of the absorbing atoms is majorly deduced from the location (energy) of the pre-edge and the main edge regions, since the main edge regions provide further details on the continuum state energy threshold.[110] Finally, information pertaining to the neighboring species of the absorbing atom, such as the interatomic distances and bond angles,[107,111] can be elucidated from the multiple scattering regions (figure 1.10). This region arises from the photoelectron scatterings by nearby atoms surrounding the central absorbing atom.

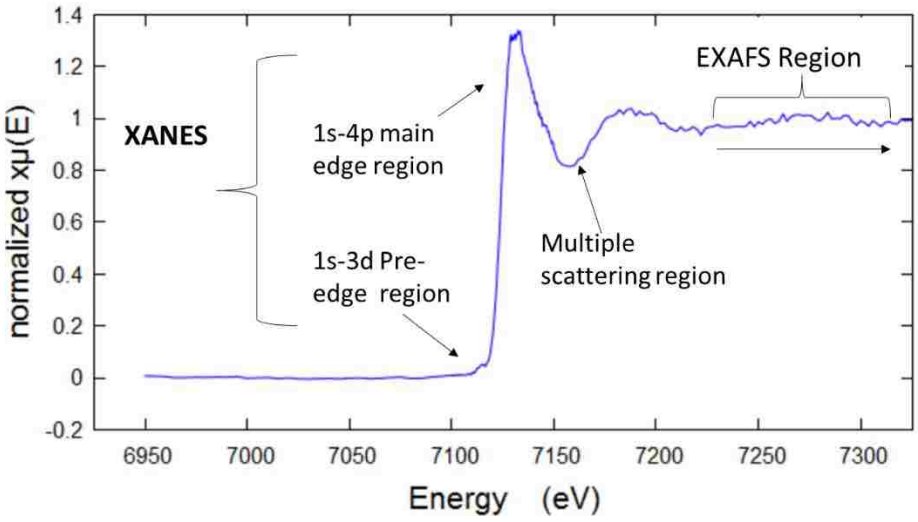

Figure 1.10 X-ray absorption spectra showing XANES and EXAFS regions

1.7.2.2 Extended X-ray absorption fine structure (EXAFS)

Extended X-ray absorption fine structure (EXAFS) is a technique employed to determine the structural information of a crystalline or amorphous sample. EXAFS provides information such as the coordination numbers, interatomic distances between an absorbing central and the neighboring atom, and the local environment of the nearby atoms that are within the range of ~5Å in a sample.[104,106-109] In EXAFS, the measurement is mainly concerned with the region which is ~50 eV to ~1000 eV above the absorption edge energy.[107] As stated earlier, the energy of the incident photon is usually higher than the binding (edge) energy resulting in the ejection of a photoelectron. Typically, a photoelectron is represented as a wave/particle and the resultant energy is given by the following equation:[104-106-108]

$$E = E_x - E_0 \quad \text{equation 1.8,}$$

where E_x is the energy of the incident X-ray photon and E_0 represents the binding energy or energy of the edge. Due to the proximity of other neighboring atoms to the specified central absorbing atom, the wave associated with the photoelectron is scattered by these nearby atoms, resulting in a constant interference pattern, which can be constructive or destructive in nature. [104-106-108]In a sample, these interference patterns result in absorption coefficient modulations, giving rise to signal oscillations which are usually evident in the EXAFS spectra. [104,107-108]

Generally, the EXAFS equation is expressed in terms of an energy oscillation function, whose value is proportional to the amplitude of the scattered photo-electron at the absorbing atom:

$$\chi(E) = \frac{\mu(E) - \mu_0(E)}{\Delta\mu_0(E)} \quad \text{equation 1.9,}$$

where $\mu(E)$ is the measured absorption coefficient, $\mu_0(E)$ is the background value of the absorption coefficient of the isolated atom, while $\Delta\mu_0(E)$ represents the difference in the measured absorption coefficient from the background energy. [104,108-109] The oscillation functions associated with the photoelectron are usually expressed interpreted in terms of a wave vector or wavenumbers, k,:[104,108-109]

$$k = \sqrt{\frac{2m_e(E - E_0)}{\hbar^2}}$$

or $$k = \frac{\sqrt{2m_e(E-E_0)}}{\hbar} \quad \text{equation 2.0,}$$

where m_e is the electron mass. When every other component is factored in, considering the oscillation from the photoelectron scattering of the nearby atoms, the oscillation wave function $x(k)$ defines the complete EXAFS equation which is stated as [104,108-109]:

$$x(k) = \sum_j \frac{N_j f_j(k) e^{-2k^2\sigma_j^2} e^{\frac{2R_j}{\lambda}}}{kR_j^2} \quad \text{equation 2.1,}$$

where N is the number of the neighboring atoms, R is the interatomic distance between the central absorbing atom and the neighboring atoms and the atomic disorder from the neighboring atom, δ^2, can be determined from the known values of the scattering properties, namely: $f(k)$ and $\delta(k)$, which are dependent on the atomic number of the neighboring atom.[104] EXAFS spectra are usually represented as Fourier transformed radial distributions. [104,108-109] EXAFS data can be collected both in transmission and fluorescence modes. In this dissertation work, XANES and EXAFS were utilized to investigate the change in the oxidation state of transition metal ion centers after EPFR formation and, in conjunction with other techniques, to determine the coordination environment of formed EPFRs.

1.7.3 X-ray powder diffraction (XRD)

X-ray powder diffraction (XRD) is a versatile analytical characterization tool, commonly utilized in the phase measurement of crystalline materials.[112-113] Materials are usually analyzed in a finely ground powdered form. XRD operates on the basic principle of the scattering of X-ray radiation by the surface of a material and depends on the arrangement of the atoms in the crystal lattice. Due to the periodic manner in which atoms are arranged in the crystal lattices, constructive inference is produced, causing a diffraction of the incident X-ray at an angle equal to the incident X-ray.[112-114] The outcome of the scattered light from a crystal surface is dependent on the number of electrons around atoms which are responsible for the coherent scattering. The diffracted light from a crystal provides information about the atomic arrangements in the crystal. [112-114] Generally, the XRD principle is based on Bragg's equation, which is stated as follows:

$$n\lambda = 2d \sin\theta \qquad \text{equation 2.2,}$$

where n represents the order of reflection of X-ray light from the crystal surface, λ is the wavelength of the incident X-ray, d represents the distance between the crystal planes, and θ is the angle of incidence of the X-ray light. In operating the XRD instrument, the powdered sample is scanned at an angle of 2θ in such a way as to obtain diffraction in all directions from the

powdered sample.[112-114] The information derived from the XRD scanning experiment is interpreted in terms of *d*-spacing and results in *d*-spacing values which are then judged against standard references. [113] An XRD spectrum is typically presented as a plot of count-per-seconds versus the rotation angle of 2θ. In the research contained in this dissertation work, XRD was utilized to corroborate the cation exchange in and dosing of montmorillonite clay.

1.7.4 X-ray photoelectron spectroscopy (XPS)

X-ray photoelectron spectroscopy (XPS) is a surface probing technique which can be applied to measure the electronic structure at the surface of a material. XPS probes electronic properties from the photoelectrons emitted from surface atoms bound up to ~10 nm deep from the surface.[114] This is accomplished by measuring the resultant kinetic energy after the ejection of an electron from an atom by an incident photon. As previously described in section 1.7.2, the decay of the excited state electron results in the filling of the *K* shell hole by an *L* shell electron. This results in the emission of an Auger electron that gives rise to characteristic electronic signal which is detected in XPS. The kinetic energy involved in the photoemission and the Auger de-excitation process from different electronic energy level transitions are unique to each element. The XPS spectrum is presented as a plot of signal intensity versus the binding energy. In this dissertation work, XPS was employed to corroborate the reduction of Fe(III) to Fe(II) that occurred in the EPFR formation process in the model Fe-containing clay-based surrogate soil system.

1.7.5 Raman Spectroscopy

Raman spectroscopy is an analytical technique based on the principle of inelastic scattering of monochromatic radiation. In Raman spectroscopy, a monochromatic laser light source of a specified frequency is applied to illuminate a sample, resulting in the interaction of photon with the sample's molecules. This interaction leads to an exchange of energy and a subsequent scattering of the incident radiation. The resulting scattered radiation possesses a frequency and wavelength different from those of the incident radiation, giving rise to a

phenomenon known as the Raman effect.[114-115] The energy of the resulting scattered radiation may be lower or higher than that of the incident photon depending on the extent of energy exchange during interactions of light with the sample's molecules. [114-115] In addition, the discrepancies in the frequency, wavelength, and energy of the scattered light are all a function of the rotational and vibrational energy of each type of molecule. The energy transition of the molecule is determined by the frequency difference of the scattered radiation. For instance, when the frequency of the scattered radiation is less than the frequency of the incident radiation, it results in the appearance of a Stokes line in the Raman spectrum.[115] This corresponds to an energy transition from a lower to a higher energy vibrational state of the sample's molecule However, anti-Stokes shifts can also be observed in Raman spectroscopy for fluorescent samples.[115] This occurs when the frequency (energy) of the scattered radiation is higher than that of the incident radiation. Raman spectra are usually presented as a plot of intensity versus the wavelength number, with the wavenumber of Raman active modes usually ranging from 400 to 4000 cm^{-1}. In this dissertation work, Raman spectroscopy was utilized to identify and characterize the organic phase poly-*p*-phenylene grafted on the cation-exchanged clay during the preparation of a clay-polymer surrogate model used to represent the SOM/mineral component of soil.

1.7.6 Fourier transform infrared (FTIR) spectroscopy

Fourier transform infrared spectroscopy is an analytical technique used to measure functional groups that absorb or emit within the infrared region of the electromagnetic spectrum. Beer's law, as previously stated in section 1.7.2, also applies to FTIR. In FTIR, a single frequency infrared (IR) radiation source is employed to illuminate a splitter which reflects and transmits the beam of light into two equal parts.[116] After splitting, the transmitted beam of radiation is cast on the sample, causing the sample to absorb radiation that is characteristic of the sample's molecular constituents. The transmitted beam from the sample is then compared against the transmitted beam obtained from the background, thus generating two single beam spectra, which are then

interpreted by Fourier transforming the corresponding interferograms to yield frequency-based data so that different functional groups are detected as a result of their vibrational frequencies.[116] FTIR spectrum can be presented as transmission or absorbance versus wavenumbers. A typical FTIR instrument has a wavenumber range of 400 to 4000 cm^{-1}, which represents the mid infrared radiation energy region. Molecular absorption of radiation in this IR region results from the difference in the ground state and excited state vibrational modes. [116] In this dissertation work, FTIR was utilized to confirm the absorption of phenols after gas phase exposure on cation-exchanged clays.

1.8 References

1. Williams, L. L.; Giesy, J. P.; DeGalan, N.; Verbrugge, D. A.; Tillitt, D. E.; Ankley, G. T.; Welch, R. L., Prediction of Concentrations of 2,3,7,8-Tetrachlorodibenzo-p-dioxin Equivalents from Total Concentrations of Polychlorinated Biphenyls in Fish Fillets. *Environmental Science & Technology* **1992,** *26* (6), 1151-1159.

2. b, C.; Liu, C.; Ding, Y.; Li, H.; Teppen, B. J.; Johnston, C. T.; Boyd, S. A., Clay Mediated Route to Natural Formation of Polychlorodibenzo-p-dioxins. *Environmental Science & Technology* **2011,** *45* (8), 3445-3451.

3. Gu, C.; Li, H.; Teppen, B. J.; Boyd, S. A., Octachlorodibenzodioxin Formation on Fe(III)-Montmorillonite Clay. *Environmental Science & Technology* **2008,** *42* (13), 4758-4763.

4. Gu, C.; Liu, C.; Johnston, C. T.; Teppen, B. J.; Li, H.; Boyd, S. A., Pentachlorophenol Radical Cations Generated on Fe(III)-Montmorillonite Initiate Octachlorodibenzo-p-dioxin Formation in Clays: Density Functional Theory and Fourier Transform Infrared Studies. Environmental Science & Technology **2011**, 45 (4), 1399-1406.

5. Boström, C.-E.; Gerde, P.; Hanberg, A.; Jernström, B.; Johansson, C.; Kyrklund, T.; Rannug, A.; Törnqvist, M.; Victorin, K.; Westerholm, R., Cancer risk assessment, indicators, and guidelines for polycyclic aromatic hydrocarbons in the ambient air. *Environmental Health Perspectives* **2002,** *110* (Suppl 3), 451-488.

6. Boffetta, P.; Jourenkova, N.; Gustavsson, P., Cancer risk from occupational and environmental exposure to polycyclic aromatic hydrocarbons. Cancer causes & control: CCC **1997**, 8 (3), 444-72.

7. Buth, J. M.; Grandbois, M.; Vikesland, P. J.; McNeill, K.; Arnold, W. A., Aquatic photochemistry of chlorinated triclosan derivatives: Potential source of polychlorodibenzo-P-dioxins. *Environmental Toxicology and Chemistry* **2009,** *28* (12), 2555-2563.

8. Takada, S.; Nakamura, M.; Matsueda, T.; Kondo, R.; Sakai, K., Degradation of polychlorinated dibenzo-p-dioxins and polychlorinated dibenzofurans by the white rot fungus Phanerochaete sordida YK624. Appl Environ Microbiol **1996**, 62 (12), 4323-8.

9. Barr, D. P.; Aust, S. D., MECHANISMS WHITE ROT FUNGI USE TO DEGRADE POLLUTANTS. *Environmental Science & Technology* **1994,** *28* (2), 78A-87A.

10. Buckley, S. M.; Casals, J., Lassa fever, a new virus disease of man from West Africa. 3. Isolation and characterization of the virus. Am J Trop Med Hyg **1970**, 19 (4), 680-91

11. Laine, M. M.; Ahtiainen, J.; Wågman, N.; Öberg, L. G.; Jørgensen, K. S., Fate and Toxicity of Chlorophenols, Polychlorinated Dibenzo-p-dioxins, and Dibenzofurans during Composting of Contaminated Sawmill Soil. Environmental Science & Technology **1997**, 31 (11), 3244-3250.

12. Aeppli, C.; Bastviken, D.; Andersson, P.; Gustafsson, Ö., Chlorine Isotope Effects and Composition of Naturally Produced Organochlorines from Chloroperoxidases, Flavin-Dependent Halogenases, and in Forest Soil. *Environmental Science & Technology* **2013,** *47* (13), 6864-6871.

13. Holmstrand, H.; Gadomski, D.; Mandalakis, M.; Tysklind, M.; Irvine, R.; Andersson, P.; Gustafsson, O., Origin of PCDDs in ball clay assessed with compound-specific chlorine isotope analysis and radiocarbon dating. *Environ Sci Technol* **2006,** *40* (12), 3730-5.

14. Aeppli, C.; Tysklind, M.; Holmstrand, H.; Gustafsson, Ö., Use of Cl and C Isotopic Fractionation to Identify Degradation and Sources of Polychlorinated Phenols: Mechanistic Study and Field Application. Environmental Science & Technology **2013**, 47 (2), 790-797.

15. Lobo, V., et al., Free radicals, antioxidants and functional foods: Impact on human health. Pharmacogn Rev, **2010**. 4(8): p. 118-26.

16. Holt, E.; von der Recke, R.; Vetter, W.; Hawker, D.; Alberts, V.; Kuch, B.; Weber, R.; Gaus, C., Assessing Dioxin Precursors in Pesticide Formulations and Environmental Samples As a Source of Octachlorodibenzo-p-dioxin in Soil and Sediment. Environmental Science & Technology **2008**, 42 (5), 1472-1478.

17. Khachatryan, L.; Dellinger, B., Environmentally Persistent Free Radicals (EPFRs)-2. Are Free Hydroxyl Radicals Generated in Aqueous Solutions? Environmental Science & Technology **2011**, 45 (21), 9232-9239.

18. Balakrishna, S.; Lomnicki, S.; McAvey, K. M.; Cole, R. B.; Dellinger, B.; Cormier, S. A., Environmentally persistent free radicals amplify ultrafine particle mediated cellular oxidative stress and cytotoxicity. *Particle and Fibre Toxicology* **2009,** *6* (1), 1-14.

19. Dellinger, B.; Lomnickia, S.; Khachatryana, L.; Maskosa, Z.; Halla, R.; Adounkpea, J.; McFerrina, C.; Truonga, H., Formation and stabilization of persistent free radicals. Proceedings of the Combustion Institute **2007**, 31, 521 - 528.

20. Vejerano, E.; Lomnicki, S.; Dellinger, B., Lifetime of combustion-generated environmentally persistent free radicals on Zn(II)O and other transition metal oxides. Journal of environmental monitoring: JEM **2012**, 14 (10), 2803-6.

21. Vejerano, E.; Lomnicki, S.; Dellinger, B., Formation and Stabilization of Combustion-Generated Environmentally Persistent Free Radicals on an Fe(III)2O3/Silica Surface. Environmental Science & Technology **2011**, 45 (2), 589-594.

22. Lomnicki, S.; Truong, H.; Vajereno, E.; Dellinger, B., Copper Oxide-Based Model of Persistent Free Radical Formation on Combustion Derived Particulate Matter. Environ Sci Technol **2008**, 42.

23. Khachatryan, L.; Vejerano, E.; Lomnicki, S.; Dellinger, B., Environmentally Persistent Free Radicals (EPFRs). 1. Generation of Reactive Oxygen Species in Aqueous Solutions. Environmental Science & Technology **2011**, 45 (19), 8559-8566.

24. Dugas, T. R.; Lomnicki, S.; Cormier, S. A.; Dellinger, B.; Reams, M., Addressing Emerging Risks: Scientific and Regulatory Challenges Associated with Environmentally Persistent Free Radicals. Int J Environ Res Public Health **2016,** 13 (6).

25. Vejerano, E.; Lomnicki, S. M.; Dellinger, B., Formation and stabilization of combustion-generated, environmentally persistent radicals on Ni(II)O supported on a silica surface. Environ Sci Technol **2012**, 46 (17), 9406-11.

26. Vejerano, E.; Lomnicki, S.; Dellinger, B., Formation and Stabilization of Combustion-Generated Environmentally Persistent Free Radicals on an Fe(III)2O3/Silica Surface. Environmental Science & Technology **2011**, 45 (2), 589-594.

27. Miguel, A. H.; Kirchstetter, T. W.; Harley, R. A.; Hering, S. V., On-Road Emissions of Particulate Polycyclic Aromatic Hydrocarbons and Black Carbon from Gasoline and Diesel Vehicles. *Environmental Science & Technology* **1998,** *32* (4), 450-455.

28. Shah, S. D.; Ogunyoku, T. A.; Miller, J. W.; Cocker, D. R., 3rd, On-road emission rates of PAH and n-alkane compounds from heavy-duty diesel vehicles. Environ Sci Technol **2005**, 39 (14), 5276-84.

29. Lough, G. C.; Schauer, J. J.; Park, J.-S.; Shafer, M. M.; DeMinter, J. T.; Weinstein, J. P., Emissions of Metals Associated with Motor Vehicle Roadways. *Environmental Science & Technology* **2005,** *39* (3), 826-836.

30. Lee, B.-K.; Vu, V. T., Sources, Distribution and Toxicity of Polyaromatic Hydrocarbons (PAHs) in Particulate Matter. 2010.

31. dela Cruz, A. L. N.; Gehling, W.; Lomnicki, S.; Cook, R.; Dellinger, B., Detection of Environmentally Persistent Free Radicals at a Superfund Wood Treating Site. *Environmental Science & Technology* **2011,** *45* (15), 6356-6365.

32. dela Cruz, A. L. N.; Cook, R. L.; Dellinger, B.; Lomnicki, S. M.; Donnelly, K. C.; Kelley, M. A.; Cosgriff, D., Assessment of environmentally persistent free radicals in soils and sediments from three Superfund sites. Environmental Science: Processes & Impacts **2014**, 16 (1), 44-52.

33. Kiruri, L. W.; Dellinger, B.; Lomnicki, S., Tar Balls from Deep Water Horizon Oil Spill: Environmentally Persistent Free Radicals (EPFR) Formation During Crude Weathering. *Environmental Science & Technology* **2013,** *47* (9), 4220-4226.

34. Huang, X.; Zalma, R.; Pezerat, H., Chemical reactivity of the carbon-centered free radicals and ferrous iron in coals: Role of bioavailable Fe2+ in coal workers' pneumoconiosis. *Free Radical Research* **1999,** *30* (6), 439-451.

35. Retcofsky, H. L.; Hough, M. R.; Maguire, M. M.; Clarkson, R. B., Nature of the free radicals in coals, pyrolyzed coals, solvent-refined coal, and coal liquefaction products. *Advances in Chemistry Series* **1981,** (192), 37-58.

36. Tian, L.; Koshland, C. P.; Yano, J.; Yachandra, V. K.; Yu, I. T.; Lee, S. C.; Lucas, D., Carbon-Centered Free Radicals in Particulate Matter Emissions from Wood and Coal Combustion. Energy & fuels : an American Chemical Society journal **2009**, 23 (5), 2523-2526.

37. Sofowote, U. M.; McCarry, B. E.; Marvin, C. H., Source Apportionment of PAH in Hamilton Harbour Suspended Sediments: Comparison of Two Factor Analysis Methods. *Environmental Science & Technology* **2008,** *42* (16), 6007-6014.

38. Xia, H.; Gomez-Eyles, J. L.; Ghosh, U., Effect of Polycyclic Aromatic Hydrocarbon Source Materials and Soil Components on Partitioning and Dermal Uptake. Environ Sci Technol **2016**, 50 (7), 3444-52.

39. Nwosu, U. G.; Cook, R. L., C Nuclear Magnetic Resonance and Electron Paramagnetic Spectroscopic Comparison of Hydrophobic Acid, Transphilic Acid, and Reverse Osmosis May 2012 Isolates of Organic Matter from the Suwannee River. Environ Eng Sci **2015**, 32 (1), 14-22.

40. Jia, H.; Nulaji, G.; Gao, H.; Wang, F.; Zhu, Y.; Wang, C., Formation and Stabilization of Environmentally Persistent Free Radicals Induced by the Interaction of Anthracene with Fe(III)-Modified Clays. Environ Sci Technol **2016**, 50 (12), 6310-9.

41. Li, H.; Pan, B.; Liao, S.; Zhang, D.; Xing, B., Formation of environmentally persistent free radicals as the mechanism for reduced catechol degradation on hematite-silica surface under UV irradiation. Environmental pollution (Barking, Essex : 1987) **2014**, 188, 153-8.

42. Li, H.; Guo, H.; Pan, B.; Liao, S.; Zhang, D.; Yang, X.; Min, C.; Xing, B., Catechol degradation on hematite/silica-gas interface as affected by gas composition and the formation of environmentally persistent free radicals. Scientific reports **2016**, 6, 24494.

43. Patterson, M. C.; Keilbart, N. D.; Kiruri, L. W.; Thibodeaux, C. A.; Lomnicki, S.; Kurtz, R. L.; Poliakoff, E. D.; Dellinger, B.; Sprunger, P. T., EPFR Formation from Phenol adsorption on Al2O3 and TiO2: EPR and EELS studies. Chemical physics **2013**, 422, 277-282.

44. Alderman, S. L.; Farquar, G. R.; Poliakoff, E. D.; Dellinger, B., An Infrared and X-ray Spectroscopic Study of the Reactions of 2-Chlorophenol, 1,2-Dichlorobenzene, and Chlorobenzene with Model CuO/Silica Fly Ash Surfaces. Environmental Science & Technology **2005**, 39 (19), 7396-7401.

45. Patterson, M. C.; Thibodeaux, C. A.; Kizilkaya, O.; Kurtz, R. L.; Poliakoff, E. D.; Sprunger, P. T., Electronic Signatures of a Model Pollutant–Particle System: Chemisorbed Phenol on TiO2(110). Langmuir **2015**, 31 (13), 3869-3875.

46. Thibodeaux, C. A.; Poliakoff, E. D.; Kizilkaya, O.; Patterson, M. C.; DiTusa, M. F.; Kurtz, R. L.; Sprunger, P. T., Probing environmentally significant surface radicals: Crystallographic and temperature dependent adsorption of phenol on ZnO. Chemical physics letters **2015**, 638, 56-60.

47. Yang, J.; Pan, B.; Li, H.; Liao, S.; Zhang, D.; Wu, M.; Xing, B., Degradation of p-Nitrophenol on Biochars: Role of Persistent Free Radicals. *Environmental Science & Technology* **2016,** *50* (2), 694-700.

48. Fang, G.; Gao, J.; Liu, C.; Dionysiou, D. D.; Wang, Y.; Zhou, D., Key Role of Persistent Free Radicals in Hydrogen Peroxide Activation by Biochar: Implications to Organic Contaminant Degradation. *Environmental Science & Technology* **2014,** *48* (3), 1902-1910.

49. Steenhof, M.; Gosens, I.; Strak, M.; Godri Krystal, J.; Hoek, G.; Cassee Flemming, R.; Mudway Ian, S.; Kelly Frank, J.; Harrison Roy, M.; Lebret, E.; Brunekreef, B.; Janssen Nicole, A. H.; Pieters Raymond, H. H., In vitro toxicity of particulate matter (PM) collected at different sites in the Netherlands is associated with PM composition, size fraction and oxidative potential - the RAPTES project. *Particle and Fibre Toxicology* **2011,** (1), 26.

50. Hu, J.; Zhang, H.; Chen, S.; Ying, Q.; Wiedinmyer, C.; Vandenberghe, F.; Kleeman, M. J., Identifying PM2.5 and PM0.1 Sources for Epidemiological Studies in California. *Environmental Science & Technology* **2014,** *48* (9), 4980-4990.

51. Thibodeaux, C. A., The Electronic Structure of Environmentally Persistent Free Radicals Formed on Metal Oxide Surfaces. PhD Dissertation, Louisiana State University and Agricultural and Mechanical College, Baton Rouge, LA, 2015.

52. Kiruri, L. W.; Khachatryan, L.; Dellinger, B.; Lomnicki, S., Effect of Copper Oxide Concentration on the Formation and Persistency of Environmentally Persistent Free Radicals (EPFRs) in Particulates. *Environmental Science & Technology* **2014,** *48* (4), 2212-2217.

53. Choi, J. H.; Kim, J. S.; Kim, Y. C.; Kim, Y. S.; Chung, N. H.; Cho, M. H., Comparative study of PM2.5 - and PM10 - induced oxidative stress in rat lung epithelial cells. *Journal of veterinary science* **2004,** *5* (1), 11-8.

54. Vallius, M. J.; Ruuskanen, J.; Mirme, A.; Pekkanen, J., Concentrations and Estimated Soot Content of PM1, PM2.5, and PM10 in a Subarctic Urban Atmosphere. *Environmental Science & Technology* **2000,** *34* (10), 1919-1925.

55. Reed, J. R.; dela Cruz, A. L.; Lomnicki, S. M.; Backes, W. L., Environmentally persistent free radical-containing particulate matter competitively inhibits metabolism by cytochrome P450 1A2. *Toxicol Appl Pharmacol* **2015,** *289* (2), 223-30.

56. Reed, J. R.; dela Cruz, A. L.; Lomnicki, S. M.; Backes, W. L., Inhibition of cytochrome P450 2B4 by environmentally persistent free radical-containing particulate matter. Biochemical pharmacology **2015**, 95 (2), 126-32.

57. Reed, J. R.; Cawley, G. F.; Ardoin, T. G.; Dellinger, B.; Lomnicki, S. M.; Hasan, F.; Kiruri, L. W.; Backes, W. L., Environmentally persistent free radicals inhibit cytochrome P450 activity in rat liver microsomes. *Toxicol Appl Pharmacol* **2014,** *277* (2), 200-9.

58. Burn, B. R.; Varner, K. J., Environmentally persistent free radicals compromise left ventricular function during ischemia/reperfusion injury. *American journal of physiology. Heart and circulatory physiology* **2015,** *308* (9), H998-h1006.

59. Balakrishna, S.; Saravia, J.; Thevenot, P.; Ahlert, T.; Lominiki, S.; Dellinger, B.; Cormier, S. A., Environmentally persistent free radicals induce airway hyperresponsiveness in neonatal rat lungs. *Part Fibre Toxicol* **2011,** *8*, 11.

60. Kelley, M. A.; Hebert, V. Y.; Thibeaux, T. M.; Orchard, M. A.; Hasan, F.; Cormier, S. A.; Thevenot, P. T.; Lomnicki, S. M.; Varner, K. J.; Dellinger, B.; Latimer, B. M.; Dugas, T. R., Model Combustion-Generated Particulate Matter Containing Persistent Free Radicals Redox Cycle to Produce Reactive Oxygen Species. Chemical Research in Toxicology **2013**, 26 (12), 1862-1871.

61. Lee, G. I.; Saravia, J.; You, D.; Shrestha, B.; Jaligama, S.; Hebert, V. Y.; Dugas, T. R.; Cormier, S. A., Exposure to combustion generated environmentally persistent free radicals enhances severity of influenza virus infection. Part Fibre Toxicol **2014**, 11, 57.

62. Liao, S.; Pan, B.; Li, H.; Zhang, D.; Xing, B., Detecting Free Radicals in Biochars and Determining Their Ability to Inhibit the Germination and Growth of Corn, Wheat and Rice Seedlings. *Environmental Science & Technology* **2014,** *48* (15), 8581-8587.

63. dela Cruz, A. L. N.; Cook, R. L.; Lomnicki, S. M.; Dellinger, B., Effect of Low Temperature Thermal Treatment on Soils Contaminated with Pentachlorophenol and Environmentally Persistent Free Radicals. *Environmental science & technology* **2012,** *46* (11), 5971-5978.

64. Bioavailability of Contaminants in Soils and Sediments: Processes, Tools, and Applications. The National Academies Press: 2003

65. Boyd, S. A.; Mortland, M. M., Dioxin radical formation and polymerization on Cu(II)-smectite. *Nature* **1985,** *316* (6028), 532-535.

66. Boyd, S. A.; Mortland, M. M., Radical formation and polymerization of chlorophenols and chloroanisole on copper(II)-smectite. Environmental Science & Technology **1986**, 20 (10), 1056-1058.

67. Rother, G.; Ilton, E. S.; Wallacher, D.; Hauβ, T.; Schaef, H. T.; Qafoku, O.; Rosso, K. M.; Felmy, A. R.; Krukowski, E. G.; Stack, A. G.; Grimm, N.; Bodnar, R. J., CO2 Sorption to Subsingle Hydration Layer Montmorillonite Clay Studied by Excess Sorption and Neutron Diffraction Measurements. *Environmental Science & Technology* **2013,** *47* (1), 205-211.

68. Meunier, A.; Velde, B.; Griffault, L., The reactivity of bentonites: a review. An application to clay barrier stability for nuclear waste storage. In Clay Minerals, **1998**; Vol. 33, p 187.

69. Odom, I. E., Smectite clay Minerals: Properties and Uses. *Philosophical Transactions of the Royal Society of London A: Mathematical, Physical and Engineering Sciences* **1984,** *311* (1517), 391-409.

70. Kloprogge, J. T.; Komarneni, S.; Amonette, J. E., Synthesis of smectite clay minerals: a critical review. Clays and Clay Minerals **1999**, 47 (5), 529-554.

71. Wilson, M. J., The origin and formation of clay minerals in soils: past, present and future perspectivesd. In *Clay Minerals*, 1999; Vol. 34, p 7.

72. Mortland, M. M.; Shaobai, S.; Boyd, S. M., CLAY-ORGANIC COMPLEXES AS ADSORBENTS FOR PHENOL AND CHLOROPHENOLS I. **1986**.

73. Nebbioso, A.; Piccolo, A., Molecular characterization of dissolved organic matter (DOM): a critical review. *Analytical and Bioanalytical Chemistry* **2013,** *405* (1), 109-124.

74. Ueno, A.; Shimizu, S.; Tamamura, S.; Okuyama, H.; Naganuma, T.; Kaneko, K., Anaerobic decomposition of humic substances by Clostridium from the deep subsurface. *Scientific reports* **2016,** *6*, 18990.

75. Trumbore, S. E., Potential responses of soil organic carbon to global environmental change. *Proceedings of the National Academy of Sciences* **1997,** *94* (16), 8284-8291.

76. Findlay, S.; Sinsabaugh, R. L., Aquatic ecosystems: interactivity of dissolved organic matter. Academic Press: 2003.

77. Sutton, R.; Sposito, G., Molecular Structure in Soil Humic Substances: The New View. *Environmental Science & Technology* **2005,** *39* (23), 9009-9015.

78. Thorn, K. A.; Folan, D. W.; MacCarthy, P. *Characterization of the International Humic Substances Society standard and reference fulvic and humic acids by solution state carbon-13 (13C) and hydrogen-1 (1H) nuclear magnetic resonance spectrometry*; 89-4196; 1989.

79. Davies, G.; Ghabbour, E. A., Humic substances. Structures, Properties and Uses, Cambridge: The Royal Society of Chemistry, 1999. 260 p.

80. Piccolo, A., THE SUPRAMOLECULAR STRUCTURE OF HUMIC SUBSTANCES. *Soil Science* **2001,** *166* (11), 810-832.

81. Zhang, C.; Zhang, D.; Li, Z.; Akatsuka, T.; Yang, S.; Suzuki, D.; Katayama, A., Insoluble Fe-Humic Acid Complex as a Solid-Phase Electron Mediator for Microbial Reductive Dechlorination. Environmental Science & Technology **2014**, 48 (11), 6318-6325. Conte, P.; Piccolo, A., Conformational Arrangement of Dissolved Humic Substances. Influence of Solution Composition on Association of Humic Molecules. *Environmental Science & Technology* **1999,** *33* (10), 1682-1690.

82. Scott, D. T.; McKnight, D. M.; Blunt-Harris, E. L.; Kolesar, S. E.; Lovley, D. R., Quinone Moieties Act as Electron Acceptors in the Reduction of Humic Substances by Humics-Reducing Microorganisms. *Environmental Science & Technology* **1998,** *32* (19), 2984-2989.

83. Perminova, I. V.; Grechishcheva, N. Y.; Kovalevskii, D. V.; Kudryavtsev, A. V.; Petrosyan, V. S.; Matorin, D. N., Quantification and Prediction of the Detoxifying Properties of Humic Substances Related to Their Chemical Binding to Polycyclic Aromatic Hydrocarbons. *Environmental Science & Technology* **2001,** *35* (19), 3841-3848.

84. Fang, G.; Gao, J.; Dionysiou, D. D.; Liu, C.; Zhou, D., Activation of Persulfate by Quinones: Free Radical Reactions and Implication for the Degradation of PCBs. Environmental Science & Technology **2013**, 47 (9), 4605-4611.

85. Cao, F.; Liu, T. X.; Wu, C. Y.; Li, F. B.; Li, X. M.; Yu, H. Y.; Tong, H.; Chen, M. J., Enhanced Biotransformation of DDTs by an Iron- and Humic-Reducing Bacteria Aeromonas hydrophila HS01 upon Addition of Goethite and Anthraquinone-2,6-Disulphonic Disodium Salt (AQDS). *Journal of Agricultural and Food Chemistry* **2012,** *60* (45), 11238-11244.

86. Aeschbacher, M.; Graf, C.; Schwarzenbach, R. P.; Sander, M., Antioxidant Properties of Humic Substances. Environmental Science & Technology 2012, 46 (9), 4916-4925.

87. Lovley, D. R.; Coates, J. D.; Blunt-Harris, E. L.; Phillips, E. J. P.; Woodward, J. C., Humic substances as electron acceptors for microbial respiration. *Nature* **1996,** *382* (6590), 445-448.

88. Zhang, H.; Weber, E. J., Elucidating the Role of Electron Shuttles in Reductive Transformations in Anaerobic Sediments. *Environmental Science & Technology* **2009,** *43* (4), 1042-1048.

89. Cervantes, F. J.; de Bok, F. A.; Duong-Dac, T.; Stams, A. J.; Lettinga, G.; Field, J. A., Reduction of humic substances by halorespiring, sulphate-reducing and methanogenic microorganisms. Environ Microbiol **2002**, 4 (1), 51-7

90. Zhang, C.; Katayama, A., Humin as an Electron Mediator for Microbial Reductive Dehalogenation. *Environmental Science & Technology* **2012,** *46* (12), 6575-6583.

91. Magar, V. S.; Stensel, H. D.; Puhakka, J. A.; Ferguson, J. F., Sequential Anaerobic Dechlorination of Pentachlorophenol: Competitive Inhibition Effects and a Kinetic Model. *Environmental Science & Technology* **1999,** *33* (10), 1604-1611.

92. Kuipers, B.; Cullen, W. R.; Mohn, W. W., Reductive Dechlorination of Nonachlorobiphenyls and Selected Octachlorobiphenyls by Microbial Enrichment Cultures. *Environmental Science & Technology* **1999,** *33* (20), 3579-3585.

93. Williams, W. A., Microbial Reductive Dechlorination of Trichlorobiphenyls in Anaerobic Sediment Slurries. Environmental Science & Technology **1994**, 28 (4), 630-635.

94. Wukasch, R.F.; Proceedings of the 48th Industrial Waste Conference, Purdue University, May 1993.

95. Cervantes, F. J.; Dijksma, W.; Duong-Dac, T.; Ivanova, A.; Lettinga, G.; Field, J. A., Anaerobic Mineralization of Toluene by Enriched Sediments with Quinones and Humus as Terminal Electron Acceptors. *Applied and Environmental Microbiology* **2001,** *67* (10), 4471-4478.

96. Gao, D.; Du, L.; Yang, J.; Wu, W. M.; Liang, H., A critical review of the application of white rot fungus to environmental pollution control. Critical reviews in biotechnology 2010, 30 (1), 70-7.

97. Dashtban, M.; Schraft, H.; Syed, T. A.; Qin, W., Fungal biodegradation and enzymatic modification of lignin. *International Journal of Biochemistry and Molecular Biology* **2010,** *1* (1), 36-50.

98. Barr, D. P.; Aust, S. D., Mechanisms white rot fungi use to degrade pollutants. *Environmental Science & Technology* **1994,** *28* (2), 78A-87A.

99. ukushima, M.; Shigematsu, S.; Nagao, S., Oxidative degradation of 2,4,6-trichlorophenol and pentachlorophenol in contaminated soil suspensions using a supramolecular catalyst of 5,10,15,20-tetrakis (p-hydroxyphenyl)porphine-iron(III) bound to humic acid via formaldehyde polycondensation. *Journal of Environmental Science and Health, Part A* **2009,** *44* (11), 1088-1097.

100. Corvaja, C., Introduction to Electron Paramagnetic Resonance. In *Electron Paramagnetic Resonance*, John Wiley & Sons, Inc.: 2008; pp 1-36.

101. dela Cruz, A. L. N. Detection and Characterization of Environmentally Persistent Free Radicals (EPFRs) in Soils and Sediments from Superfund Sites. Faculty of the Louisiana State University and Agricultural and Mechanical College in partial fulfillment of the requirements for the degree of Doctor of Philosophy in The Department of Chemistry by dela Cruz, Albert Leo N., 2015.

102. Duin, E., Electron Paramagnetic Resonance Theory. https://www.auburn.edu/~duinedu/epr/1_theory.pdf (accesed July 20, 2016)

103. Höfer, P., Basic Experimental Methods in Continuous Wave Electron Paramagnetic Resonance. In *Electron Paramagnetic Resonance*, John Wiley & Sons, Inc.: 2008; pp 37-82.104. Newville, M., Fundamentals of XAFS. Reviews in Mineralogy and Geochemistry **2014**, 78 (1), 33-74.

104. Newville, M., Fundamentals of XAFS. Reviews in Mineralogy and Geochemistry **2014**, 78 (1), 33-74.

105. Li, Z.; Dervishi, E.; Saini, V.; Zheng, L.; Yan, W.; Wei, S.; Xu, Y.; Biris, A. S., X-ray Absorption Fine Structure Techniques. *Particulate Science and Technology* **2010,** *28* (2), 95-131.

106 Vlaic, G.; Olivi, L.; EXAFS Spectroscopy: a Brief Introduction. CROATICA CHEMICA ACTA CCACAA **2004**, 77 (3) 427-433

107. Gaur, A.; Shrivastava, B. D.; Nigam, H., X-Ray Absorption Fine Structure (XAFS) Spectroscopy–A Review. *Proceedings of the Indian National Science Academy* **2013,** *79* (Part B), 921-966.

108. Koningsberger, D. C.; Prins, R., X-ray absorption: Principles, applications, techniques of EXAFS, SEXAFS and XANES. 1987; p Medium: X; Size: Pages: 624.

109. Bechthold, P.S; X-ray Absorption Spectroscopy. Institut f¨ur Festkorperforschung

110. Forschungszentrum J¨ulich GmbH. http://www.fzjuelich.de/SharedDocs/Downloads/PGI/PGI-6/EN/E9_XAS_Bechthold07_a.pdf?__blob=publicationFilee

111. XANES: Theory http://chem.libretexts.org/Core/Physical_Chemistry/Spectroscopy/X-ray_Spectroscopy/XANES%3A_Theory (accessed 19 July 2016)

112. Speakman, S.A.; Basics of X-Ray Powder Diffraction Training to Become an Independent User of the X-Ray SEF at the Center for Materials Science and Engineering at MIT. http://prism.mit.edu/xray/oldsite/Basics%20of%20X-Ray%20Powder%20Diffraction.pdf. (accessed, 23 July, 2016)

113. Dutrow, B.L.; Christine M. Clark., X-ray Powder Diffraction (XRD) http://serc.carleton.edu/research_education/geochemsheets/techniques/XRD.html. (accessed, 23 July, 2016)

114. van der Heide, P., Introduction. In *X-Ray Photoelectron Spectroscopy*, John Wiley & Sons, Inc.: 2011; pp 1-12.

115. Bumbrah, G. S.; Sharma, R. M., Raman spectroscopy – Basic principle, instrumentation and selected applications for the characterization of drugs of abuse. *Egyptian Journal of Forensic Sciences*.

116. Griffiths, P. R.; de Haseth, J. A., Introduction to Vibrational Spectroscopy. In *Fourier Transform Infrared Spectrometry*, John Wiley & Sons, Inc.: 2006; pp 1-18.

CHAPTER 2
FORMATION OF ENVIRONMENTALLY PERSISTENT FREE RADICAL (EPFR) IN IRON(III) CATION-EXCHANGED SMECTITE CLAY*

2.1 Introduction

Clay minerals are important components of soils and act as a potential reservoir of metals and toxic organic pollutants.[1,2] Sorption of polycyclic aromatic hydrocarbons (PAHs) and chlorinated aromatic hydrocarbons to clay minerals has been used to remediate organic pollutants;[2,3] however, the possible formation of undesirable dioxins render this practice detrimental to the environment.[4,5] Organochlorinated contaminants, formed as products and by-products of such remediation processes, are not only toxic in their own right, but the intermediate reactions leading to their formation are also of major concern to environmental safety.[6,7] In particular, these intermediate processes result in the formation of surface-stabilized environmentally persistent free radicals (EPFRs).[2,8,9] Traditionally, EPFRs have been misidentified as molecular pollutants in soils and particulate matter.10 The stability of an EPFR is associated with the ability of mostly aromatic organic contaminants to undergo chemisorption and form complexes with a redox (transition metal) centre, with the EPFR being formed through a single electron transfer.[9,11] In addition to EPFRs playing a role in the transformation of pollutants, radical processes involving EPFRs and organic compounds impact the formation of humic substances, and hence, carbon sequestration.[12] It has also been found that EPFR-containing particles can generate reactive oxygen species (ROS) which, in turn, may induce oxidative stress. This can occur in three steps: 1) EPFRs reduce molecular oxygen to superoxide, 2) the superoxide, through disproportion, forms hydrogen peroxide; 3) the reduced metal species formed

---

* This chapter previously appeared as Ugwumsinachi G. Nwosu, Amitava Roy, Albert Leo N. dela Cruz, Barry Dellinger and Robert Cook, “Formation of environmentally persistent free radical (EPFR) in iron(III) cation-exchanged smectite clay. ***Environ. Sci.: Processes Impacts****, 2016,**18**, 42-50.* Reproduced by permission of The Royal Society of Chemistry

via EPFR formation participate in Fenton chemistry which, in turn, generates ROS.[7] EPFRs have recently been found at elevated concentrations in numerous soil/sediment samples from a range of pentachlorophenol-polluted Superfund sites.[13,14] A detailed top-down study found that the EPFRs were almost solely associated with the clay/humic soil fraction.[14]

Other studies have shown that: 1) dioxin radicals can form in the presence of Cu(II) smectite montmorillonite clay mineral,[15] 2) pentachlorophenol (PCP) radical cations are generated in Fe(III)-montmorillonite clay,[2] and 3) transition metal centres in clay minerals play a key role in the formation of the intermediate radicals in the formation of dioxins.[2,5] However, these studies were carried out at conditions not relevant to the EPFR-contaminated Superfund sites as organic solvents were used and/or high temperature and reflux conditions were applied. Our previous investigations also demonstrated the catalytic role of transition metal centres, Cu(II) and Fe(III) supported on silica particles metal surfaces, in the formation of intermediate EPFRs.[9,11,16] While important, these studies did not address the type of conditions present at the Superfund sites in which soil EFPRs have been found.

With the remediation of EPFR-contaminated soil systems being the ultimate goal of this research, it is important to first gain a fundamental molecular level understanding of how EPFRs are formed in soils at environmental conditions. The soil matrix, however, due to its complexity, poses major technical challenges for modern molecular level analytical methods, thus a bottom-up approach is appropriate, in which a soil is broken down into its biological, organic, and inorganic components and the role of each of these components is determined individually and in combination with each other. In this effort to systematically reconstruct the geosorbant (here soil) and understand at a molecular level the mechanism of EPFR formation in contaminated soil systems, we report on the use of Fe(III) exchanged montmorillonite clay, designed to model the clay component of a real soil in which EPFR have been shown to concentrate.[14] Iron was chosen as the redox centre of interest as it was found to be the most abundant transition metal in the

contaminated Superfund sites.[13] Phenol was utilized as a simplified model of organic contaminants as it is a well-known soil contaminant itself and can be easily produced by microbial reductive dechlorination of chlorophenol and polychlorophenols in contaminated soils,[17] and is considered as priority pollutant by U.S. EPA.[18] The following analytical techniques were combined in this study: 1) Fourier transformed infrared (FTIR) spectroscopy and X-ray diffraction (XRD) to demonstrate the sorption of the model pollutant, phenol, 2) X-ray photoelectron spectroscopy (XPS) to study the changes in chemical environment of Fe species, the redox centre of interest in this study, and other elements in the clay, 3) electron paramagnetic resonance (EPR) spectroscopy for radical detection and quantification, and 4) X-ray absorption near edge structure (XANES) spectroscopy to investigate the redox change of the Fe centres. This non-biological approach offers insights into the mechanism of the EPFR formation in soils and allows one to measure EPFR lifetimes under environmentally relevant conditions.

2.2 Experimental

2.2.1 Materials

Smectite clay (CaM), STx-1b (Montmorillonite) with a cation exchange capacity (CEC) of 84.4 meq/100 g and a surface area of 83.79 ± 0.22 m^2/g, was purchased from the Source Clay Repository (Purdue University, West Lafayette, IN). Iron(III) chloride, $FeCl_3$, was obtained from Sigma Aldrich, analytical grade phenol (loose crystal) was obtained from Mallinckrodt, and trace metal grade nitric acid, HNO_3, was obtained from Fisher Scientific.

Preparation of Fe-Exchanged Clay Samples: Cation-exchange was performed following well established protocols.[2,19] Briefly, a 4 g sample of clay was placed in a 250 mL beaker and mixed with 25 mL of 0.012 M $FeCl_3$ solution for proper hydration and dispersion. The resulting suspension was then diluted up to 100 mL with additional $FeCl_3$ solution and stirred for 48 h. The Fe(III) clay suspension was transferred to a dialysis tube and immersed into 18 MΩ•cm water.

The water was replaced every 12 h in order to wash out free chloride ions associated with $FeCl_3$ until a negative $AgNO_3$ test. The resulting clay material (Fe(III)CaM) was filtered using a suction vacuum filtration set-up and allowed to dry for 48 h at 60 °C. The sample was then crushed and homogenized using mortar and pestle and utilized for subsequent experiments.

2.2.2 ICP-OES-Analysis

The metal content of the clay samples was determined by inductively coupled plasma optical emission spectroscopy (ICP-OES) using a Varian Vista-MPX CCD Simultaneous ICP-OES. For this analysis, a 0.2 g sample of clay was digested in 5 mL of concentrated HNO_3 for approximately 8 h, cooled, and the resultant digestate was diluted to a total volume of 50 mL with 18 MΩ•cm water and analyzed.

2.2.3 Gas Phase Phenol Dosing of Clay Samples

Clay samples were dosed with phenol following a previously reported method.14 Briefly, 50 mg of samples, contained in a 4 mm glass detachable bulb-shaped pyrex reactor with a protruding Suprasil® quartz EPR tube, were exposed to phenol at room temperature in vapor phase by dosing in a custom-made vacuum exposure system. Sample dosing commenced after the attainment of a ~10^{-2} mm Hg vacuum to allow the removal of interfering organic contaminants. Unreacted physisorbed phenol was evacuated by applying a vacuum of 10^{-2} mmHg. This procedure resulted in the production of four different samples, namely: pristine montmorillonite (PureCaM), phenol-exposed pristine montmorillonite (DosedCaM), Fe(III)-cation-exchanged montmorillonite (Fe(III)CaM), and phenol-exposed Fe(III)-cation-exchanged montmorillonite (DosedFe(III)CaM). All phenol-exposed samples were protected from light throughout the study.

2.2.4 Sample Exposures

Three different sample exposures were used in this study. First, the sample was simply left under vacuum. Secondly, the sample was exposed to ambient air. The third experiment

involved exposing the sample to humid air inside a Model 3940 Series Forma Environmental Chamber with the relative humidity and temperature set at 75% and 25 °C, respectively.

2.2.5 Electron Paramagnetic Resonance (EPR) Spectroscopic Analysis

EPR measurements were conducted using a dual cavity Bruker EMX 10/2.7 EPR spectrometer with a X-band microwave frequency of 9.78 GHz at room temperature and spectra were recorded under the following instrumental conditions: sweep width of 150 G and 6000 G, attenuator of 20 dB, power of 2.03 mW, modulation frequency of 100 kHz, modulation amplitude of 4 G, sweep time of 41.94 s, time constant of 1.28 ms, conversion time of 20.48 ms, static field of 3460.059 G, centre field of 3488.00 G, receiver gain of 1.0×10^4, and a total of 5 scans. The instrument was calibrated with a 2,2-diphenyl-1-picrylhydrazyl (DPPH) standard.[11,20]

2.2.6 FTIR Analysis

Infrared spectra were collected on a Bruker Alpha or Tensor 27 Fourier transform infrared (FT-IR) spectrometer. Powdered clay samples were dispersed directly onto a Pike Miracle ATR cell sample plate as to cover the Pt-diamond crystal. Spectra acquisition was recorded within the frequency ranges of 400 cm^{-1} to 4000 cm^{-1} at a minimum resolution of 4 cm^{-1} by averaging 16 scans.

2.2.7 X-Ray Analysis

X-ray absorption near edge structure (XANES) spectra were obtained at the wavelength shifter Double Crystal Monochromator (WDCM) beam line of the J. Bennett Johnston, Sr., Center for Advanced Microstructures and Devices (CAMD) located on the 7 T wavelength shifter. Germanium 220 crystals were used in a Lemonnier-type monochomator with design modifications made at Bonn University, Germany. Iron metal foil was used for monochromator calibration at 7112 eV. Samples were prepared by spreading a few μm thick clay powders onto a Kapton™ tape. The measurements in fluorescence mode were made with a 13-element germanium solid state detector (Canberra Industries, Meridian, Connecticut, USA). Multiple scans (2-5 scans each)

were performed at room temperature and were averaged using the Demeter software (Ravel and Newville, 2005). Spectra of reagent grade standards of Fe_2O_3, FeO and Fe_3O_4 were also collected for least squares fitting. The X-ray diffraction (XRD) data were collected on a PANalytical Empyrean diffractometer using the Cu Kα radiation of λ = 1.5419 Å within 2Θ scan range of 5 – 90°. The X-ray photoelectron spectroscopy (XPS) measurements were performed using the Kratos AXIS 165 XPS/AES system equipped with a monochromatic Al-Kα source and a charge neutralizer, at pass energy of 80 eV for high resolution scans. The step size of 0.05 eV was applied and shifts in binding energies were corrected with a 284.6 carbon 1s peak as internal reference.

2.3 Results and discussion

Our previous research on particulate matter ($PM_{2.5}$) proposed that EPFR formation involves an initial physisorption of an organic pollutant, followed by chemisorption and a concurrent single electron transfer process to an active redox (transition metal) centre.[9,11,16] In this study we wish to (i) determine if the same processes could take place on a very simple soil surrogate system, namely Fe(III)CaM, under ambient environmental conditions, (ii) monitor the sorption of the organic pollutant (in this case phenol), the formation of the EPFRs, and the reduction of the transition metal centre, (iii) quantify the amount of EFPRs formed and metal centres reduced, as well as (iv) determine the influence of environmental conditions on EPFR stability.

2.3.1 PureCaM and Fe(III)CaM Characterization

As shown in Figure 2.1, a reduced basal spacing in the XRD pattern from 1.53 nm for the PureCaM sample to 1.31 nm for the Fe(III)CaM sample indicates the replacement of interlayer Ca(II) cations by Fe(III).[21] An XPS survey spectra (Figure 2.1, B) show intense oxygen peaks associated to the major silicate Si (2s, 2p) and aluminate Al (2s, 2p) metal framework that forms the tetrahedral and octahedral layers in calcium montmorillonite clay.[22] The Fe 2p region in the

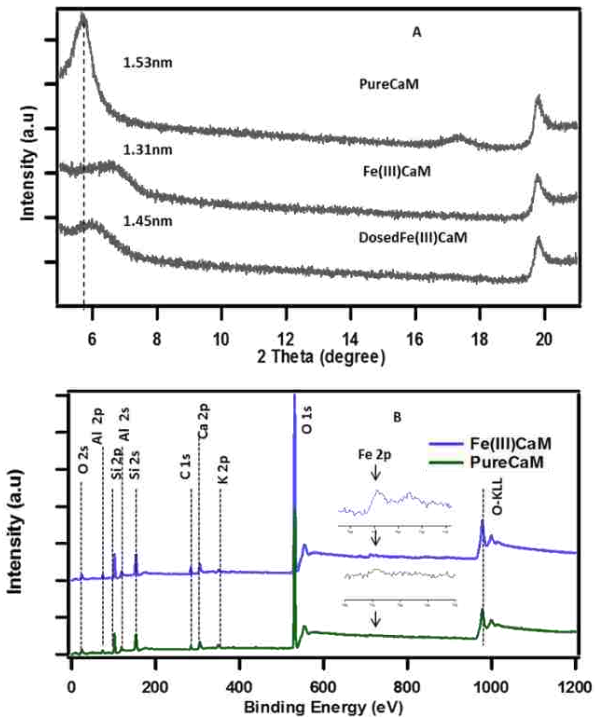

Figure 2.1 XRD pattern spectra of A) PureCaM, Fe(III)CaM and DosedFe(III)CaM, B) XPS survey spectra of (Fe(III)CaM) and PureCaM. Experiment performed with 1.8 x 104 mg/kg Fe loading.

survey after cation exchange appears to intensify after treatment with Fe(III) (inset spectra). This is an indication of Fe(III) exchange with the Al(III) interstitial lattice sites of the octahedral aluminate clay layers.[23] Similarly, the intercalation and the replacement of calcium and other interlayer cations with by Fe(III) species are also known to be responsible for such changes.[24] Overall, these data strongly suggest that the Fe(III) introduced in the cation exchange procedure is interstitial in nature; however, the possibility of FeOOH coating a small percentage of the clay surface cannot be completely disregarded.

2.3.2 Phenol Sorption

The sorption of phenol to the clay samples following the dosing procedure was confirmed using FTIR spectroscopy by the presence of phenol vibrational frequencies in the phenol-dosed samples.

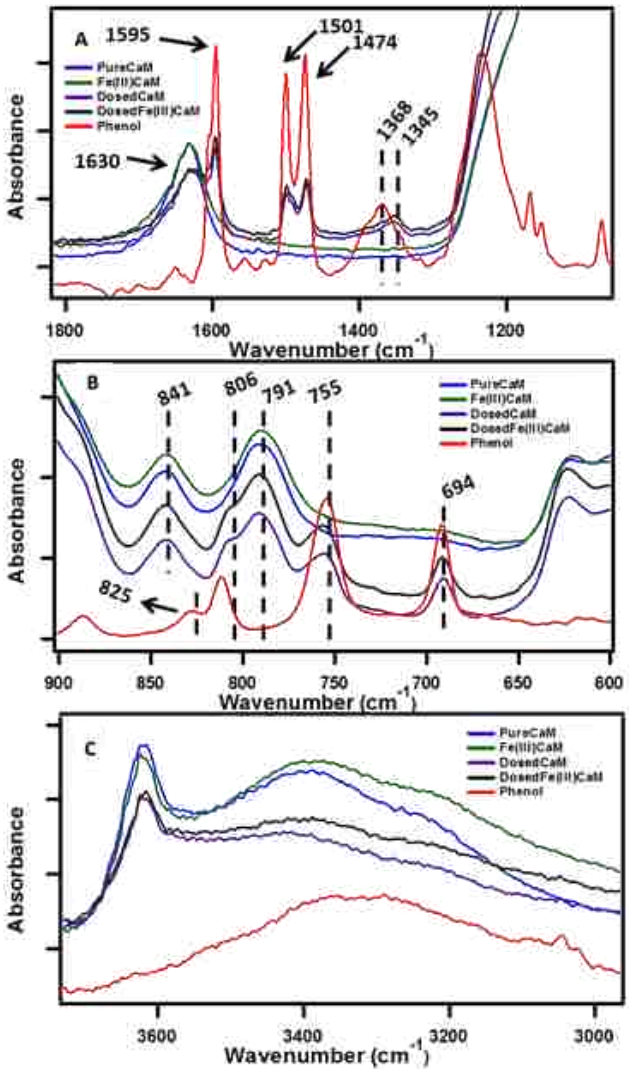

Figure 2.2 FTIR spectra showing sorption of phenol at different wavenumbers, ranging from 4000 cm–1 to 600 cm–1, with Fe loading of 1.8 x 104 mg/kg. (Expanded view)

The spectral regions presented in Figure 2.2, A and Figure 2.2, B are highly diagnostic of phenol sorption. In Figure 2.2, A sorption of phenol to the DosedCaM and DosedFe(III)CaM samples is shown via the absorption bands at 1595 cm^{-1}, 1501 cm^{-1}, 1474 cm^{-1}, and 1345 cm^{-1}. The double peaks at 1501 cm^{-1} and 1474 cm^{-1}, along with the peak at 1595 cm^{-1}, are all attributable to the carbon-carbon stretching vibration of phenol, while the bands at 1368 cm–1 and 1345 cm^{-1} for pure phenol, DosedCaM, and DosedFe(III)CaM are assignable to the in-plane -OH bending.[25-26] Other bands seen in Figure 2.2, B that are associated with the adsorption of

phenol appear in the lower frequency region at 755 cm^{-1} and 694 cm^{-1} and correspond to the out-of-plane C–H bending.[26] Similarly, a shoulder peak at 806 cm^{-1}, typical of the aromatic C–H bending region, indicates adsorption of phenol to the metal cation.[26-27] The sorption of phenol is further supported by the increase in the basal spacing observed from the XRD patterns (cf. Figure 2.1) between the Fe(III)CaM and DosedFe(III)CaM samples from 1.31 nm to 1.45 nm, respectively. Spectra shown in Figure 2.2, C reveal a broad and rather featureless envelope of peaks between 3200 cm^{-1} and 3583 cm^{-1} for all clay samples and pure phenol, which can be assigned to a number of different hydroxyl group types. The sharp peak at 3628 cm^{-1} for the clay samples can be assigned to the -OH groups associated with Si(IV) and Al(III) or Fe(III) in the tetrahedral and octahedral sheets.[28-30] Figure 2.2, C further shows the corresponding -OH bending absorption bands between 841 cm^{-1} and 791 cm^{-1} for octahedral cations (Si(IV), Al(III), and Fe(III)), mainly Al-OH-Fe and Al-OH-Mg.[24,28] In addition, H–O–H stretching vibrations from inherent and adsorbed interfacial water molecules and weak hydrogen bonding within the Si–O surfaces have also been known to show strong absorption bands within these regions.[28-31]

2.3.3 EPFR Formation and Analysis

The presence of organic radicals, EPFRs, were detected by EPR shortly after the dosing of the Fe(III)CaM with phenol.

EPR Analysis: The EPR spectrum presented in Figure 2.3, A provides clear evidence of EPFR formation when Fe(III)CaM is dosed with phenol. The EPFR signal in Figure 2.3, A is a nearly symmetrical peak with the magnetic field centred at 3460 G, an average g-factor of 2.0034, and peak-to-peak line width (ΔHp-p) of ~6.1; these values correspond to an oxygen-centred phenoxyl-type organic radical.[11,16] The EPR spectrum at 6000 G, presented in Figure 2.3, B provides further insight into the chemical environment of the unpaired electron. A broad peak at g-factor = 2.03 and a somewhat narrower peak towards the lower magnetic field at g-factor = 4.21

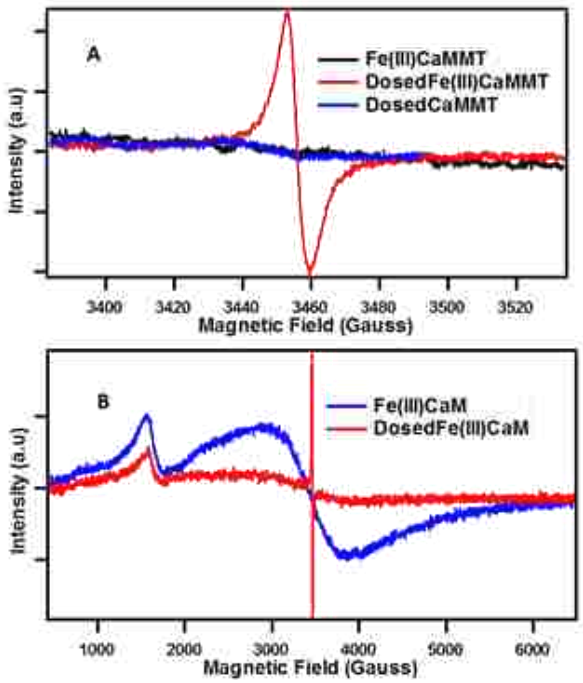

Figure 2.3 EPFR generation: EPR spectra for Fe(III)CaM with Fe loading of 1.8 x 104 mg/kg and DosedFe(III)CaM at A) 150 G and B) 6000 G spectral width.

are attributed to low and high spin octahedral and tetrahedral paramagnetic Fe(III) ion sites, respectively.[32-33] The peak at g-factor = 2.03 is superimposed by the peak associated with the organic radical formation after phenol exposure.

The example of Fe(III) illustrates the importance of transition metal centres and their exact speciation. It is further supported by the fact that the DosedCaM system does not form EPFRs. While PureCaM does inherently possess Fe(III) centres, they are located at the enclosed inner lattice sites in the octahedral clay layer. This hinders phenol-Fe(III) interactions, preventing EPFR formation, as indicated by no radicals being detected in the DosedCaM system. This demonstrates that intercalated Fe(III) species are mainly responsible for the formation of the organic radicals through a single-electron oxidation of phenol.[11,16] Furthermore, a change in colour from brownish yellow for Fe(III)CaM to greyish green for the DosedFe(III)CaM also confirms the

occurrence of a redox process; this has been previously observed for the Fe(III) reduction to Fe(II) in montmorillonite clays.[34]

2.3.4 Role of Redox Centres in EPFR Formation

The role of the Fe(III) redox centre was further studied by a combination of high resolution XPS and XANES. High Resolution XPS: The high resolution XPS scans of the Fe 2p region in the survey scan in Figure 2.1, B can be employed to further explain the changes in the chemical state of Fe(III) after cation exchange and subsequent radical formation. Figure 2.4, A-C highlights the Fe 2p3/2 and Fe 2p1/2 binding energy peaks of iron. The peaks at 711.6 and 725.0 eV for the PureCaM are assignable to the structural Fe, confirming that Fe(II) and Fe(III) are embedded in the montmorillonite lattice.[35] After cation exchange with Fe(III), the Fe 2p1/2 peak remains nearly unchanged (724.8 eV for Fe(III)CaM and 724.7 eV for DosedFe(III)CaM). On the other hand, the Fe 2p3/2, which is considered to be the main Fe 2p peak, partitions into two sub-peaks positioned at 710.7 eV and 713.0 eV, that may be attributed to structural and intercalated Fe species, respectively.[35] Upon dosing with phenol, the position of the peak ascribed to the intercalated Fe(III) shows a 0.6 eV shift from 713.0 eV to 712.4 eV. This suggests a change in chemical state of Fe(III), consistent with a reduction of Fe(III) to Fe(II).

XANES Studies: In order to further confirm the mechanism by which EPFRs are formed, Fe(III)CaM and DosedFe(III)CaM samples were analyzed by XANES, with the focus on the Fe redox centre. The data in Figure 2.5 show, based on the K-edge energy shift, the partial reduction of Fe(III) to Fe(II) (100% Fe(III) for Fe(III)CaM and 77%Fe(III) and 23%Fe(II) for DosedFe(III)CaM) after phenol dosing. These data, when synthesized with the FT-IR and EPR data discussed above, lead to the mechanism proposed in Scheme 1, whereby the initial phenol adsorption in the Fe(III)-exchanged clay results in the abstraction of a hydrogen atom from phenol and a single electron transfer from the phenol molecule to the Fe(III) centre, leading to the EPFR formation.

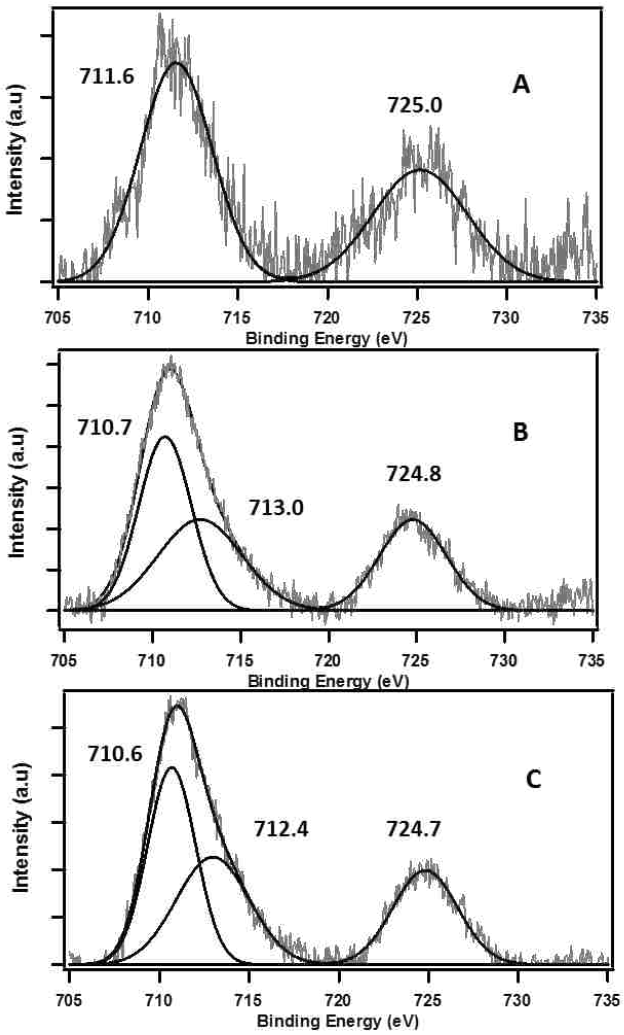

Figure 2.4 Deconvoluted high resolution XPS spectra of Fe 2p binding energy peak regions for A) PureCaM, B) Fe(III)CaM, and C) DosedFe(III)CaM. Experiment performed with 1.8 x 10^4 mg/kg Fe loading.

This mechanism is consistent with the EPFR formation mechanism proposed for $PM_{2.5}$.[36-37] The XANES data presented in Figure 2.5 reveal additional mechanistic information beyond the oxidation state of Fe redox centres in the formation of EPFRs. Least squares fitting of the spectra demonstrates a decrease in the main-edge intensity of the spectra for the probed post phenol-dosed sample (Fit_Fe(II&III)) compared to the iron standards (Fe(II) and Fe (III)).

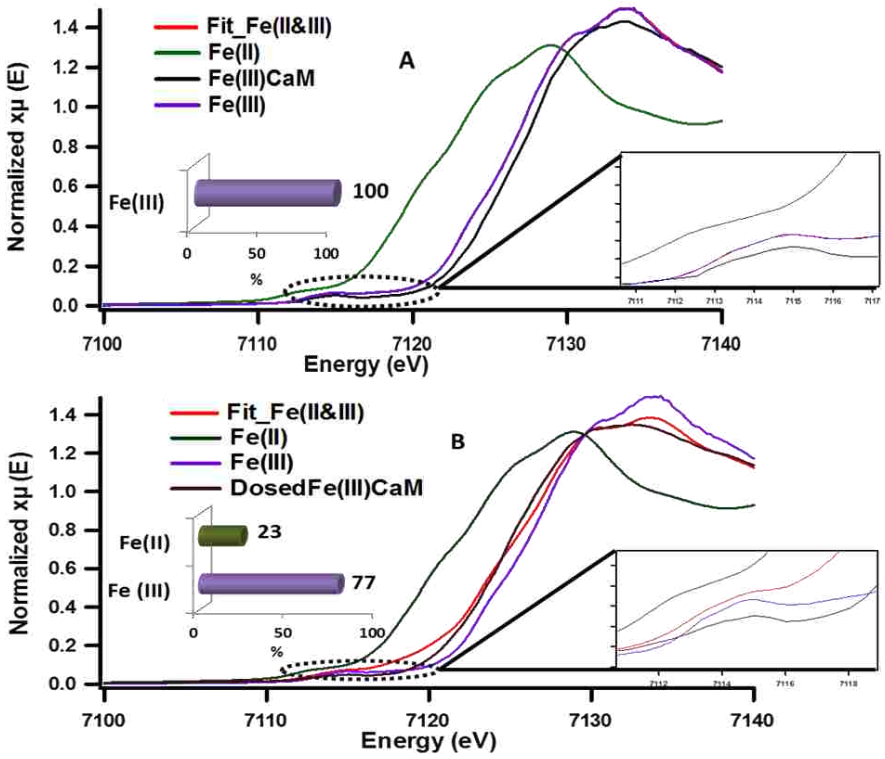

Figure 2.5 XANES spectra showing the changes in redox state of iron pre- and post-phenol dosing A) Iron standards (Fe(II) and Fe(III)), Fe(III)CaM, and the Fe(III)CaM Fit, B) Iron standards (Fe(II) and Fe(III)), Fe(III)CaM dosed with phenol, and the Fe(III)CaM dosed with phenol Fit. Experiment performed with 1.8 x 104 mg/kg Fe loading.

This suggests an alteration typical of the octahedral or near octahedral coordination environment of Fe in the post phenol-dosed sample.[38-42] A significant edge shift from 7125.5 eV to 7124.0 eV and 7122 eV to 7120 eV at the centre and the base of the K-edge towards the Fe(II) energy for the phenol-dosed sample (Fit_Fe(II&III)), when compared to the Fe(III) standard, provides further strong evidence of the change in oxidation state of iron from Fe(III) to Fe(II).[38-41]

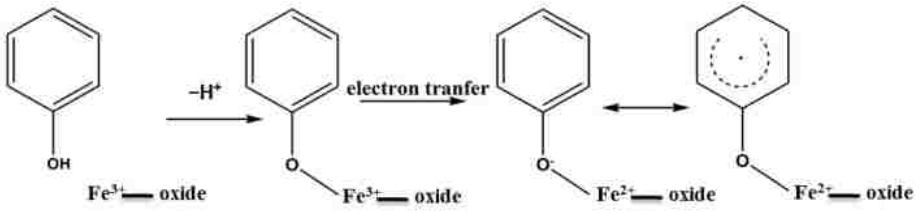

Scheme 2.1**.** General mechanism for EPFR formation with phenol on Fe(III)CaM.

The expanded insets of the Figure 2.5, A-B show the emergence of an intense and broad peak in the post phenol-dosed sample spectrum DosedFe(III)CaM and in its spectral fit (Fit_Fe(II&III)). It results in a slight deviation from the pre-edge centroid position. This type of shift has been previously associated with a change in oxidation state of Fe(III).[38-42] However, further explanation can be ascribed to the distortion in the coordinating ligands after chemisorption, with the subsequent replacement of ligating species, such as -OH and H_2O, following a single electron transfer from phenol molecules.[38-39,42] This possible distortion in the 1s→3d pre-edge transitions during electron transfer (Fe(III) → Fe(II)) in the octahedral coordination environment, may explain the intensity gain observed for Fit_Fe(II&III) as a result of their quadrupolar character.[38,40-41] This finding corroborates the initial EPR observations. Furthermore, the Fe(III)CaM and Fit_Fe(II&III) spectra appear to align with the standard Fe(III) spectrum, both in the 1s→4s (main-edge) and in the 1s→3d (pre-edge) transition regions, demonstrating a 100% Fe(III) composition in the pre-phenol-dosed sample (Fe(III)CaM) with no distortion in the coordination environment. In summary, the XANES data support the proposal that phenol is chemisorbed to the Fe redox centre and, via electron donation, reduces Fe(III) to Fe(II), and reinforce the EPFR formation mechanism presented in Scheme 2.1.

Radical Density: The combination of ICP-OES and XANES results allows for an estimation of the Fe(II) concentration (in atoms per gram), while EPR analysis allows for the determination of spins (EPFRs) per gram. Thus, by linking the data from these three techniques, one can obtain an estimate of EPFR density per Fe(II) atom (in spins /atom). Remarkably, it was found that there were 1.5×10^{-2} spins/Fe(II) atom. Stated differently, only 3 EPFRs are produced per 200 Fe(III) atoms reduced (or 200 electrons transferred). While steric effects between metal atoms have been reported to be the biggest factor affecting the accessibility of phenol to the transition metal surface,[11] steric effects due to phenol orientation on the metal surface are bound to affect the lifetime of the radical as well, increasing the chances of radical recombination and decay. Thus,

the low ratio of EPFRs to Fe(II) redox centres reported here can be explained by a large number of the initially formed radicals combining with other radicals in the areas of high radical density— in short, phenoxyl radical polymerization— leading to the relatively rare event of long-lived EPFR formation in the areas of low radical density.

2.3.5 Influence of Fe(III) Loading in Fe(III)CaM on EPFR Concentration

To further investigate the relationship between Fe concentration and EPFR formation, Fe(III)CaM samples with different Fe loadings were prepared from Fe solutions of varying concentrations, ranging from 0.0021 M to 0.025 M, following previously stated procedures.[19] Upon exposure to phenol, an increase in the Fe(III) loading concentration from ~8 x 10^3 mg/kg to ~2.4 x 10^4 mg/kg caused a non-linear increase in the EPFR concentration (cf. Figure 2.6, A). EPFR concentrations obtained when the Fe loading concentrations were between ~ 1.8 x 10^4 and 2.4 x 10^4 mg/kg were found to be statistically within the same range. This observation can be explained as follows: at low Fe loadings (8 x 10^3 mg/kg – 1.0 x 10^4 mg/kg) only a few Fe(III) centres are available for EPFR formation. Due to steric effects, the adsorbed phenoxyl radicals prevent additional phenol molecules from accessing Fe(III) centres.[11] However, at higher Fe loading concentrations (> 1.0 x 10^4 mg/kg), more and more Fe(III) centres become available for reaction with phenol. The data also show that, at 1.8 x 10^4 mg/kg, an optimum number of the appropriate Fe(III) centres are available, beyond which no further EPFR formation occurs. This EPFR saturation can be explained by the fact that, at higher (1.8 x 10^4 mg/kg) Fe(III) concentrations, there are either no additional isolated Fe(III) centres, causing any radicals formed to react with each other instead of facilitating EPFR formation or additional Fe(III) are not accessible to sorbed phenol molecules due to steric reasons.

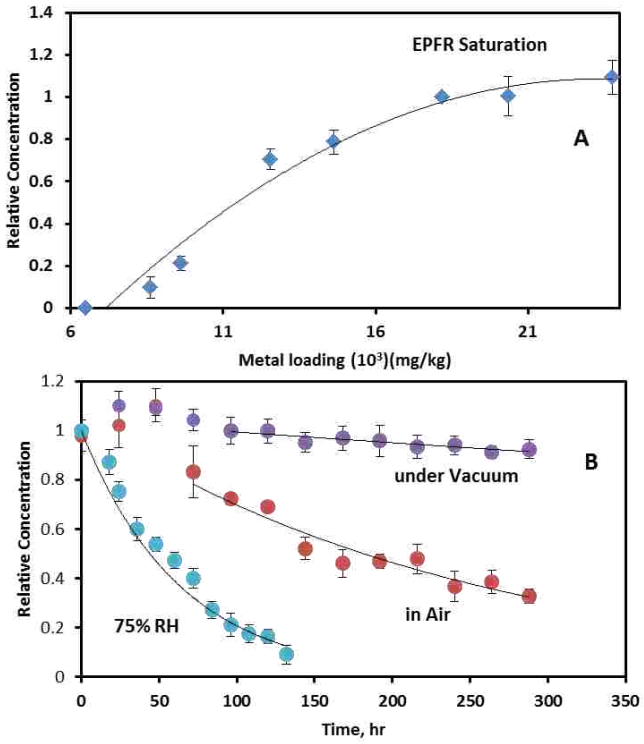

Figure 2.6 A) Relationship between EPFR concentration and Fe(III) loading concentration B) EPFR lifetimes for DosedFe(III)CaM in vacuum (purple), after exposure to ambient air (red) and at 75% relative humidity (RH; blue).

2.3.6 EFPR Lifetime Analysis

The stability of EPFRs in the atmosphere contributes to their environmental impact. We have investigated this by exposing the Fe(III)CaM-associated EFPRs to air.

Effect of Air on EPFR Persistence: EPFR lifetimes have been widely studied as a way to express their persistency and stability after exposure to molecular oxygen in the environment.[11,16,43] The EPFR concentrations in DosedFe(III)CaM samples (at an approximate $1.8x10^4$ mg/kg Fe(III) loading concentration) were monitored immediately upon exposure to air and under relative humidity (RH) range of 22%–38%, both in the dark (to minimize the chance of a photoreaction). The same procedures were carried out with EPFRs under vacuum to serve as a control experiment for an oxygen-free atmosphere. The results for these experiments are shown in Figure 6, B with two time periods being apparent: the growth period, during which EPFRs were

formed, and the subsequent decay period. The growth period is attributed to the migration of phenol to more active Fe(III) sites in the clay.

The growth period also resulted in the g-factor and ΔHp-p of the EPFRs increasing from 2.0034 to 2.0036 and from 6.1 to ~ 6.6–6.9 G, respectively. The increase in ΔHp-p is a consequence of concentration broadening.[37] The EPFR decay rates and lifetimes were determined employing the pseudo-first-order integrated rate law expression (ln ($R/R0$) = –kt, where $t_\tau = 1/k$, τ =1/e, e is the base of the natural logarithm, and $R/R0$ is the ratio of the final to initial radical concentrations).[11,16,43] When suspended in vacuum, EPFRs showed significant stability, with decay occurring at a very slow rate of 0.00028 h^{-1}, yielding a 1/e lifetime of τ = 148.8 days . During this decay period, the g-factor and ΔHp-p remained unchanged. For EPFR decay monitored in air, a 1/e lifetime of 10.4 days was observed with a decay rate of 0.0040 h^{-1}. During the in-air decay period, the g-factor and ΔHp-p decreased to 2.0032 and 5.2 G, respectively. The total EPFR lifetimes for the systems under study here are 151.8 days (with 72 h of radical growth) under vacuum compared to 12.4 days (with 48 h of radical growth) in air.

The above lifetimes are longer than the 3.8 days previously reported for EPFRs generated (in air) on a $Fe(III)_2O_3$/silica system, a model surrogate of the $PM_{2.5}$ systems,[16] dosed with phenol at 230 °C, but shorter than those reported for EPFRs in pentachlorophenol-contaminated soils and real $PM_{2.5}$ systems. Conversely, multiple decays with longer combined EPFR lifetimes of 39 and 21− 5028 days were reported for PCP-contaminated soil and real $PM_{2.5}$ systems, respectively.[37,43] The complex nature of the soil matrix, which can consist of polymeric aromatic components of soil organic matter (SOM) and assorted transition metals (Fe(III), Cu(II), Mn(III)),[13-14,36,43] may account for the longer lifetimes encountered in the contaminated soil system due to local effects, such as hydrophobic associations and π-stacking, which are common with the SOM systems.[13-14,43] Additionally, the long EPFR lifetimes for real $PM_{2.5}$ samples have been previously explained by the presence of trapped EPFRs, also known as ‘internal radicals’. This trapping, or

internalization, protects radicals from molecular oxygen in the environment, hindering the oxidation, and hence, slowing decay processes of these 'internal' EPFRs.[37] It has also been reported that phenol intercalation can occur in a montmorillonite clay containing organic cations, constricting phenol molecules to their interlayer domain.[44] The same intercalation can be assumed for the system under study here, as evidenced by the increase of the basal spacing from 1.31 nm to 1.45 nm for Fe(III)CaM and DosedFe(III)CaM (cf. Figure 2.1), causing similar internalization and hindrance to oxidation, resulting in longer EPFR lifetimes for the DosedFe(III)CaM than for the $Fe(III)_2O_3$/silica system. Radical dimerization provides another plausible explanation of the prolonged EPFR lifetimes, especially during the radical growth period after air exposure.43 For example, a cyclopentadienyl radical formed from a phenoxyl radical via chlorophenoxyl radical intermediates, was previously implicated in the formation of different types of dioxins.[16] Such an occurrence may can also contribute to the slight change in the g-factor and ΔHp-p observed during the radical growth period in this work.

Effect of Humidity on EPFRs Persistence: The observed EPFR decay after exposure to air may also be due to the adsorption of water molecules to, and desorption of the organic precursor from active metal sites. To verify this assertion, DosedFe(III)CaM EPFRs were exposed for 4 h to 75% RH air at 25 °C and their decay was monitored. As shown in Figure 2.6, B, a much faster decay rate of 0.02 h^{-1} was found under these conditions, amounting to a 1/e lifetime of 2.1 days and no initial growth period. During the EPFR decay period, the g-factor decreased from the 2.0033 – 2.0035 range to 2.0030, while the ΔHp-p showed a swift decrease from 6.2 to 4.7 G, suggesting a more homogenous radical system.20 The increase in the RH of air to 75% resulted in EPFRs decaying 5 times faster than in air with RH ranging from 22% to 38%, and 71 times faster than under vacuum. This observation suggests that humidity is a more important factor than the presence of oxygen in the EPFR decay processes taking place in the environment.

Additionally, at 75% RH conditions, no prolonged growth period was observed, presumably due to the water molecules blocking all available active Fe(III) sites, inhibiting further reaction.

2.4 Conclusions

It has previously been found that soils with iron concentrations between 14 and 23 x 10^3 mg/kg, contaminated with phenols and, to a lesser extent, other organic pollutants, have EFPR concentrations ranging from 5.83 x 10^{17} to 20.2 x 10^{17} spins/g.[13] The complex tri-component biological/mineral/SOM soil system is an analytical challenge, especially for mechanistic studies. This study is an initial step in gaining a mechanistic understanding of how EPFR form in contaminated soils by simplifying the soil system to its mineral components. The mineral component, represented here by montmorillonite clay, was chosen as it has been shown that the vast majority of EPFRs in contaminated soils are associated with this fraction, and that clay systems act as a major metal repository and a sorbent of organic pollutants.[13-14,43] This model system yielded EPFR concentrations and lifetimes close to, but lower than those reported for real world soil samples, with no biological component present. The differences in concentration can be explained by other processes, such as enzyme-enhanced EPFR formation.[13,14] The longer EPFR lifetimes for real world soil samples can be explained by SOM stabilization, as we have previously suggested.[14]

Mechanistically, the Fe-loaded montmorillonite system revealed that, under environmentally relevant conditions, an EPFR can be formed by the intercalation sorption of phenol, followed by a transfer of an electron from the phenol to an Fe(III) centre, which results in the reduction of iron to Fe(II). The intercalation of phenol results in the intercalated EPFR, which reduces the ability of oxygen to oxidize this radical, and hence, allows for a long-lived radical. This mechanism can be further extended by the fact that the concentration of EPFRs (spins) are much lower than that of the Fe(II) centres per gram of clay, which leads to the conclusion that a large number of the formed radicals dimerize and form non-radical final products, such as dioxins,

and only the isolated radicals become EPFRs. Finally, it was found that high humidity resulted in faster EPFR decay, hence EPFR toxicity may be lower in humid climates.

The strong resistance to oxidation and the stability of these radicals after exposure to air imply that, even without the stabilizing effect of SOM, the formed EPFRs can persist long enough in the soil to increase the chance of the EPFR-containing clay particles being suspended in air by wind and, in turn, inhaled, ultimately causing oxidative stress.[7] The critical environmental implication of this work lies in the observation that the clay system, when contaminated, in the absence of any biological components, can form EPFRs at concentrations close to those found in real contaminated soils at ambient temperature, which has wide ranging environmental and human health implications, especially when humidity is relatively low.

2.5 References

1. Holmstrand, H.; Gadomski, D.; Mandalakis, M.; Tysklind, M.; Irvine, R.; Andersson, P.; Gustafsson, Ö., Origin of PCDDs in Ball Clay Assessed with Compound-Specific Chlorine Isotope Analysis and Radiocarbon Dating. *Environmental Science & Technology* **2006,** *40* (12),3730-3735.

2. Gu, C.; Liu, C.; Johnston, C. T.; Teppen, B. J.; Li, H.; Boyd, S. A., Pentachlorophenol Radical Cations Generated on Fe(III)-Montmorillonite Initiate Octachlorodibenzo-p-dioxin Formation in Clays: Density Functional Theory and Fourier Transform Infrared Studies. *Environmental Science & Technology* **2011,** *45* (4), 1399-1406.

3. Soma, Y.; Soma, M., Chemical reactions of organic compounds on clay surfaces. *Environmental Health Perspectives* **1989,** *83*, 205-214.

4. Kunisue, T.; Nakanishi, S.; Oka, N.; Sato, F.; Tsurumi, M.; Tanabe, S., Dioxins and Related Compounds in Albatrosses from the Torishima Island, Japan: Accumulation Features by Growth Stage and Toxicological Implications. *Environmental Science & Technology* **2006,** *40* (22), 6919-6927.

5. Ferré-Huguet, N.; Nadal, M.; Schuhmacher, M.; Domingo, J. L., Environmental Impact and Human Health Risks of Polychlorinated Dibenzo-p-dioxins and Dibenzofurans in the Vicinity of a New Hazardous Waste Incinerator: A Case Study. *Environmental Science & Technology* **2006,** *40* (1), 61-66.

6. Dellinger, B.; Pryor, W. A.; Cueto, R.; Squadrito, G. L.; Hegde, V.; Deutsch, W. A., Role of Free Radicals in the Toxicity of Airborne Fine Particulate Matter. *Chemical Research in Toxicology* **2001,** *14* (10), 1371-1377.

7. Kelley, M. A.; Hebert, V. Y.; Thibeaux, T. M.; Orchard, M. A.; Hasan, F.; Cormier, S. A.; Thevenot, P. T.; Lomnicki, S. M.; Varner, K. J.; Dellinger, B.; Latimer, B. M.; Dugas, T. R., Model Combustion-Generated Particulate Matter Containing Persistent Free Radicals Redox Cycle to Produce Reactive Oxygen Species. *Chemical Research in Toxicology* **2013,** *26* (12), 1862-1871.

8. Truong, H.; Lomnicki, S.; Dellinger, B., Mechanisms of molecular product and persistent radical formation from the pyrolysis of hydroquinone. *Chemosphere* **2008,** *71* (1), 107-113.

9. Lomnicki, S.; Truong, H.; Vejerano, E.; Dellinger, B., Copper Oxide-Based Model of Persistent Free Radical Formation on Combustion-Derived Particulate Matter. *Environmental Science & Technology* **2008,** *42* (13), 4982-4988.

10. Truong, H.; Lomnicki, S.; Dellinger, B., Potential for Misidentification of Environmentally Persistent Free Radicals as Molecular Pollutants in Particulate Matter. *Environmental Science & Technology* **2010,** *44* (6), 1933-1939.

11. Kiruri, L. W.; Khachatryan, L.; Dellinger, B.; Lomnicki, S., Effect of Copper Oxide Concentration on the Formation and Persistency of Environmentally Persistent Free Radicals (EPFRs) in Particulates. *Environmental Science & Technology* **2014,** *48* (4), 2212-2217.

12. Sun, Z.; Tang, B.; Xie, H., Treatment of Waste Gases by Humic Acid. *Energy & Fuels* **2015,** *29* (3), 1269-1278.

13. dela Cruz, A. L. N.; Cook, R. L.; Dellinger, B.; Lomnicki, S. M.; Donnelly, K. C.; Kelley, M. A.; Cosgriff, D., Assessment of environmentally persistent free radicals in soils and sediments from three Superfund sites. *Environmental Science: Processes & Impacts* **2014,** *16* (1), 44-52.

14. dela Cruz, A. L. N.; Gehling, W.; Lomnicki, S.; Cook, R.; Dellinger, B., Detection of Environmentally Persistent Free Radicals at a Superfund Wood Treating Site. *Environmental Science & Technology* **2011,** *45* (15), 6356-6365.

15. Boyd, S. A.; Mortland, M. M., Radical formation and polymerization of chlorophenols and chloroanisole on copper(II)-smectite. *Environmental Science & Technology* **1986,** *20* (10), 1056-1058.

16. Vejerano, E.; Lomnicki, S.; Dellinger, B., Formation and Stabilization of Combustion-Generated Environmentally Persistent Free Radicals on an Fe(III)2O3/Silica Surface. *Environmental Science & Technology* **2011,** *45* (2), 589-594.

17. Tront, J. M.; Amos, B. K.; Löffler, F. E.; Saunders, F. M., Activity of Desulfitobacterium sp. Strain Viet1 Demonstrates Bioavailability of 2,4-Dichlorophenol Previously Sequestered by the Aquatic Plant Lemna minor. *Environmental Science & Technology* **2006,** *40* (2), 529-535.

18. Fu, F.; Dionysiou, D. D.; Liu, H., The use of zero-valent iron for groundwater remediation and wastewater treatment: A review. *Journal of Hazardous Materials* **2014,** *267*, 194-205.

19. Ma, Y.-L.; Xu, Z.-R.; Guo, T.; You, P., Adsorption of methylene blue on Cu(II)-exchanged montmorillonite. *Journal of Colloid and Interface Science* **2004,** *280* (2), 283-288.

20. Nwosu, U. G.; Cook, R. L., 13C Nuclear Magnetic Resonance and Electron Paramagnetic Spectroscopic Comparison of Hydrophobic Acid, Transphilic Acid, and Reverse Osmosis May 2012 Isolates of Organic Matter from the Suwannee River. *Environmental Engineering Science* **2014,** *32* (1), 14-22.

21. Wallis, P. J.; Chaffee, A. L.; Gates, W. P.; Patti, A. F.; Scott, J. L., Partial Exchange of Fe(III) Montmorillonite with Hexadecyltrimethylammonium Cation Increases Catalytic Activity for Hydrophobic Substrates. *Langmuir* **2010,** *26* (6), 4258-4265.

22. Tran, N. H.; Wilson, M. A.; Milev, A. S.; Dennis, G. R.; Kannangara, G. S. K.; Lamb, R. N., Dispersion of silicate nano-plates within poly (acrylic acid) and their interfacial interactions. *Science and Technology of Advanced Materials* **2006,** *7* (8), 786-791.

23. Martin-Luengo, M.; Martins-Carvalho, H.; Ladriere, J.; Grange, P., Fe(III)-pillared montmorillonites; preparation and characterization. *Clay Minerals* **1989,** *24* (3), 495-504.

24. Huang, Z.; Wu, P.; Li, H.; Li, W.; Zhu, Y.; Zhu, N., Synthesis and catalytic properties of La or Ce doped hydroxy-FeAl intercalated montmorillonite used as heterogeneous photo Fenton catalysts under sunlight irradiation. *RSC Advances* **2014,** *4* (13), 6500-6507.

25. Popov, A.; Kondratieva, E.; Gilson, J.-P.; Mariey, L.; Travert, A.; Maugé, F., IR study of the interaction of phenol with oxides and sulfided CoMo catalysts for bio-fuel hydrodeoxygenation. *Catalysis Today* **2011,** *172* (1), 132-135.

26. Katti, D. R.; Katti, K. S.; Raviprasad, M.; Gu, C., Role of Polymer Interactions with Clays and Modifiers on Nanomechanical Properties and Crystallinity in Polymer Clay Nanocomposites. *Journal of Nanomaterials* **2012,** *2012*, 15.

27. Hao, Q.-Q.; Wang, G.-W.; Liu, Z.-T.; Liu, Z.-W., Insights into Structural and Chemical Properties of Activated Montmorillonite for Fischer-Tropsch Synthesis over Supported Cobalt Catalysts. In *Nanocatalysis for Fuels and Chemicals*, American Chemical Society: 2012; Vol. 1092, pp 167-193.

28 Amorim, L. V.; Gomes, C. M.; Lira, H. d. L.; França, K. B.; Ferreira, H. C., Bentonites from Boa Vista, Brazil: physical, mineralogical and rheological properties. *Materials Research* **2004,** *7* (4), 583-593.

29. Ji, Y.-Q.; Black, L.; Weidler, P. G.; Janek, M., Preparation of Nanostructured Materials by HeterocoagulationInteraction of Montmorillonite with Synthetic Hematite Particles. *Langmuir* **2004,** *20* (22), 9796-9806.

30. Elkhalifah, A. E.; Murugesan, T.; Bustam, M. A. In *Characterization of different cationic forms of montmorillonite by FTIR, XRD and TGA techniques*, National Postgraduate Conference (NPC), 2011, IEEE: 2011; pp 1-6.

31. Madejová, J., FTIR techniques in clay mineral studies. *Vibrational Spectroscopy* **2003,** *31* (1), 1-10.

32. Flogeac, K.; Guillon, E.; Aplincourt, M., Adsorption of several metal ions onto a model soil sample: Equilibrium and EPR studies. *Journal of Colloid and Interface Science* **2005,** *286* (2), 596-601.

33. Muralidhara, R. S.; Kesavulu, C. R.; Rao, J. L.; Anavekar, R. V.; Chakradhar, R. P. S., EPR and optical absorption studies of Fe3+ ions in sodium borophosphate glasses. *Journal of Physics and Chemistry of Solids* **2010,** *71* (12), 1651-1655.

34. Manjanna, J.; Kozaki, T.; Kozai, N.; Sato, S., A New Method for Fe(II)-montmorillonite Preparation Using Fe(II)-nitrilotriacetate Complex. *Journal of Nuclear Science and Technology* **2007,** *44* (7), 929-932.

35. Huang, Z.; Wu, P.; Li, H.; Li, W.; Zhu, Y.; Zhu, N., Synthesis and catalytic properties of La or Ce doped hydroxy-FeAl intercalated montmorillonite used as heterogeneous photo Fenton catalysts under sunlight irradiation. *RSC Advances* **2014,** *4* (13), 6500-6507.

36. Dellinger, B.; Lomnicki, S.; Khachatryan, L.; Maskos, Z.; Hall, R. W.; Adounkpe, J.; McFerrin, C.; Truong, H., Formation and stabilization of persistent free radicals. *Proceedings of the Combustion Institute* **2007,** *31* (1), 521-528.

37. Gehling, W.; Dellinger, B., Environmentally Persistent Free Radicals and Their Lifetimes in PM2.5. *Environmental Science & Technology* **2013,** *47* (15), 8172-8178.

38 Westre, T. E.; Kennepohl, P.; DeWitt, J. G.; Hedman, B.; Hodgson, K. O.; Solomon, E. I., A Multiplet Analysis of Fe K-Edge 1s → 3d Pre-Edge Features of Iron Complexes. *Journal of the American Chemical Society* **1997,** *119* (27), 6297-6314.

39. Petit, P. E.; Farges, F.; Wilke, M.; Sole, V. A., Determination of the iron oxidation state in earth materials using XANES pre-edge information. *Journal of synchrotron radiation* **2001,** *8* (Pt 2), 952-4.

40. Galoisy, L.; Calas, G.; Arrio, M. A., High-resolution XANES spectra of iron in minerals and glasses: structural information from the pre-edge region. *Chemical Geology* **2001,** *174* (1–3), 307-319.

41. Ingall, E. D.; Diaz, J. M.; Longo, A. F.; Oakes, M.; Finney, L.; Vogt, S.; Lai, B.; Yager, P. L.; Twining, B. S.; Brandes, J. A., Role of biogenic silica in the removal of iron from the Antarctic seas. *Nat Commun* **2013,** *4*, 1981.

42. Pokrovski, G. S.; Schott, J.; Farges, F.; Hazemann, J.-L., Iron (III)-silica interactions in aqueous solution: insights from X-ray absorption fine structure spectroscopy. *Geochimica et Cosmochimica Acta* **2003,** *67* (19), 3559-3573.

43. Cruz, A. L. N. d.; Cook, R. L.; Lomnicki, S. M.; Dellinger, B., Effect of Low Temperature Thermal Treatment on Soils Contaminated with Pentachlorophenol and Environmentally Persistent Free Radicals. *Environmental Science & Technology* **2012,** *46* (11), 5971-5978.

44. Okada, T.; Watanabea, Y.; Ogawa, M., Photocontrol of the adsorption behavior of phenol for an azobenzene-montmorillonite intercalation compound. *Chemical Communications* **2004,** (3), 320-321.

CHAPTER 3
MODEL SYSTEM STUDY OF ENVIRONMENTALLY PERSISTENT FREE RADICALS FORMATION IN A SEMICONDUCTING POLYMER MODIFIED COPPER CLAY SYSTEM AT AMBIENT TEMPERATURE*

3.1 Introduction

Decades of experimental research on the remediation of polluted soils have led to the concept that, after much aging, soil acts as an environmentally inert sink for organic pollutants.[1,2] However, the discovery of environmentally persistent free radicals (EPFRs) in soils has caused a reconsideration of this notion.[3,4] Detected in combustion particulate matter, soils, and sediments, EPFRs appear to be ubiquitous in the environment.[3-7] EPFRs are oxidation resistant organic radical complexes, may be aromatic or polycyclic aromatic in nature, and are formed via the reduction of transition metal ions by the adsorbed aromatic organic pollutant.[3-8]

Our early studies were aimed at the understanding the role of transition metals and aromatic organics in the formation of dioxins in combustion particulate matter.[4,9] EPFRs are of similar concern as dioxins[10-12], as they have been shown to induce the formation of reactive oxygen species (ROS) and can lead to cardiopulmonary diseases and cancer.[13-15] The formation of EPFRs in combustion particulate matter implies an important role of high temperatures in the formation of EPFRs.[6,16] In addition, it has been recently shown that UV radiation can also induce the formation of EPFRs[17] in the presence of a redox centre and an appropriate organic contaminant. While there is evidence that high temperatures or UV radiation may induce the formation of EPFRs, the detection of EPFRs

---

* This chapter previously appeared as Ugwumsinachi G. Nwosu, Lavrent Khachatryan, Sang Gil Youm, Amitava Roy, Albert Leo N. dela Cruz, Evgueni E. Nesterov, Barry Dellinger and Robert L. Cook “Model system study of environmentally persistent free radicals formation in a semiconducting polymer modified copper clay system at ambient temperature.” ***RSC Adv.***, 2016,**6**, 43453-43462. Reproduced by permission of The Royal Society of Chemistry.

in subsurface soil and sediment samples as well as our recent study on Fe(III)CaMMT systems,[3-4,8] raise a number of questions regarding the fundamental mechanisms of EPFR formation. In particular, is there truly a need for any added energy beyond what is thermally available under environmentally relevant conditions? To address these questions, an understanding of the possible soil EPFR-forming components must be developed.

Soil (and sediment) can be viewed as a complex matrix, that can be broken down into three major components, namely: biological, mineral, and organic.[3,4,18] The formation of radicals by the biological and mineral components has been documented. For instance, white rot fungi are known to utilize a number of enzymes to break down organic molecules via radical pathways in the presence of a redox centre, such as iron.[19,20] On the mineral side, it has been shown that loading clays or coating silica with a redox centre (Fe) can yield EPFRs with the addition of either thermal or UV energy.[16,17] Among soil components, the soil organic matter (SOM), can be viewed as the most complex.[21] A number of studies have shown that SOM can act as an electron shuttle within soils.[22,23] This means that a redox centre may not have to be directly accessible *if* it is coated with SOM. In this context, to-date, the Superfund site with the highest EPFR concentrations had 1) high concentrations of redox-active transition metals, such as copper, iron, and manganese, all of which could act as catalytic templates for the chemisorption of pollutants resulting in EPFR formation[4] and 2) high SOM content,[3,4,18] which despite potentially coating such catalytic templates, due to their electron shuttling potential, allow the redox centres to remain accessible.

Consequently, in order to understand the mechanisms of EPFR formation in contaminated soils, it is necessary to conduct a systematic multifaceted study of the individual components of the soil system and their respective roles in EPFR formation. A “top-down” approach was employed in our prior work on the detection of EPFRs in a

contaminated soil from a Superfund wood-treatment site.[3] Here we turn our attention to the contributions of the soil organic matter and the clay mineral components in the formation and stabilization of EPFRs under environmentally relevant conditions. We have developed and employed a poly-*p*-phenylene-modified, copper(II)-loaded montmorillonite clay composite (PPP-Cu(II)CaMMT) as a model for the SOM-clay/mineral components and utilized phenol as a precursor pollutant. Poly-*p*-phenylene (PPP) is a semiconducting polymer, that can act as a simple model for the complex organic phase in natural soil. It was used to investigate the degree to which extended conjugated aromatic systems can affect the stability and lifetimes of EPFRs and the potential for electron shuttling, as seen in SOM. Montmorillonite clay, a naturally abundant smectite clay, containing stacked octahedral aluminate layers assembled between two tetrahedral silicate layers with exchangeable interlayer cations,[24-26] was employed to facilitate the inclusion of the transition metal (redox centre). The amounts, nature, and lifetimes of the EPFRs formed on this surrogate soil, as well as the potential of EPFRs to generate ROS at environmentally relevant conditions were also investigated.

3.2. Experimental Section

3.2.1 Materials

Clay samples, smectite clay, STx-1b (Montmorillonite) with a cation exchange capacity (CEC) of 84.4 meq/100 g and surface area of 83.79 ± 0.22 m^2/g were purchased from the Source Clay Repository (Purdue University, West Lafayette, IN). High purity 5,5-dimethyl-1-pyrroline N-oxide (DMPO, 99%+, GLC) and Copper(II) chloride (anhydrous, 99%) were obtained from Enzo Life Sciences, and Acros Organics, respectively. Isopropylmagnesium chloride (2.0 M solution in THF) was purchased from Acros Organics. All other reagents and solvents were obtained from Aldrich and Alfa Aesar and used without further purification.

3.2.2 Experimental Design

To-date, the highest concentration of EPFRs detected in a real soil was from a wood treating site in Georgia.[18] A “top-down” analysis of the contaminated soil from this site revealed that the EPFRs were almost entirely associated with the clay/humin fraction. This soil also had greatly elevated levels of Cu compared to the neighbouring soils that did not contain EPFRs (differences in Fe were minimal). Based on this finding and the high SOM content of these EFPR-containing soils, the conjugated aromatic assemblies within the SOM were proposed to act as stabilizers of the soil EFPRs. In order to determine if Cu could act as a redox centre—in terms of electron acceptance—in the formation of EPFRs at environmental conditions and to elucidate the role of conjugated aromatics in the stabilization of EPFRs in soils, an engineered soil surrogate (ESS) was synthesized. This surrogate was a novel poly-*p*-phenylene-modified copper(II)-loaded montmorillonite clay composite (PPP-Cu(II)CaMMT). Its make-up echoes the important aspects of the field site—the dominance of Cu and SOM and the presence of the clay/humin soil component with which the vast majority of the detected EPFRs were associated. The use of such a surrogate system allows for a detailed mechanistic study of EPFR formation and stabilization, which in turn will result in better understanding of toxicity data and improved remediation strategies. Such investigations are not possible with real soil samples due to their inherent extreme complexity.

3.2.3 Preparation of Clay Systems

The method used followed our previous work.[8] Briefly, 4 g of clay was homogenized, stirred in 100 mL of a freshly prepared 0.02 M solution of $CuCl_2$ for 48 hours and vacuum filtered. The wet clay was dried at 60 °C for 48 hours. For the metal analysis, clay samples were digested in 5 mL trace metal grade concentrated HNO_3 for 24 hours and then diluted in 50 mL of de-ionized water. The digested sample was analyzed for

metals using Varian Vista-MPX CCD simultaneous inductively coupled plasma–optical emission spectroscopy (ICP–OES) instrument and found to contain 24 mg/g of copper. The procedure for the synthesis of the PPP-modified montmorillonite clay by surface-confined Kumada catalyst-transfer chain-growth polymerization is provided in the Supporting Information (appendix A). For the purpose of this study, samples were identified as CaMMT, Cu(II)CaMMT, PPP-Cu(II)CaMMT, Dosed_Cu(II)CaMMT and Dosed_PPP-Cu(II)CaMMT for pristine, copper-loaded, copper-loaded poly-*p*-phenylene, phenol-exposed copper-loaded and phenol-exposed copper-loaded poly-*p*-phenylene montmorillonite clays, respectively.

3.2.4 Raman Spectrometry Measurements

The Raman spectroscopic measurements were performed using a Jobin Yvon Horiba LabRAM Raman spectrometer employing the following conditions: HeNe laser source (632.81 nm), incident power of 17 mW, grating of 1800 lines per mm, and confocal hole aperture of 180 μm. Measurements were carried out in the scan range of 150 – 2000 cm^{-1}.

3.2.5 Gas Phase Phenol Exposure Experiments

The samples were exposed to phenol in a controlled temperature and vacuum chamber employing a previously developed procedure.[6,8] Briefly, 50 mg of Cu(II)CaMMT and PPP-Cu(II)CaMMT were preheated under vacuum at 40 °C in a 4-mm ID suprasil quartz EPR tube prior to phenol exposure. Phenol vapour deposition was performed for 5 minutes at ~10^{-2} mm Hg, followed by evacuation for additional 5 minutes to allow the removal of an unreacted adsorbate.

3.2.6 EPR Measurements

EPR measurements were performed using a Bruker EMX-10/2.7 EPR spectrometer (X-band) with dual cavities under the following parameters: microwave frequency of 9.77

GHz, power of 2.01 mW, 5 scans, modulation amplitude of 4.00 G, modulation frequency of 100 kHz, centre field of 3488.46 G, sweep width of 150 G and 6000 G, time constant of 1.280 ms, conversion time of 20.5 ms, sweep time of 41.93 s, resolution of 2048 points, and receiver gain of 1.0×10^4. Measurements were done at room temperature and quantitative analyses were conducted using Bruker's WINEPR program.[8,18] Radical concentrations and the g-factor were estimated relative to the standard 2,2-diphenyl-1-picrylhydrazyl (DPPH), which was used to calibrate the field position.[27] The EPR parameters for the spin trapping experiments, to detect DMPO-OH adducts, were as follows: sweep width of 100 G, EPR microwave power of 10 mW, modulation amplitude of 0.8 G, time constant of 40.96 ms, and sweep time of 167.77 s.

3.2.7. X-ray Diffraction (XRD) Measurements

The XRD data were collected on a PANalytical Empyrean diffractometer using the Cu Kα radiation of λ = 1.5419 Å within 2Θ scan range of 5 – 90°.

3.2.8. Extended X-Ray Absorption Fine Structure (EXAFS) and X-Ray Absorption Near Edge Structure (XANES) Measurements

The EXAFS data were collected at the high energy X-ray absorption spectroscopy beamline of the J. Bennett Johnston, Sr., Center for Advanced Microstructures and Devices (CAMD) electron storage ring at Louisiana State University, Baton Rouge, Louisiana, USA. The beamline is equipped with a Bonn University modified Le Monnier type water-cooled double crystal monochromator, located on the 11-pole and a 7.5 T multi-pole wiggler. A Ge 111 crystal set was used in the monochromator for the EXAFS measurements. The monochromator beam energy was calibrated with a standard Cu metal foil at the energy of 8979 eV and the fluorescence mode measurements were made with a single element Ketek™ 80 mm^2 silicon drift detector. Samples were prepared by spreading a few μm thick clay powder onto a Kapton™ tape. Multiple scans (2-5 scans

each) were performed at room temperature and were processed using the IFEFFIT Demeter software 0.9.21.[28] FEFF paths for EXAFS fitting were obtained from the copper cyclohexasilicate crystal structure,[29] via Inorganic Crystal Structure Database.

For X-ray absorption spectroscopy near edge measurements Ge 220 crystals were used in the monochromator. A Ketek™ 150 mm^2 silicon drift detector was used for the measurements. Each spectrum was measured with following steps: from -100 to 30 eV below the edge with 5 eV, from -30 eV to 30 eV around the edge in 0.5 eV, 100 to 200 eV in 2eV, 200 to 400 eV in 5 eV. At least two spectra were averaged each with 7 seconds integration time.

3.2.9 Hydroxyl Radical Detection

Hydroxyl radicals (•OH) were trapped using DMPO with the following procedure: 10 µL of a sonicated suspension containing 2 mg/mL of homogenized Cu(II)CaMMT, Dosed_Cu(II)CaMMT, PPP-Cu(II)CaMMT, or Dosed_PPP-Cu(II)CaMMT samples were mixed with a 10 µL of freshly prepared 3 M DMPO solution and the suspension was made up to 200 µL. All sample suspensions were made in a pH 7.4 10 mM phosphate buffered saline (PBS) solution (using organic free 18 MΩ·cm ultra-pure de-ionized water). Aeration was carried out by bubbling air through the PBS solution for 10 minutes prior to introducing the samples. The reaction mixture was stirred vigorously at room temperature and subjected to EPR analysis. The concentration of the •OH radical generated in solution was estimated assuming a 1:1 stoichiometric ratio between DMPO and •OH. [12] Finally, •OH radical concentration was estimated relative to the standard radical 3-line spectra of 4-hydroxyl-2,2,6,6-tetramethylpiperidine-1-oxyl, TEMPOL.[13]

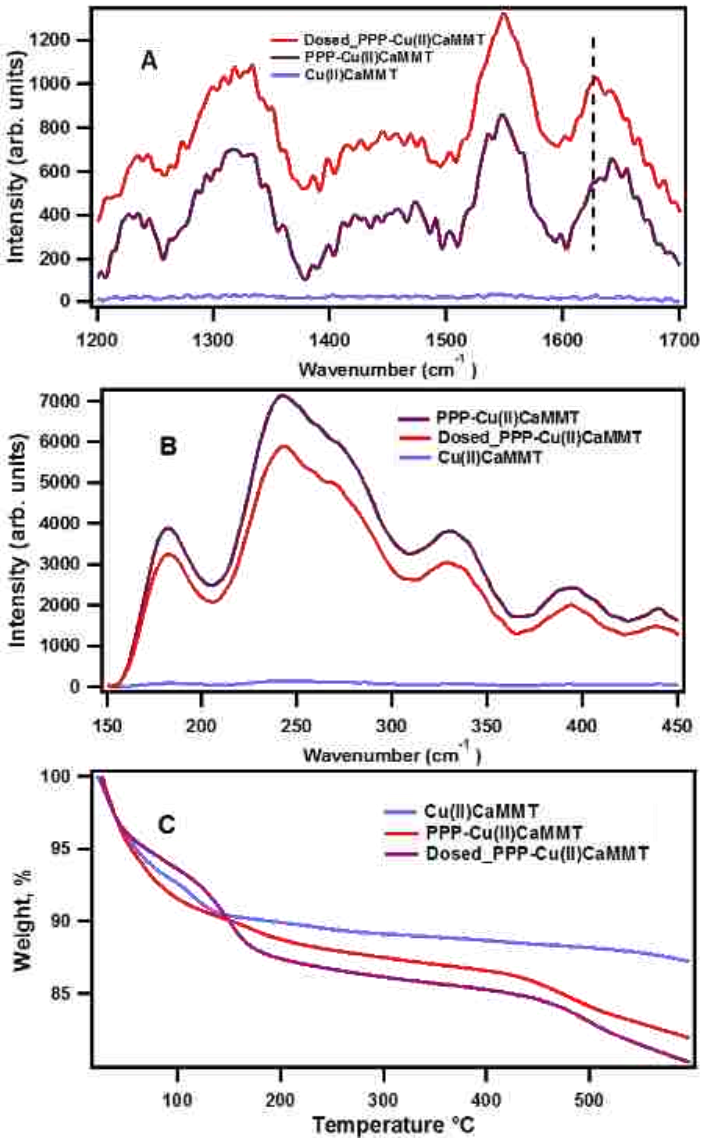

Figure. 3.1 Raman spectra and thermogravimetric analysis (TGA) data of PPP-Cu(II)CaMMT, DosedPPP-Cu(II)CaMMT and Cu(II)CaMMT showing (A) D and G bands between 1200 cm^{-1} – 1700 cm^{-1}; (B) Stretching bands between 150 cm^{-1} – 400 cm^{-1}; (C) TGA data collected at 10 °C/minute from 0 °C to 600 °C under nitrogen.

3.3 Results and Discussion

3.3.1 Characterization of the Model Soil System

3.3.1.1 Raman

Samples of Cu(II)CaMMT, PPP-Cu(II)CaMMT and Dosed_PPP-Cu(II)CaMMT were characterized by Raman spectroscopy to determine the presence of the polymer, the

sorption of phenol, and possible changes resulting from electron delocalization in the conjugated aromatic polymer system. The obtained results are presented in Figure 3.1 (A and B).

The results in Figure 3.1, A show characteristic observable changes in the different clay samples in the prominent Raman D, D' and G band modes at 1342 cm^{-1}, 1641 cm^{-1}, and 1548 cm^{-1} for the clay composite samples (PPP-Cu(II)CaMMT and Dosed_PPP-Cu(II)CaMMT). These bands are characteristic of stretching vibrations of bonds between sp^2-hybridized carbons typical for aromatic polymers, graphene, and carbon nanotubes.[30-34] The in-plane bending vibrations of the methine C–H bonds are recognized as responsible for the shoulder peaks appearing at 1234 cm^{-1}.[31-32] These peaks were absent in the Cu(II)CaMMT, thus indicating the presence of PPP phase in the clay composite PPP-Cu(II)CaMMT.[33] The 13 cm^{-1} shift in D' band splitting from 1641 cm^{-1} to 1628 cm^{-1}, observed in Figure 3.1, A (marked by the dashed vertical line), is consistent with the electronic delocalization after exposure to phenol.[31,34] Another distinguishable feature is the decreased Raman intensity in the stretching bands between 150 cm^{-1} and 400 cm^{-1} observed for Dosed_PPP-Cu(II)CaMMT (Figure 3.1, B). This further corroborates the prior evidence of aromatic ring interactions after phenol exposure and polymerization of PPP within the Cu(II)CaMMT system.[34] Similar trends have been noted in single-walled carbon nanotube (SWCNT) systems for which reduction in Raman intensities within radial breathing mode band regions were correlated to the sorption of organic molecules on, or modification of, SWCNT surfaces.[34, 35, 36]

3.3.2. Thermogravimetric analysis (TGA)

TGA was used to determine the amount of PPP in the clay composite, with the results presented in Figure 3.1, C. Approximately 5% (0.101 mg) mass loss of the clay composite sample that occurred between 425 and 500 °C for both PPP-Cu(II)CaMMT and

Dosed_PPP-Cu(II)CaMMT, was due to the loss of PPP.[37-38] The TGA data also reveal three distinct weight loss patterns between 60 and 190 °C. For PPP-Cu(II)CaMMT there is a swift loss of mass until about 100 °C, which can be associated with the loss of water.[39] For Cu(II)CaMMT the pattern is somewhat more complex, with a small shoulder between 60 and 120 °C, which can be attributed to water loss, including the surface-bound water.[39] The majority of this surface water appears absent in PPP-Cu(II)CaMMT, which is consistent with the hydrophobicity of the PPP coating. The large shoulder apparent between 60 and 200 °C for Dosed_PPP-Cu(II)CaMMT can be attributed to the loss of the sorbed phenol due to vaporization.[40]

3.3.3. X-ray Diffraction (XRD)

The XRD data presented in Figure 3.2 show 1) a shift in the interlayer peak for CaMMT from 1.53 nm to 1.28 nm for Cu(II)CaMMT, as clear evidence of Cu(II) exchanging with interlayer cations (Ca^{2+}, Mg^{2+} and Na^{+}) in montmorillonite[41], 2) a shift in the interlayer peak from 1.28 nm to 1.52 nm between Cu(II)CaMMT and PPP-Cu(II)CaMMT, serving as a clear evidence that the majority of the PPP polymer is formed in the interlayer, and 3) an increase in interlayer spacing after phenol dosing, which is indicative of phenol being sorbed into the interlayer space.

3.3.4 Formation and Characterization of EPFRs

3.3.4.1 Cu(II)CaMMT versus PPP-Cu(II)CaMMT

After exposure to phenol, EPFRs were formed by both Cu(II)CMMT and PPP-Cu(II)CaMMT, as evidenced by the EPR spectra in Figure 3.3, A, with g-factor values of 2.0034 and 2.0033 and peak to peak line widths, $\Delta Hp\text{-}p$, of ~5 and 7, respectively. These values are consistent with phenoxyl-type radicals.[6,8,42] When CaMMT was exposed to phenol, no radicals were formed, providing reasonable evidence that EPFRs formation in the studied systems involves both an organic precursor and an active transition metal (redox) centre.

PPP-Cu(II)CaMMT inherently contains radicals—either intrinsically present (solitons), or resulting from PPP oxidation in air (polarons) (Scheme 3.1A).[43] These radicals have a

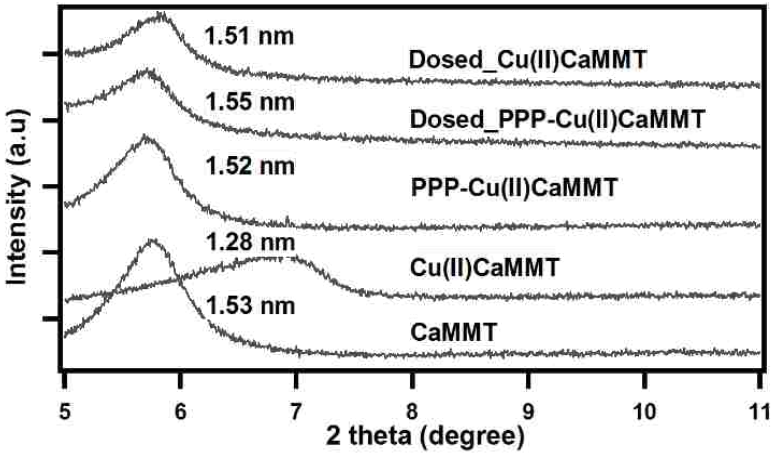

Figure 3.2 Powder XRD patterns showing the interlayer spacing for pre-phenol-exposed samples: CaMMT, Cu(II)CaMMT, PPP-Cu(II)CaMMT and post phenol-exposed samples: Dosed_PPP-Cu(II)CaMMT, and Dosed_Cu(II)CaMMT.

g-factor of 2.0024, indicating that the radical resonates mostly within the benzene rings of the conjugated PPP system and compares well with the g-factor of a free electron (2.0023) and PPP systems (2.0023 – 2.0025). [44-46] A shift in g-factor from 2.0024 to 2.0033 was observed after phenol exposure, indicating a combination of carbon and oxygen-centred organic radical of phenoxyl type,[42, 47-49] as well as a new source of radicals (as depicted in Scheme 3.1, B). A new source of radicals is also supported by the g-factor of 2.0034 for the Dosed_Cu(II)CaMMT which, along with results from previous studies,[42,44,47] demonstrates that, for copper-phenol systems with an adjacent oxygen atom, the radical mostly resides on the oxygen centres. Only slightly lower g-factor of 2.0033 for the Dosed_PPP-Cu(II)CaMMT strongly suggests the presence of a new but very similar radical to that present in the Dosed_Cu(II)CaMMT.

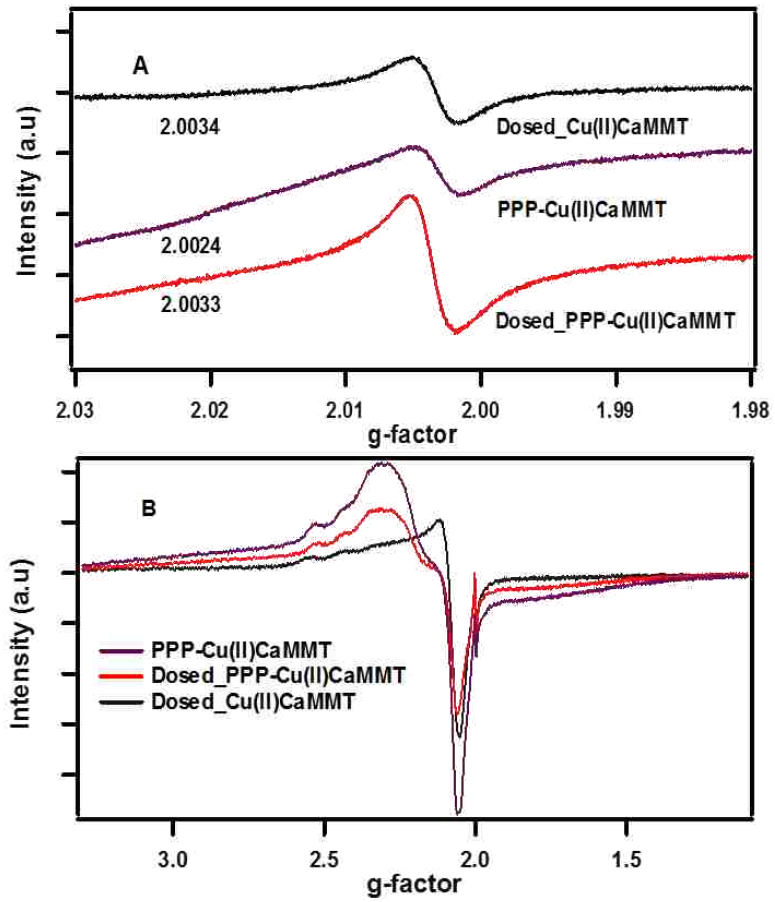

Figure 3.3 EPR Spectra of phenol exposed Cu-loaded clay (black), Cu-loaded-poly-p-phenylene clay, (purple), and phenol-exposed Cu-loaded clay-poly-p-phenylene (red) composite. Spectra were collected at (A) 150 G and (B) 6000 G magnetic fields.

This new source of radicals also explains the fact that the same exposure to phenol leads to more radicals being formed in PPP-Cu(II)CaMMT (1.58×10^{17} spins/g, corrected to account for the radical inherent to PPP) compared to Cu(II)CaMMT (1.22×10^{17} spins/g). Scheme 3.1B proposes a model for the formation of these radicals within the Dosed_PPP-Cu(II)CaMMT. The mechanisms put forward in Scheme 1 are supported by further EPR analysis at a magnetic field of 6000 G (*cf*. Figure 3, B). This analysis indicates a splitting of the hyperfine components ($g_{\parallel} = 2.345$, $g^{\perp} = 2.075$), which are typical of paramagnetic Cu(II) ions.[49-50] However, the distortion in shapes and positions of the hyperfine components at these regions after

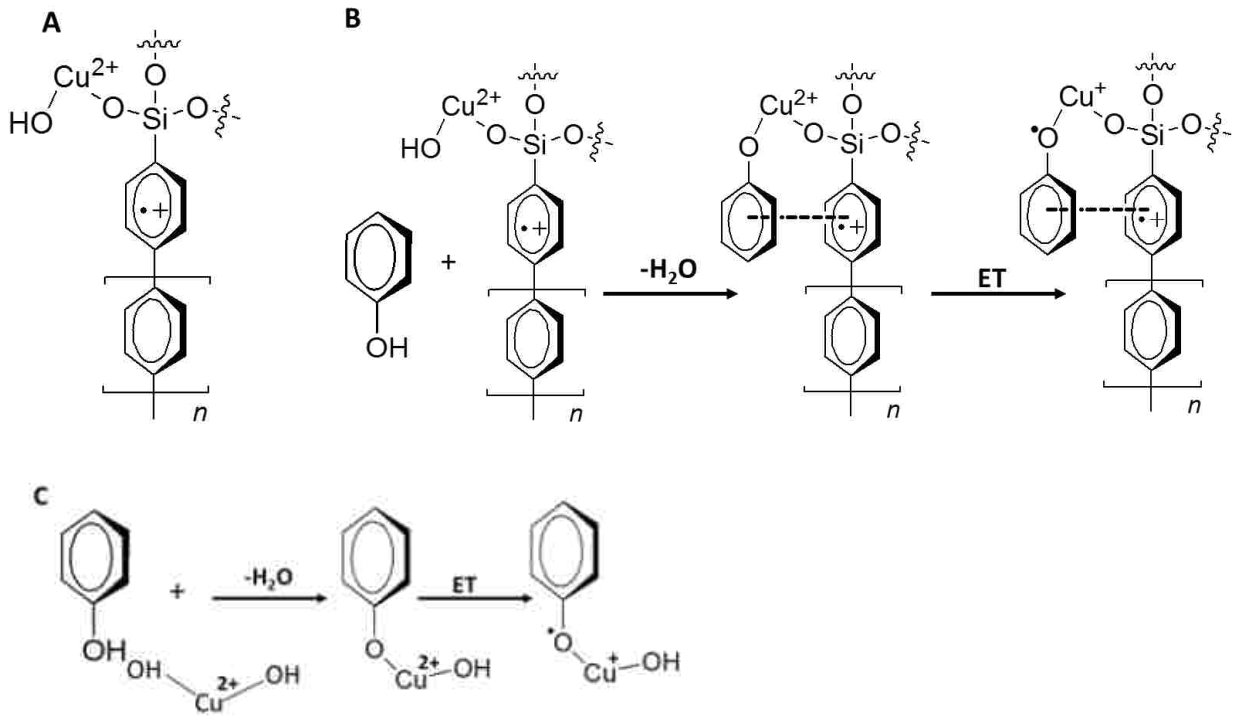

Scheme 3.1 Proposed structures and mechanisms of EPFR formation in Cu-loaded clay and the PPP semiconducting polymer modified clay, showing possible π-π stacking interaction between polymer molecule and adsorbed phenol. The silyl group which can bind Cu(II) is an intrinsic part of the clay-confined PPP.

polymerization imply a mononuclear or binuclear copper-poly-*p*-phenylene complex formed on a fraction of Cu(II) paramagnetic centres.[51-52] The required binding sites on PPP polymers are provided by the silyl groups which are used as anchoring units for clay immobilization of PPP polymer (see the Supporting Information for experimental details). These findings are consistent with the mechanisms illustrated in Scheme 3.1. The mechanism presented in Scheme 3.1(B and C) is also consistent with the formation of EPFRs through the chemisorption of an aromatic organic molecule to a transition metal centre and the subsequent reduction of the transition metal centre via the formation of a metal-oxygen complex.[6,8, 16, 27]

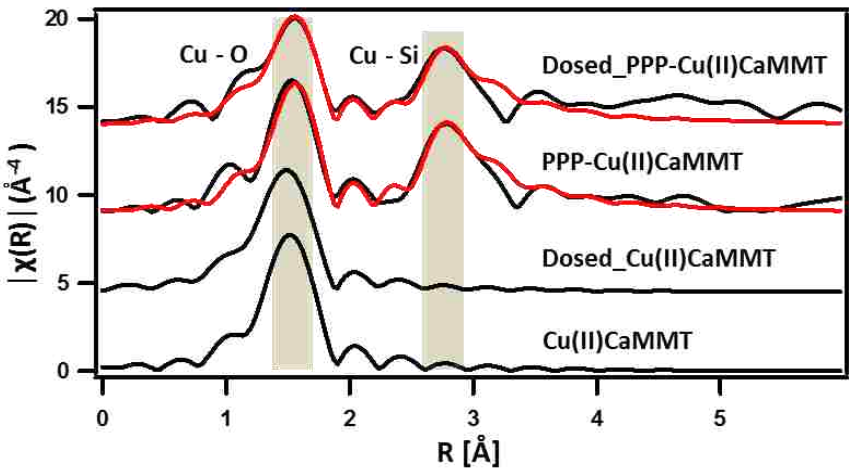

Figure 3.4 Fourier transform of Cu K-edge K^3-weighted EXAFS of Cu(II)CaMMT, Dosed_Cu(II)CaMMT, PPP-Cu(II)CaMMT Dosed_PPP-Cu(II)CaMMT. Black lines represent experimental data while red lines represent best fit to cyclohexasilicate crystal structure. Phase shift correction was not applied.

3.3.5 Extended X-Ray Absorption Fine Structure (EXAFS)

The EXAFS data shown in Figure 3.4, represent the Fourier transform χ(R) (R space) of Cu(II)CaMMT, PPP-Cu(II)CaMMT, Dosed_Cu(II)CaMMT and Dosed_PPP-Cu(II)CaMMT, and further confirm the presence of a polymer unit bonded to Si in close proximity to the copper-oxygen bond, as hypothesized in Scheme 3.1A. The radial distances for the Cu-O and Cu-Si/Cu shells were clearly observed in PPP-Cu(II)CaMMT and Dosed_PPP-Cu(II)CaMMT. The peaks due to Cu-Si/Cu were absent in Cu(II)CaMMT and Dosed_Cu(II)CaMMT. This is supported strongly by fitting PPP-Cu(II)CaMMT and Dosed_PPP-Cu(II)CaMMT with a copper cyclohexasilicate crystal structural model, which best describes a Cu-O-Si structural backbone, as proposed in Scheme 3.1B. The first set of peaks represents Cu–O interatomic distances observed to be ~1.93 Å for Cu(II)CaMMT and Dosed_Cu(II)CaMMT and ~1.96 Å for PPP-Cu(II)CaMMT and Dosed_PPP-Cu(II)CaMMT (based on the fit to copper cyclohexasilicate crystal structure). According to the fit, the presence of Cu-Si coordination shell peak with a distance of ~3.17Å may suggest the presence of PPP polymer since it was anchored on the silica oxide. With the Cu–Cu distance of ~3.12 Å falling within the same range, a possible backscattering from the

binuclear copper portion of the complex may also be possible by the presence of the polymer. This corroborates the previously presented Raman and EPR spectra, which indicate the presence of a copper-PPP complex.

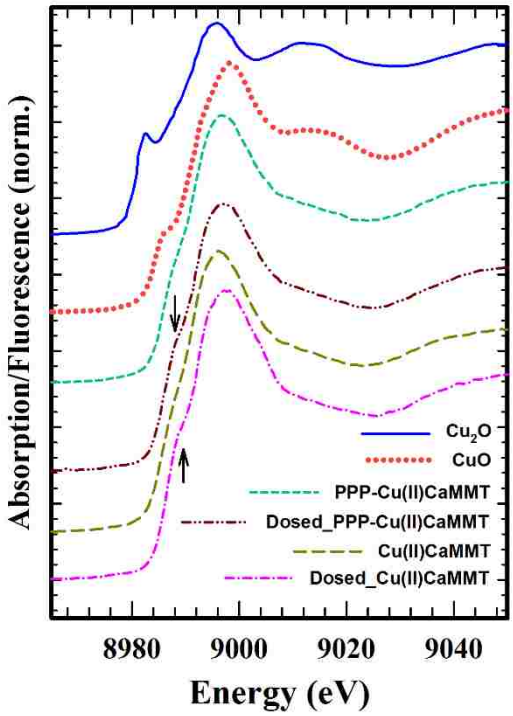

Figure 3.5 Cu K-edge XANES spectra of Cu(II)CaMMT, Dosed_Cu(II)CaMMT, PPP-Cu(II)CaMMT, Dosed_PPP-Cu(II)CaMMT, and standards Cu_2O and CuO.

3.3.6 X-ray Absorption Near Edge Spectroscopy (XANES)

XANES experiments were also performed in order to investigate the changes in the oxidation state of copper in the EPFR forming process. Evidence of the redox process involved in the formation of EPFRs was observed at the 1s → 4p transition edge region of the Cu K-edge XANES spectra, as illustrated in Figure 3.5. The result showed the appearance of a shoulder at ~8989.3 eV, as evidence of the absorption edge energy, after dosing for both Dosed_Cu(II)CaMMT and Dosed_PPP-Cu(II)CaMMT, a feature absent in the spectra for Cu(II)CaMMT and PPP-Cu(II)CaMMT, indicating Cu(II) to Cu(I) reduction, as previously reported in an EPFR forming process.[53] Generally, Cu in +1 oxidation state

is marked with prominent sharp peaks at the 1s → 4p transition region, as seen in Cu_2O, while shifts to lower and higher energies in this region have been reported to indicate reduction and oxidation of Cu species, respectively.[54]

3.3.7 EPFR Lifetimes

In order to gain insight into the decay kinetics of EPFRs present in Dosed_Cu(II)CaMMT and Dosed_PPP-Cu(II)CaMMT, time dependent open air exposure studies were carried out, and the results are presented in Figure 3.6. The data in Figure 3.6. were used to calculate the lifetimes (τ) according to the pseudo-first-order integrated rate law expression: $\ln(R/R_0) = -kt$, where $t_\tau = 1/k$ and k and e represent the slope of the regression and the base of the natural logarithm, respectively.[8]

3.3.7.1 Dosed_Cu(II)CaMMT

A decay lifetime of ~20 h (τ_1 = ~20 h) was found for the Dosed_Cu(II)CaMMT-associated EPFRs, as shown with the pseudo-first-order rate law expression fit line (red) in Figure 3.6. A shorter decay lifetime has been found for EPFRs formed on silica-supported Cu(II)O (τ_1 = ~74 min).[16] The ~1.5 orders slower decay of the Dosed_Cu(II)CaMMT EPFRs can be attributed to the confined environment of the adsorbed (physisorbed and chemisorbed) phenol to the Cu(II) metal centre.[8] Due to the layered structure of montmorillonite clay, phenoxyl radicals can be formed through binding of phenol with cation-exchanged copper in the interlayer (as well as edges) of the clay, resulting in the entrapment of radicals within the clay matrix (internal radicals).[47, 55-56]

The XRD data (*cf.* Figure 3.2) strongly support this assertion, with a significant shift in the interlayer peak spacing for Cu(II)CaMMT from 1.28 nm to 1.51 nm after phenol exposure (Dosed_ Cu(II)CaMMT). This presents an additional barrier to the decomposition of the EPFRs formed in the clay, making them more stable than the EPFRs formed on silica-supported Cu(II)O.[16]

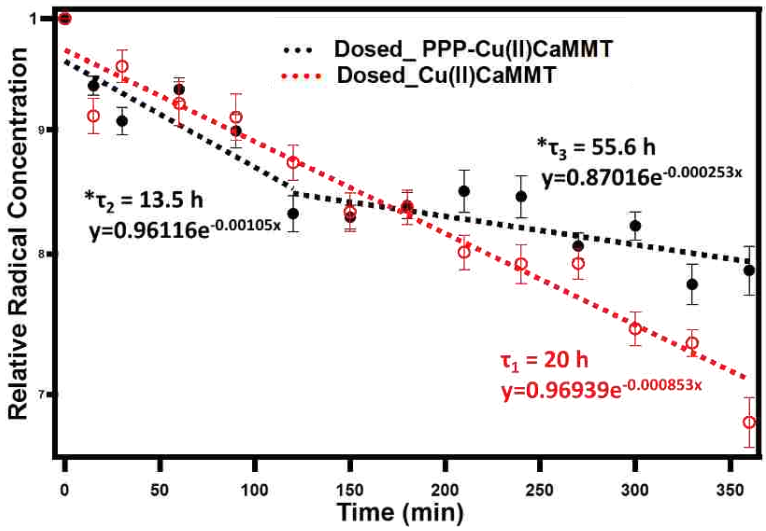

Figure 3.6 Lifetimes of phenoxyl radical (EPFR) formed under 30 minutes thermal pre-heating at 40 °C in ambient air with 5 min gas phase phenol exposure to Cu(II)CaMMT (open red circles and dashed red fit line) and PPP-Cu(II)CaMMT (closed black circles and dashed black fit lines). Igor Pro 6.37 was used for all line fitting. * Corrected lifetime-utilizing a 0.843 PPP decay factor [to account for the decay of the radicals associated with PPP]).

3.3.7.2 Dosed_PPP-Cu(II)CaMMT

The EPFRs associated with the Dosed_PPP-Cu(II)CaMMT yielded two decay lifetimes of ~13.5 h and 55.6 h (τ_2 and τ_3), as shown with the pseudo-first-order rate law expression fit lines (black) in Figure 3.6, after accounting for the PPP radical decay. The two decay periods occurred: from the initial air exposure (0 min) to 180 min and from 180 to 360 min. The g-factor and $\Delta Hp\text{-}p$ values varied between 2.0030 and 2.0034 and between 6.0 and 7.2, respectively, and are consistent with previously reported results of the decay of phenoxyl-type oxygen-centred EPFRs.[8,42,47] In addition, EPFRs formed in real soil samples contaminated with pentachlorophenol (PCP) have shown similar multiple decays.[18]

These two decays can be assigned to 1) the faster decaying EPFRs chemisorbed to Cu(II) metal centres, as in the case of Dosed_Cu(II)CaMMT (Scheme 1C) and 2) the slower decaying Cu(II)-bound PPP polymer chain-associated EFPRs with a possible

electron shuttling taking place between the phenol and the PPP polymer chain, utilizing the conjugated backbone system.

The XRD data presented in Figure 3.2 show interlayer peak positions of 1.52 and 1.55 nm for PPP-Cu(II)CaMMT and Dosed_PPP-Cu(II)CaMMT, respectively, indicating the presence of the PPP and the subsequent phenol intercalation after dosing. These patterns are similar to those exhibited by Dosed_Cu(II)CaMMT, and serve as strong evidence of phenol being adsorbed between clay layers, as illustrated in Scheme 3.1B. It can be speculated that the larger interlayer spacing in Dosed_PPP-Cu(II)CaMMT compared to Dosed_Cu(II)CaMMT allows for an easier oxygen access, and hence, shorter decay lifetimes of the Cu(II)-chemisorbed EPFRs in Dosed_PPP-Cu(II)CaMMT (~13.5 h versus ~20h).

While the second mechanism is not fully understood, previous works have proposed that aromatic ring stacking between the polymer and phenol allows for π-π interactions resulting in the formation of sandwich dimers,[27,57] as illustrated in Scheme 3.1B. These dimers would stabilize the formed EPFRs by delocalizing the unpaired electron over the polymer's extended conjugated π system. This is consistent with the longer EPFR lifetime associated with the Dosed_PPP-Cu(II)CaMMT. Also, PPP could be envisioned to assume a "flapping" orientation within the clay matrix, resulting in a π-cation interaction,[57-58] thus increasing the chances of the sorption of phenol onto the polymer. This is equivalent to the interaction that leads to the formation of stable copper-quinone complexes,[59] as may be found in the real soil system, where quinone moieties act as the main electron shuttling agents.[60-61] With the sorption of phenol onto the PPP chain, electron shuttling possibilities cannot be disregarded.

In regards to the exact EPFR decay mechanism, a potential pathway would be a pseudo-first order interaction between the radical with oxygen, as has been previously proposed.[18]

Surface reaction models, such as Langmuir−Hinshelwood and Eley−Rideal, have also been suggested as possible routes by which EPFRs form and decompose to yield dioxins or other products of radical recombination.[18,62]

3.3.8 Detection of Hydroxyl Radicals by EPR-Spin Trapping

EPFRs have been shown to initiate the generation of superoxide and hydroxyl radicals through the reduction of oxygen. In order to investigate hydroxyl radical ($^{\bullet}OH$) generation, EPR spin trapping experiments were carried out using 5,5-dimethyl-1-pyrroline-N-oxide (DMPO). The concentration of DMPO-OH adduct was estimated from the double integration of the DMPO-OH characteristic 1:2:2:1 EPR peak signals with hyperfine splitting of a_N = 15.066 G, a_H = 14.735 G (Figure S1)(Appendix A), which is the chemical signature of the trapped $^{\bullet}OH$. In the present study, Cu(II)CaMMT was combined with molecular oxygen and used as a reference for $^{\bullet}OH$ generation. The results for the $^{\bullet}OH$ generated by this none EPFR containing system were subtracted from those obtained for $^{\bullet}OH$ generated by PPP-Cu(II)CaMMT (no EPFRs), Dosed_Cu(II)CaMMT, and Dosed_PPP-Cu(II)CaMMT systems and are presented in Figure 3.7 for incubation times of 1, 3, 5, and 8 h.

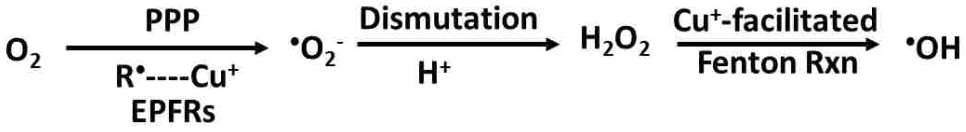

Scheme 3.2 Proposed $^{\bullet}OH$ radical generation routes involving redox-active conjugated polymer (PPP) and EPFRs in the presence of molecular oxygen.[13]

The data presented in Figure 3.7 provide two very clear general trends: (i) the EPFR-containing particles (dosed systems) yield significantly more $^{\bullet}OH$ radicals than the

non-EPFR containing systems, and (ii) there is an increase in the trapped •OH radical with increasing time.

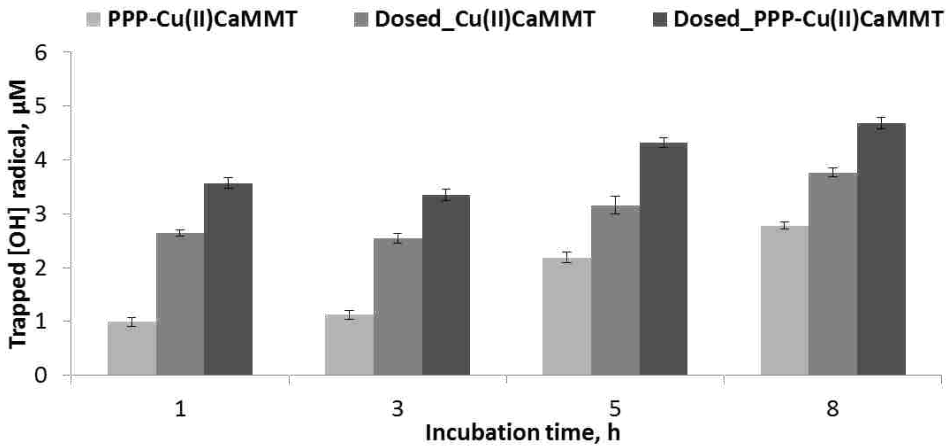

Figure 3.7 Chart derived from the EPR spectra of spin trapped [OH] for PPP-Cu(II)CaMMT, Dosed_Cu(II)CaMMT, and Dosed_PPP-Cu(II)CaMMT. All Samples were incubated in buffer (PBS pH 7.4) suspension with DMPO.

In addition to the redox cycling route involving the reduction of molecular oxygen into superoxide radical ion, which generates hydrogen peroxide and hydroxyl radical through disproportionation and Fenton chemistry (Scheme 3.2), other EPFR decay routes can also result in the production •OH for the systems under study. For example, nucleophilic addition of water is often considered as artefactual to •OH generation.[12, 63] To account for these possibilities, the undosed Cu(II)CaMMT was used. Likewise, the undosed PPP-(Cu(II)CaMMT was used as an additional control to account for the radicals inherently present in the PPP-Cu(II)CaMMT conjugated polymer-based systems. After the first hour of incubation, due to the presence of EPFRs, Dosed_PPP-Cu(II)CaMMT were shown to generate 72% more •OH compared to the PPP-Cu(II)CaMMT. This number represents 98% of the •OH generated by the Dosed_Cu(II)CaMMT, after the •OH radicals generated by the PPP in the system are accounted for. Similar results have been

previously reported with a 50% increase in the number of •OH radicals generated between a tarball-associated EPFRs compared to the non-EPFR particle systems.[27] However, as noted, a fraction of the •OH generated by this system can be attributed to the radicals within the PPP-Cu(II)CaMMT conjugated polymer system being active in •OH generation. This implies that conjugated polymer PPP catalyzes the generation of •OH in a similar fashion to how EPFR-containing systems do, due to the π-electron conjugated chain ability to donate electrons via the formation of cation radical (polaron)[43] as seen in Scheme 3.2. This means that conjugated polymer can facilitate reduction of molecular oxygen to superoxides. Analogously, •OH can be generated through quinone-quinoid redox cycling, as demonstrated with quinone moieties inherent in SOM. This may help explain the ability of natural organic matter (NOM) to induce the formation of ROS in biological entities.[64-66]

Also, this is in agreement with the explanation that a range of aromatic functionalities, such as graphene oxide and biochars, catalyze the formation of •OH through the activation of molecular O_2 to produce superoxide radical ($^{\bullet}O_2^-$).[67-68] The superoxide radical produced in this process may further act as an oxidant, initiating a Fenton-type reaction that ultimately results in •OH generation.[13,63]

3.4 Conclusions

Fundamental: Our results demonstrate that a simple copper-exchanged montmorillonite clay system (Cu(II)CaMMT) and an electron shuttling organic polymer-modified clay system (PPP-Cu(II)CaMMT) can yield EPFRs when exposed to phenol under environmentally relevant conditions. This finding illustrates that EPFRs may be formed on just the Cu-containing clay components of soils and provides evidence that soil organic matter (SOM) may act as an electron shuttle between mineral/clay redox centres and pollutants, aiding in the formation of EPFRs as well as stabilizing the formed radicals. Our results provide insights into the role of soil component in the formation of EPFRs at

Superfund sites and that even with the minimum quantity of SOM (e.g., 5% polymer) in the soil, the radical can persist longer due to aromatic stabilization. The type of organic radicals and the different decay patterns, as those observed for the Dosed_PPP-Cu(II)CaMMT system, are akin to those observed in PCP-contaminated soils, biochar, and tarballs, all of which are identical in composition in terms of the presence of aromatic moieties as well as metal redox centres. While the complex nature of these materials makes mechanistic studies into radical formation very difficult, this work demonstrates how such studies can be facilitated by the use of properly designed model systems.

Health and Remediation: From a health perspective, the real concern is that, in windy conditions, EPFR-contaminated soil can turn into airborne dust particulate matter, especially during periods of low precipitation, and subsequently become inhaled or ingested by humans. Since EPFRs are known to induce oxidative stress through the formation of reactive oxygen species, they can lead to cardiopulmonary diseases and cancer.[13-14] The results for the Dosed_PPP-Cu(II)CaMMT system indicate that soil remediation methods must be developed, in which the native SOM is penetrated in order to destroy the EPFRs present.

The approach put forward in this work allows one to systematically study and understand the underlying mechanisms of EPFR formation in single and bi-component surrogate soil models. However, when applying the findings from this study to real world soils, caution must be exercised as the role of a number of other important soil components, such as biological enzymes (e.g., laccase), and various environmental conditions have not been accounted for. Nevertheless, the results from this study will benefit future efforts that take these additional variables into account.

3.5 References

1. Doick, K. J.; Klingelmann, E.; Burauel, P.; Jones, K. C.; Semple, K. T., Long-Term Fate of Polychlorinated Biphenyls and Polycyclic Aromatic Hydrocarbons in an Agricultural Soil. *Environmental Science & Technology* **2005,** *39* (10), 3663-3670.

2. Moeckel, C.; Nizzetto, L.; Guardo, A. D.; Steinnes, E.; Freppaz, M.; Filippa, G.; Camporini, P.; Benner, J.; Jones, K. C., Persistent Organic Pollutants in Boreal and Montane Soil Profiles: Distribution, Evidence of Processes and Implications for Global Cycling. *Environmental Science & Technology* **2008,** *42* (22), 8374-8380.

3. dela Cruz, A. L. N.; Gehling, W.; Lomnicki, S.; Cook, R.; Dellinger, B., Detection of Environmentally Persistent Free Radicals at a Superfund Wood Treating Site. *Environmental Science & Technology* **2011,** *45* (15), 6356-6365.

4. dela Cruz, A. L. N.; Cook, R. L.; Dellinger, B.; Lomnicki, S. M.; Donnelly, K. C.; Kelley, M. A.; Cosgriff, D., Assessment of environmentally persistent free radicals in soils and sediments from three Superfund sites. *Environmental Science: Processes & Impacts* **2014,** *16* (1), 44-52.

5. Dellinger, B.; Lomnicki, S.; Khachatryan, L.; Maskos, Z.; Hall, R. W.; Adounkpe, J.; McFerrin, C.; Truong, H., Formation and stabilization of persistent free radicals. *Proceedings of the Combustion Institute* **2007,** *31* (1), 521-528.

6. Vejerano, E.; Lomnicki, S.; Dellinger, B., Formation and Stabilization of Combustion-Generated Environmentally Persistent Free Radicals on an Fe(III)2O3/Silica Surface. *Environmental Science & Technology* **2011,** *45* (2), 589-594.

7. Truong, H.; Lomnicki, S.; Dellinger, B., Mechanisms of molecular product and persistent radical formation from the pyrolysis of hydroquinone. *Chemosphere* **2008,** *71* (1), 107-113.

8. Nwosu, U. G.; Roy, A.; dela Cruz, A. L. N.; Dellinger, B.; Cook, R., Formation of environmentally persistent free radical (EPFR) in iron(iii) cation-exchanged smectite clay. *Environmental Science: Processes & Impacts* **2016,** *18* (1), 42-50.

9. Truong, H.; Lomnicki, S.; Dellinger, B., Potential for Misidentification of Environmentally Persistent Free Radicals as Molecular Pollutants in Particulate Matter. *Environmental Science & Technology* **2010,** *44* (6), 1933-1939.

10. Kunisue, T.; Nakanishi, S.; Oka, N.; Sato, F.; Tsurumi, M.; Tanabe, S., Dioxins and Related Compounds in Albatrosses from the Torishima Island, Japan: Accumulation Features by Growth Stage and Toxicological Implications. *Environmental Science & Technology* **2006,** *40* (22), 6919-6927.

11. Holt, E.; Weber, R.; Stevenson, G.; Gaus, C., Polychlorinated Dibenzo-p-Dioxins and Dibenzofurans (PCDD/Fs) Impurities in Pesticides: A Neglected Source of Contemporary Relevance. *Environmental Science & Technology* **2010,** *44* (14), 5409-5415.

12. Ferré-Huguet, N.; Nadal, M.; Schuhmacher, M.; Domingo, J. L., Environmental Impact and Human Health Risks of Polychlorinated Dibenzo-p-dioxins and Dibenzofurans in the Vicinity of a New Hazardous Waste Incinerator: A Case Study. *Environmental Science & Technology* **2006,** *40* (1), 61-66.

13. Khachatryan, L.; Vejerano, E.; Lomnicki, S.; Dellinger, B., Environmentally Persistent Free Radicals (EPFRs). 1. Generation of Reactive Oxygen Species in Aqueous Solutions. *Environmental Science & Technology* **2011,** *45* (19), 8559-8566.

14. Dellinger, B.; Pryor, W. A.; Cueto, R.; Squadrito, G. L.; Hegde, V.; Deutsch, W. A., Role of Free Radicals in the Toxicity of Airborne Fine Particulate Matter. *Chemical Research in Toxicology* **2001,** *14* (10), 1371-1377.

15. Kelley, M. A.; Hebert, V. Y.; Thibeaux, T. M.; Orchard, M. A.; Hasan, F.; Cormier, S. A.; Thevenot, P. T.; Lomnicki, S. M.; Varner, K. J.; Dellinger, B.; Latimer, B. M.; Dugas, T. R., Model Combustion-Generated Particulate Matter Containing Persistent Free Radicals Redox Cycle to Produce Reactive Oxygen Species. *Chemical Research in Toxicology* **2013,** *26* (12), 1862-1871.

16. Lomnicki, S.; Truong, H.; Vejerano, E.; Dellinger, B., Copper Oxide-Based Model of Persistent Free Radical Formation on Combustion-Derived Particulate Matter. *Environmental Science & Technology* **2008,** *42* (13), 4982-4988.

17. Li, H.; Pan, B.; Liao, S.; Zhang, D.; Xing, B., Formation of environmentally persistent free radicals as the mechanism for reduced catechol degradation on hematite-silica surface under UV irradiation. *Environmental Pollution* **2014,** *188*, 153-158.

18. Cruz, A. L. N. d.; Cook, R. L.; Lomnicki, S. M.; Dellinger, B., Effect of Low Temperature Thermal Treatment on Soils Contaminated with Pentachlorophenol and Environmentally Persistent Free Radicals. *Environmental Science & Technology* **2012,** *46* (11), 5971-5978.

19. Martinez, A. T.; Speranza, M.; Ruiz-Duenas, F. J.; Ferreira, P.; Camarero, S.; Guillen, F.; Martinez, M. J.; Gutierrez, A.; del Rio, J. C., Biodegradation of lignocellulosics: microbial, chemical, and enzymatic aspects of the fungal attack of lignin. *International microbiology: the official journal of the Spanish Society for Microbiology* **2005,** *8* (3), 195-204.

20. Hall, S. J.; Silver, W. L., Iron oxidation stimulates organic matter decomposition in humid tropical forest soils. *Global Change Biology* **2013,** *19* (9), 2804-2813.

21. Schulten, H.-R., The three-dimensional structure of humic substances and soil organic matter studied by computational analytical chemistry. *Fresenius' Journal of Analytical Chemistry* **1995,** *351* (1), 62-73.

22. Kappler, A.; Benz, M.; Schink, B.; Brune, A., Electron shuttling via humic acids in microbial iron(III) reduction in a freshwater sediment. *FEMS Microbiology Ecology* **2004,** *47* (1), 85-92.

23. Piepenbrock, A.; Schröder, C.; Kappler, A., Electron Transfer from Humic Substances to Biogenic and Abiogenic Fe(III) Oxyhydroxide Minerals. *Environmental Science & Technology* **2014,** *48* (3), 1656-1664.

24. Gu, C.; Liu, C.; Ding, Y.; Li, H.; Teppen, B. J.; Johnston, C. T.; Boyd, S. A., Clay Mediated Route to Natural Formation of Polychlorodibenzo-p-dioxins. *Environmental Science & Technology* **2011,** *45* (8), 3445-3451.

25. Gu, C.; Liu, C.; Johnston, C. T.; Teppen, B. J.; Li, H.; Boyd, S. A., Pentachlorophenol Radical Cations Generated on Fe(III)-Montmorillonite Initiate Octachlorodibenzo-p-dioxin Formation in Clays: Density Functional Theory and Fourier Transform Infrared Studies. *Environmental Science & Technology* **2011,** *45* (4), 1399-1406.

26. Gu, C.; Li, H.; Teppen, B. J.; Boyd, S. A., Octachlorodibenzodioxin Formation on Fe(III)-Montmorillonite Clay. *Environmental Science & Technology* **2008,** *42* (13), 4758-4763.

27. Kiruri, L. W.; Dellinger, B.; Lomnicki, S., Tar Balls from Deep Water Horizon Oil Spill: Environmentally Persistent Free Radicals (EPFR) Formation During Crude Weathering. *Environmental Science & Technology* **2013,** *47* (9), 4220-4226.

28 Ravel, B.; Newville, M., ATHENA, ARTEMIS, HEPHAESTUS: data analysis for X-ray absorption spectroscopy using IFEFFIT. *Journal of synchrotron radiation* **2005,** *12* (4), 537-541.

29. Breuer, K. H.; Eysel, W.; Müller, R., Structural and chemical varieties of dioptase, Cu6[Si6O18] ·6H2O. In *Zeitschrift für Kristallographie - Crystalline Materials*, 1989; Vol. 187, p 15.

30. Cervantes, T. N. M.; Bento, D. C.; Maia, E. C. R.; Zaia, D. A. M.; Laureto, E.; da Silva, M. A. T.; Moore, G. J.; de Santana, H., In situ and ex situ spectroscopic study of poly(3-hexylthiophene) electrochemically synthesized. *Journal of Materials Science: Materials in Electronics* **2012,** *23* (10), 1916-1921.

31. Wang, Z.; Rothberg, L. J., Structure and Dynamics of Single Conjugated Polymer Chromophores by Surface-Enhanced Raman Spectroscopy. *ACS Nano* **2007,** *1* (4), 299-306.

32. Rao, S.; Bálint, Š.; Cossins, B.; Guallar, V.; Petrov, D., Raman Study of Mechanically Induced Oxygenation State Transition of Red Blood Cells Using Optical Tweezers. *Biophysical Journal* **2009,** *96* (1), 209-216.

33. Wu, J.; Gherghel, L.; Watson, M. D.; Li, J.; Wang, Z.; Simpson, C. D.; Kolb, U.; Müllen, K., From Branched Polyphenylenes to Graphite Ribbons. *Macromolecules* **2003,** *36* (19), 7082-7089.

34. Takenobu, T.; Takano, T.; Shiraishi, M.; Murakami, Y.; Ata, M.; Kataura, H.; Achiba, Y.; Iwasa, Y., Stable and controlled amphoteric doping by encapsulation of organic molecules inside carbon nanotubes. *Nat Mater* **2003,** *2* (10), 683-688.

35. Lefrant, S.; Baibarac, M.; Baltog, I.; Mevellec, J. Y.; Godon, C.; Chauvet, O., Functionalization of single-walled carbon nanotubes with conducting polymers evidenced by Raman and FTIR spectroscopy. *Diamond and Related Materials* **2005,** *14* (3–7), 867-872.

36. Hupp, J. T.; Williams, R. D., Using Resonance Raman Spectroscopy to Examine Vibrational Barriers to Electron Transfer and Electronic Delocalization. *Accounts of Chemical Research* **2001,** *34* (10), 808-817.

37. Ahn, T.; Jang, M. S.; Shim, H.-K.; Hwang, D.-H.; Zyung, T., Blue Electroluminescent Polymers: Control of Conjugation Length by Kink Linkages and Substituents in the Poly(p-phenylenevinylene)-Related Copolymers. *Macromolecules* **1999,** *32* (10), 3279-3285.

38. Stack, S.; O'Donoghue, O.; Birkinshaw, C., The thermal stability and thermal degradation of blends of syndiotactic polystyrene and polyphenylene ether. *Polymer Degradation and Stability* **2003,** *79* (1), 29-36.

39. Elkhalifah, A. E.; Murugesan, T.; Bustam, M. A. In *Characterization of different cationic forms of montmorillonite by FTIR, XRD and TGA techniques*, National Postgraduate Conference (NPC), 2011, IEEE: 2011; pp 1-6.

40. Zhou, J.; Yao, Z.; Chen, Y.; Wei, D.; Wu, Y.; Xu, T., Mechanical and thermal properties of graphene oxide/phenolic resin composite. *Polymer Composites* **2013,** *34* (8), 1245-1249.

41. Seger, M. R.; Maciel, G. E., NMR Investigation of the Behavior of an Organothiophosphate Pesticide, Chlorpyrifos, Sorbed on Montmorillonite Clays. *Environmental Science & Technology* **2006,** *40* (3), 797-802.

42. Kiruri, L. W.; Khachatryan, L.; Dellinger, B.; Lomnicki, S., Effect of Copper Oxide Concentration on the Formation and Persistency of Environmentally Persistent Free Radicals (EPFRs) in Particulates. *Environmental Science & Technology* **2014,** *48* (4), 2212-2217.

43. Bredas, J. L.; Street, G. B., Polarons, bipolarons, and solitons in conducting polymers. *Accounts of Chemical Research* **1985,** *18* (10), 309-315.

44. L. Tian, C. P. Koshland, J. Yano, V. K. Yachandra, I. T. S. Yu, S. C. Lee and D. Lucas, Energy & Fuels, 2009, **23**, 2523-2526.

45. List, E. J. W.; Partee, J.; Shinar, J.; Scherf, U.; Müllen, K.; Zojer, E.; Petritsch, K.; Leising, G.; Graupner, W., Localized triplet excitations and the effect of photo-oxidation in ladder-type poly(p-phenylene) and oligo(p-phenylene). *Physical Review B* **2000,** *61* (16), 10807-10814.

46. Vescoli, V.; Degiorgi, L.; Dressel, M.; Schwartz, A.; Henderson, W.; Alavi, B.; Grüner, G.; Brinckmann, J.; Virosztek, A., Spin-density-wave gap in the Bechgaard salts (TMTSF}2X. *Physical Review B* **1999,** *60* (11), 8019-8027.

47. Gehling, W.; Dellinger, B., Environmentally Persistent Free Radicals and Their Lifetimes in PM2.5. *Environmental Science & Technology* **2013,** *47* (15), 8172-8178.

48. Liao, S.; Pan, B.; Li, H.; Zhang, D.; Xing, B., Detecting Free Radicals in Biochars and Determining Their Ability to Inhibit the Germination and Growth of Corn, Wheat and Rice Seedlings. *Environmental Science & Technology* **2014,** *48* (15), 8581-8587.

49. Calvo, R.; Passeggi, M. C.; Isaacson, R. A.; Okamura, M. Y.; Feher, G., Electron paramagnetic resonance investigation of photosynthetic reaction centers from Rhodobacter sphaeroides R-26 in which Fe2+ was replaced by Cu2+. Determination of hyperfine interactions and exchange and dipole-dipole interactions between Cu2+ and QA. *Biophysical Journal* **1990,** *58* (1), 149-165.

50. Contel, M.; Villuendas, P. R.; Fernández-Gallardo, J.; Alonso, P. J.; Vincent, J.-M.; Fish, R. H., Fluorocarbon Soluble Copper(II) Carboxylate Complexes with Nonfluoroponytailed Nitrogen Ligands as Precatalysts for the Oxidation of Alkenols and Alcohols under Fluorous Biphasic or Thermomorphic Modes: Structural and Mechanistic Aspects. *Inorganic Chemistry* **2005,** *44* (26), 9771-9778.

51. Alves, W. A.; Almeida-Filho, S. A. d.; Santos, R. H. d. A.; Paduan-Filho, A.; Ferreira, A. M. d. C., Equilibria and catalytic properties of a chloro-bridged Diimine copper(II) complex in the N,N,N',N'-tetramethyl-p-phenylenediamine (TMPD) oxidation. *Journal of the Brazilian Chemical Society* **2004,** *15*, 872-883.

52. Pavlova, S. V.; To, H. L.; Chan, E. S. H.; Li, H.-W.; Mak, T. C. W.; Lee, H. K.; Chan, S. I., Synthesis, structure and dioxygen reactivity of a bis([small micro]-iodo)dicopper(i) complex supported by the [N-(3,5-di-tert-butyl-2-hydroxybenzyl)-N,N-di-(2-pyridylmethyl)]amine ligand. *Dalton Transactions* **2006,** (18), 2232-2243.

53. Alderman, S. L.; Farquar, G. R.; Poliakoff, E. D.; Dellinger, B., An Infrared and X-ray Spectroscopic Study of the Reactions of 2-Chlorophenol, 1,2-Dichlorobenzene, and Chlorobenzene with Model CuO/Silica Fly Ash Surfaces. *Environmental Science & Technology* **2005,** *39* (19), 7396-7401.

54. Dubale, A. A.; Pan, C.-J.; Tamirat, A. G.; Chen, H.-M.; Su, W.-N.; Chen, C.-H.; Rick, J.; Ayele, D. W.; Aragaw, B. A.; Lee, J.-F.; Yang, Y.-W.; Hwang, B.-J., Heterostructured Cu2O/CuO decorated with nickel as a highly efficient photocathode for photoelectrochemical water reduction. *Journal of Materials Chemistry A* **2015,** *3* (23), 12482-12499.

55. T. Okada, T.; Watanabea, Y.; Ogawa, M., Photocontrol of the adsorption behavior of phenol for an azobenzene-montmorillonite intercalation compound. *Chemical Communications* **2004,** (3), 320-321.

56. Wang, Q.; Peng, L.; Li, G.; Zhang, P.; Li, D.; Huang, F.; Wei, Q., Activity of Laccase Immobilized on TiO2-Montmorillonite Complexes. *International Journal of Molecular Sciences* **2013,** *14* (6), 12520.

57. Wheeler, S. E., Local Nature of Substituent Effects in Stacking Interactions. *Journal of the American Chemical Society* **2011,** *133* (26), 10262-10274.

58. Keiluweit, M.; Kleber, M., Molecular-Level Interactions in Soils and Sediments: The Role of Aromatic π-Systems. *Environmental Science & Technology* **2009,** *43* (10), 3421-3429.

59. Roy, S.; Sarkar, B.; Bubrin, D.; Niemeyer, M.; Záliš, S.; Lahiri, G. K.; Kaim, W., Stabilizing the Elusive ortho-Quinone/Copper(I) Oxidation State Combination through π/π Interaction in an Isolated Complex. *Journal of the American Chemical Society* **2008,** *130* (46), 15230-15231.

60. Scott, D. T.; McKnight, D. M.; Blunt-Harris, E. L.; Kolesar, S. E.; Lovley, D. R., Quinone Moieties Act as Electron Acceptors in the Reduction of Humic Substances by Humics-Reducing Microorganisms. *Environmental Science & Technology* **1998,** *32* (19), 2984-2989.

61. Nevin, K. P.; Lovley, D. R., Potential for Nonenzymatic Reduction of Fe(III) via Electron Shuttling in Subsurface Sediments. *Environmental Science & Technology* **2000,** *34* (12), 2472-2478.

62. Boyd, S. A.; Mortland, M. M., Dioxin radical formation and polymerization on Cu(II)-smectite. *Nature* **1985,** *316* (6028), 532-535.

63. Burkitt, M. J.; Ying Tsang, S.; Ching Tam, S.; Bremner, I., Generation of 5,5-Dimethyl-1-pyrrolineN-Oxide Hydroxyl and Scavenger Radical Adducts from Copper/H2O2Mixtures: Effects of Metal Ion Chelation and the Search for High-Valent Metal–Oxygen Intermediates. *Archives of Biochemistry and Biophysics* **1995,** *323* (1), 63-70.

64. Hseu, Y.-C.; Senthil Kumar, K. J.; Chen, C.-S.; Cho, H.-J.; Lin, S.-W.; Shen, P.-C.; Lin, C.-W.; Lu, F.-J.; Yang, H.-L., Humic acid in drinking well water induces inflammation through reactive oxygen species generation and activation of nuclear factor-κB/activator protein-1 signaling pathways: A possible role in atherosclerosis. *Toxicology and Applied Pharmacology* **2014,** *274* (2), 249-262.

65. Qi, S.; Hartog, G. J. M. d.; Bast, A., Damage to lung epithelial cells and lining fluid antioxidant defense by humic acid. *Environmental Toxicology and Pharmacology* **2008,** *26* (1), 96-101.

66. Schepetkin, I. A.; Khlebnikov, A. I.; Ah, S. Y.; Woo, S. B.; Jeong, C.-S.; Klubachuk, O. N.; Kwon, B. S., Characterization and Biological Activities of Humic Substances from Mumie. *Journal of Agricultural and Food Chemistry* **2003,** *51* (18), 5245-5254.

67. Fang, G.; Gao, J.; Liu, C.; Dionysiou, D. D.; Wang, Y.; Zhou, D., Key Role of Persistent Free Radicals in Hydrogen Peroxide Activation by Biochar: Implications to Organic Contaminant Degradation. *Environmental Science & Technology* **2014,** *48* (3), 1902-1910.

68. Su, C.; Acik, M.; Takai, K.; Lu, J.; Hao, S.-j.; Zheng, Y.; Wu, P.; Bao, Q.; Enoki, T.; Chabal, Y. J.; Ping Loh, K., Probing the catalytic activity of porous graphene oxide and the origin of this behaviour. *Nat Commun* **2012,** *3*, 1298.

CHAPTER 4
EFFECTS OF ENVIRONMENTAL FACTORS ON ENVIRONMENTALLY PERSISTENT FREE RADICALS FORMATION ON CU AND FE - LOADED MONTMORRILONITE CLAY

4.1 Introduction

Soils serve as natural reservoirs for persistent organic pollutants (POP)[1-3], and hence, as determine the fate and transportation, persistency, and degradation of these pollutants through transformation into either more or less toxic compounds.[2-7] Environmentally persistent free radicals (EPFRs) have emerged as soil pollutants of concern given their highly reactive nature to biological entities and ability to initiate the formation of other toxic molecular entities known to induce further damage to the soil and the environment at large.[8-13] For instance, previous studies have shown the formation of various dioxin products through polymerization and dimerization of EPFR intermediates, such as phenoxyl and semiquinone radicals in the presence of Cu(II) and Fe(III).[9,12-13] Since soil plays host to both organic and metal contaminants, soil properties and conditions are bound to affect the sorption of contaminants and EPFR formation. Soil pH is one of the most important factors in determining the chemistry that can take place in a soil.[14-19] A number of studies have shown that pH affects the metal and organic contaminant speciation, dissociation, complexation, and dissolution of both metal oxides with aromatic organic molecules as catechol, resorcinol and dopamine.[20-24] These studies, however, were not focused on soil chemistry as it relates to EPFRs formation. Soil pH can range from very acidic pH of ~ 2.5 – 4 for acidic peat soils, up to strongly alkaline pH ~9 –10, for mineral soils in desert regions.[25] Another important factor that affects the chemistry of soil pollutants is the relative humidity (RH). Desorption ranging from 40 to 60% of the organic pollutants content at 66% relative humidity has been reported in literature [26-27]; similarly, our previous research on EPFR formation on a Fe(III) loaded clay system in the gas phase [28] showed that EPFR stability and persistence can be drastically impacted by high relative humidity (78% RH). However, in our previous studies, the

effect of soil pH was not examined. In perspective, soil pH conditions and ambient humidity conditions are factored into the present work in such a way as to encompass relevant environmental conditions. Another important environmental factor that can directly affect the formation of EPFRs is UV irradiation, such as from sunlight. Numerous studies have shown that UV irradiation can induce degradation and transformation of organic pollutants through such pathways as the photo Fenton reaction, especially in the presence of transition metals, such as Fe, Cu and TiO_2, and are strongly influenced by pH.[29-35] Even without EPFR intermediates, EPFR forming processes can still be affected by photolysis-induced photo Fenton reactions[36], mainly with Fe species at acidic pHs. Thus, soil pH can be postulated to be an important factor in EPFR formation, with or the presence of UV irradiation.

Surrogate models have been employed in the past, employing catechol, phenol, dichlorophenol, pentachlorophenol, and anthracene as contaminant precursors, while cation (Fe and Cu) loaded clays and iron and copper oxide nanoparticles have been used to model the soil mineral component. [28,30,37, 38,39] However, to our knowledge, to-date no study has been conducted to investigate the effects of ambient environmental conditions, such as pH, UV irradiation, and high relative humidity on EPFR formation. In the present work, we have employed a liquid phase exposure, which more closely mimics the real situation in soils and sediments, than the previously used gas phase exposure. Also, due to the high concentration of iron and copper in the studied Superfund soils, coupled with the higher EPFR concentrations detected in contaminated soils compared to the non-contaminated soils, we have utilized Fe(III) and Cu(II)-loaded montmorillonite clays, labeled as (Fe(III)CaMMT) and (Cu(II)CaMMT), respectively, as models to represent the presence of metals in the soil. This course of action was chosen as our previous studies of the Superfund soils have revealed that the vast majority of the detected EPFRs were associated with the soils' clay fractions.[40-42] Similarly, catechol was utilized as a model aromatic contaminant due to its (i) ability to form phenoxyl and semiquinone-type radicals, which are the

type of EPFRs most commonly detected in Superfund site samples [40-42], (ii) high water solubility, and (iii) prominent presence among soil contaminants.[43] Catechol also has the ability to exhibit two dissociation constants (pK_a) with values at 9.25 and 13.0 respectively[44], making it more unique as a model contaminant for EPFRs study in liquid phase. EPFR formation was investigated at various pH conditions, ranging from 3.4 to 9.5 under ambient conditions. In addition, the effect of solar irradiation on EPFRs formation was studied using a simulated UV irradiation system both during and post EPFR formation. Finally, EPFR decay was studied at 55% and 78% RH, which are, respectively, considered to fall within the range of annual mean normal and high humidity conditions that can easily be attained in the ambient environment.[45-46]

4.2. Materials and Methods

4.2.1 Materials

Ca-montmorillonite clay was purchased from the Source Clay Repository (Purdue University, West Lafayette, IN), STx-1b 250 grams/unit. Copper(II)chloride, anhydrous (99%), $CuCl_2$, and iron(III)chloride (97%), $FeCl_3$, were purchased from Acros Organics and Aldrich, respectively. UltraPure™ Tris buffer was obtained from ThermoFisher Scientific. Acetic acid, glacial (≥ 99.7%), trace metal grade nitric acid, HNO_3, and sodium acetate anhydrous (≥ 99%) were purchased from Fisher Scientific. MES hydrate (≥ 99.5%) and 1,2-dihydroxybenzene (≥ 99%) were purchased purchased from Sigma Aldrich. Spectra/Por® membrane dialysis pre-treated RC tubing (MWCO: 50KD), was purchased from Spectrum Labs.

4.2.2 Preparation of Cu-and Fe-Exchanged Clays

The loading of clays with Fe(III) and Cu(II) cations, following previously developed procedures [28,39], is described briefly. About 4 g of pristine clay samples (as purchased) were placed in a 250 mL beaker, properly dispersed, and hydrated with 25 mL of a 0.0021 M solution of $FeCl_3$ or $CuCl_2$ for Fe(III) and Cu(II) loading, respectively. The clay suspension was then diluted to 100 mL utilizing the 0.0021 M $FeCl_3$ or $CuCl_2$ solutions and stirred with a magnetic stirrer for

48 h at room temperature. The treated suspensions, in order to remove chloride ions, were subsequently subjected to dialysis for approximately 24 h, (replacing the water in 12 h intervals) until a negative $AgNO_3$ chloride test was achieved. Following dialysis, the cation exchanged clays were filtered out using a suction vacuum filtration set-up and subsequently dried at 60 °C for 48 h. The dried clays were smashed and homogenized into a fine powder using mortar and pestle.

4.2.3. ICP-OES-analysis

The cation-exchanged clays (Fe(III)CaMMT and Cu(II)CaMMT) were analyzed for metal content using the same methods as described in chapter 2 and in the previously published work.[28,39] Briefly, 5 mL of concentrated nitric acid was used to digest 0.2g of cation exchanged clay then the filtered digestate solution was diluted with 50 mL 18 MΩ cm water and subjected to metal content analysis with the simultaneous inductively coupled plasma optical emission spectroscopy (ICP-OES) using a Varian Vista-MPX CCD.

4.2.4 X-ray diffraction (XRD)

The XRD measurements were carried out at room temperature over a PANalytical Empyrean diffractometer equipped with a quartz monochromator using a Cu Kα radiation of λ = 1.5419Å within 2θ scan range of 5–90°.

4.2.5 Liquid phase catechol dosing

Catechol was exposed to the pristine and cation-exchanged clay samples (CaMMT, Fe(III)CaMMT, and Cu(II)CaMMT) following a slight modification of previously developed liquid phase dosing protocols.[30,38] Briefly, stock solutions of catechol (85 mM and 170 mM) were prepared in freshly made 0.01 M acetate, 0.01 M MES, 0.01 M Tris and 0.01 M carbonate buffer solutions with pH ranging from 3.4 to 9. Subsequently, 10 mL of buffer solution was added to 500 mg of clay samples contained in a 20 mL borosilicate glass scintillation vial with tightly teflon-lined screw caps for each different pH preparations and the total suspension was left to equilibrate under mechanical shaking (New Brunswick Scientific Classic Series C24KC) at 150 rpm in a

refrigerated incubator shaker for 4 days at 25 °C. Each sample was prepared in triplicate. The suspension was centrifuged at 5000 rpm for 10 min using a Kendro D-37520 Osterode centrifuge with a heraeus #3334 19Krpm rotor. The supernatants were then used to quantify the amount of catechol sorbed via HPLC, while the solid clay residues were dried for 4 days at 40 °C and subjected to radical detection using EPR. All experiments were performed in triplicates under dark conditions by wrapping the vials with aluminum foil.

4.2.6 HPLC analysis

The samples for HPLC analysis were prepared as followed: 200 µL of the resulting supernatant from previously centrifuged catechol dosed CaMMT, Fe(III)CaM and Cu(II)CaM samples was introduced into 8 mL vials containing 5 mL of the corresponding buffer solutions. After thorough shaking using a vortex mixer (Vortex Genie-2), about 1.5 mL of each solution was drawn and filtered into a 1.8 mL amber glass Agilent HPLC vial. A 1100 series Agilent HPLC (Santa Clara, CA) equipped with a reverse phase-C18 analytical column (Zorbax Eclispe XDB, 5 µm $\times$ 4.6 mm $\times$ 150 mm) and a quaternary pump was used to quantify catechol concentration in the solution phase throughout the study. The catechol peak was detected at the optimum absorbance wavelength of 250 nm, as obtained from the UV analysis of 0.001 M catechol solution, with the in-built HPLC ultraviolet-diode array detector. The optimum conditions used for the analysis are stated as follows: a mobile phase of 65:35 (%v/v) of water (pH 3.25 adjusted with 0.05% *o*-phosphoric acid) to acetonitrile, a flow rate of 0.8 mL min^{-1}, and a sample volume of 20 µL. Concentration of catechol adsorbed was calculated by subtracting the catechol in the supernatant solution from the catechol concentration of the control sample, while the adsorbed catechol fraction was determined by dividing the concentration of the adsorbed catechol with the initial catechol concentration. Control experiments were carried out following the same procedure, however, without the clay samples in the scintillation vial, and standards for calibration curves

were prepared at five different concentrations: 0.00168 M, 0.0033 M, 0.0065 M, 0.0096 M, and 0.012 M, respectively.

4.2.7 UV irradiation

UV irradiation of solid-clay particles and in-situ clay-catechol aqueous suspension samples were carried out inside a Model 3940 Series Forma Environmental Chamber, with an arc lamp light source (Newport, Oriel Instruments, USA) equipped with a 150 W xenon lamp. For the in-situ clay-catechol irradiation, 10 mL of each of the four 85 mM catechol solutions (at pH values of 3.4, 5.4, 7.4, and 9.5) was added to 500 mg of clay samples contained in a 20 mL borosilicate glass scintillation vials, the sample set-up was placed 19 cm away from the light source and continuously stirred during irradiation using an overhead stirrer for 6 h, the temperature of the reaction mixture was monitored and observed to fluctuate between 28 °C and 30 °C throughout the experiment. The same experiment was also performed in the dark without the light source at 30 °C for non-irradiated samples. The suspensions were then centrifuged at 5000 rpm for 10 min and the clay residue was dried at 40 °C and used for the EPR radical measurements, while the supernatants were used for catechol quantification.

The UV irradiation of dried solid clay samples was carried out by filling 100 mm long, 4 mm thin wall quartz EPR tubes (707-SQ-100M) with 25 mg of catechol-dosed clay samples (Fe(III)CaMMT and Cu(II)CaMMT) and placed them 34 cm away from the UV light source at different irradiation time intervals ranging from 30 to 360 min at room temperature.

4.2.8 Lifetime studies under controlled humidity

Controlled lifetime studies and relative humidity studies were performed inside a Model 3940 Series Forma Environmental Chamber with the humidity set at 55% and 78% for 4 h daily at 25 °C, after which samples were exposed to ambient air with RH variation between 22 and 56%. All experiments were protected (by wrapping them in aluminum foil and kept in a dark room) from light as much possible in order to minimize photo oxidation. Experiments were performed in

triplicates and the 1/e lifetimes were calculated with pseudo first-order integrated rate law mathematical expression ($\ln(R/R_0) = -kt$, as previously discussed extensively in Chapters 2 and 3.

4.2.9 EPR measurements

The EPR data were collected under similar conditions to those stated in chapter 2 and in previous works.[28,39] Briefly, EPR measurements were performed at room temperature on a dual cavity Bruker EMX 10/2.7 EPR spectrometer. The parameters used for the experiments were: microwave frequency of 9.75 GHz, modulation frequency of 100 kHz, modulation amplitude of 4 G, microwave power of 2.03 mW, receiver gain of 1.0×10^4, sweep width of 150 G and 6000 G, attenuator of 20 dB, sweep time of 41.94 s, time constant of 1.28 ms, conversion time of 20.48 ms, static field of 3460.059 G, center field of 3488.00 G, and a total of 5 scans. EPFR concentration was determined utilizing a 2,2-diphenyl-1-picrylhydrazyl (DPPH) standard.[28,39]

4.3 Results and Discussions

4.3.1 Metal Analyses

Metal concentrations in CaMMT, FeCaMMT, and Cu(II)CaMMT were analyzed with ICP-OES, XRD and EPR. As shown in Table 4.1, prior to cation exchange with Fe(III) and Cu(II), CaMMT contained high concentrations of Ca and Mg, which are considered to be the major interlayer cations in the pristine clay. After cation exchange, for Fe(III)CaMMT, the concentrations of Ca (9763.00 mg/kg) and Mg (9284.50 mg/kg) decreased by 14.55% for Ca and 5.86% for Mg in order to accommodate the Fe(III) ions. For Cu(II)CaMMT, the cation exchange resulted in a 14.72% and 7.16% decrease in Ca and Mg concentrations in order to accommodate the exchanged Cu(II) cation.

Table 4.1 Representing the metal concentrations as obtained by the ICP-OES

Sample/Transition metal Concentration	Ca(mg/kg)	Mg(mg/kg)	Fe(mg/kg)	Cu(mg/kg)
CaMMT	9763.00(±145.66)	9284.50(±67.17)	4390.67(±54.07)	---------
Fe(III)CaMMT	8342.00(±245.66)	8739.50(±314.66)	6487.00(±141.42)	---------
Cu(II)CaMMT	8325.00(±52.33)	8619.50(±218.49)	3885.50(±84.15)	2761.33(±18.45)

The XRD results (*cf* Figure 4.1, A) with an interlayer position, originally at 1.54 nm for CaMMT, being shifted to 1.45 nm and 1.37 nm for Fe(III)CaMMT and Cu(II)CaMMT respectively, which corroborates the ICP-OES results. Similarly, EPR spectra with high and low spin paramagnetic Fe(III) ion peaks at g-values of 4.22 and 2.02 for CaMMT, Fe(III)CaMMT, and Cu(III)CaMMT further confirm the presence of Fe(III). A concentration of 4390.67 mg of Fe per 1 kg of CaMMT represent inherent structural and intercalated Fe(III). For Cu(II)CaMMT, the signals with g-values at $g_{\parallel}$ = 2.33 and $g_{\perp}$ = 2.08 are typical hyperfine signatures of paramagnetic Cu(II) ion. The presence of Fe(III) and Cu(II) provided catalytic templates for EPFR formation.

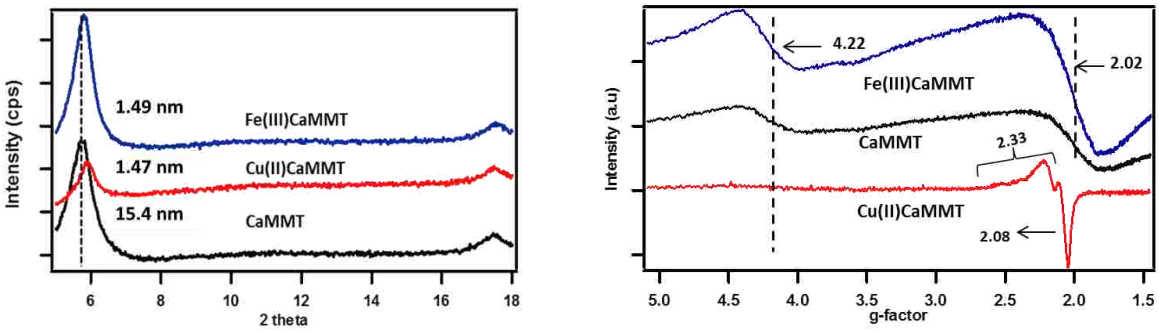

Figure 4.1 (A) XRD and (B) EPR spectra of Fe(III)CaMMT, Cu(II)CaMMT and CaMMT at 6000 G spectra width.

4.3.2 Effect of pH on Catechol Sorption

The sorbed fraction of catechol on CaMMT, Cu(II)CaMMT, and Fe(III)CaMMT was determined using HPLC, with the results presented in Figure 4.2, A. At all the pH values (3.4 –

9.5) the fraction of catechol adsorbed in CaMMT was lower compared to Cu(II)CaMMT and Fe(III)CaMMT samples, indicating the role of the exchanged cations, both Fe(III) and Cu(II), in the sorption of catechol. Catechol is known to adsorb on silica and alumina surfaces [47-51], which could be solely responsible for the detected sorption to CaMMT, in addition to the inherent Fe species. If one now compares the sorption of catechol to Cu(II)CaMMT and Fe(III)CaMMT, it can be seen that a higher fraction of catechol is sorbed to Cu(II)CaMMT. This difference in sorption could be a result of 1) the covalent contribution of the coordinate bond compared the electrostatic bond between Fe(III) and Cu(II) in catechol solution [52], in combination with the possible disintegration of the tris-catechol iron complex to form mono-catechol complexes at higher iron concentrations [53], 2) the slightly larger ionic radius of Cu(II) ion compared to Fe(III) with subsequent higher hydration of Fe(III) ions may pose hindrance to ligation by a catechol molecule, all of which may contribute to the lower catechol sorption to Fe (III) compared to Cu(II) ions. In addition, catechol sorption is observed to increase as pH increases from 6.5 to 9.5; within this pH range bis– and tris– catechol-metal coordination complexes predominate through electrostatic, non-covalent, and covalent bond formation mechanisms[44,55-63] (Scheme 1). Furthermore, the increasing sorption trend of catechol as the pH increases (especially from near neutral to alkaline pH) trend can be attributed to the tendency of catechol deprotonation to occur as the pH increases [22,44, 55-63], since the first pK_a value of catechol is ~9.3.[44] Considering the reaction's duration (4 days), it is possible that the competition between dissociative sorption and electrostatic repulsion[22,60] will limit additional catechol sorption at pH 9.5, resulting in the plateau. Also, it is envisaged that the sorption between pH 7.4 and pH 9.5 may result in the formation of mononuclear monodentate and binuclear bidentate complexes[22,44,55-63], which have been reported to predominate at high pH conditions and can be associated with higher catechol sorption.[57-60,63]

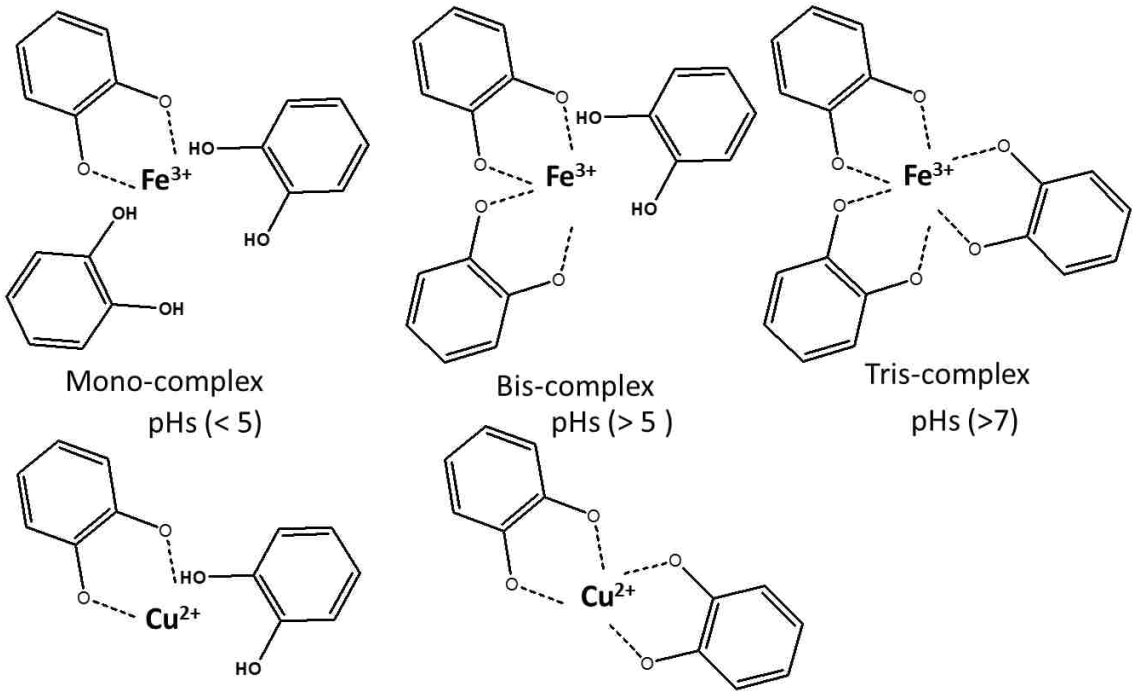

Scheme 4.1. Different types of adsorption modes of catechol on Fe(III) and Cu(II) ions at different pH conditions.

At a low (3.4 - 5.4) pH range, however, the sorption of catechol appears to be clearly lower for all three clay types. The competition for active metal sorption sites between the catechol molecules and the excess protons present at acidic pH can be seen as factors contributing to the lowering of the catechol sorption at these low pH conditions.[67,68] In addition, the excess protons present in acidic conditions can cause the protonation of the hydroxyl groups of the catechol [67], and the subsequent elimination of H_2O, resulting in less catechol being sorbed.[64-68] This may explain the previously reported presence of mono-catecholate iron(III) complex in this pH region.[55-64]

4.3.3 Effects of pH on EPFR formation

The formation of EPFRs on Fe(III)CaMMT and Cu(II)CaMMT is significantly affected by pH, as depicted in Figure 4.2, B and C. The EPR spectra displayed in Figure 4.2, C show a nearly symmetric organic radical peak, signifying the EPFR formation at pH 7.4, for CaMMT,

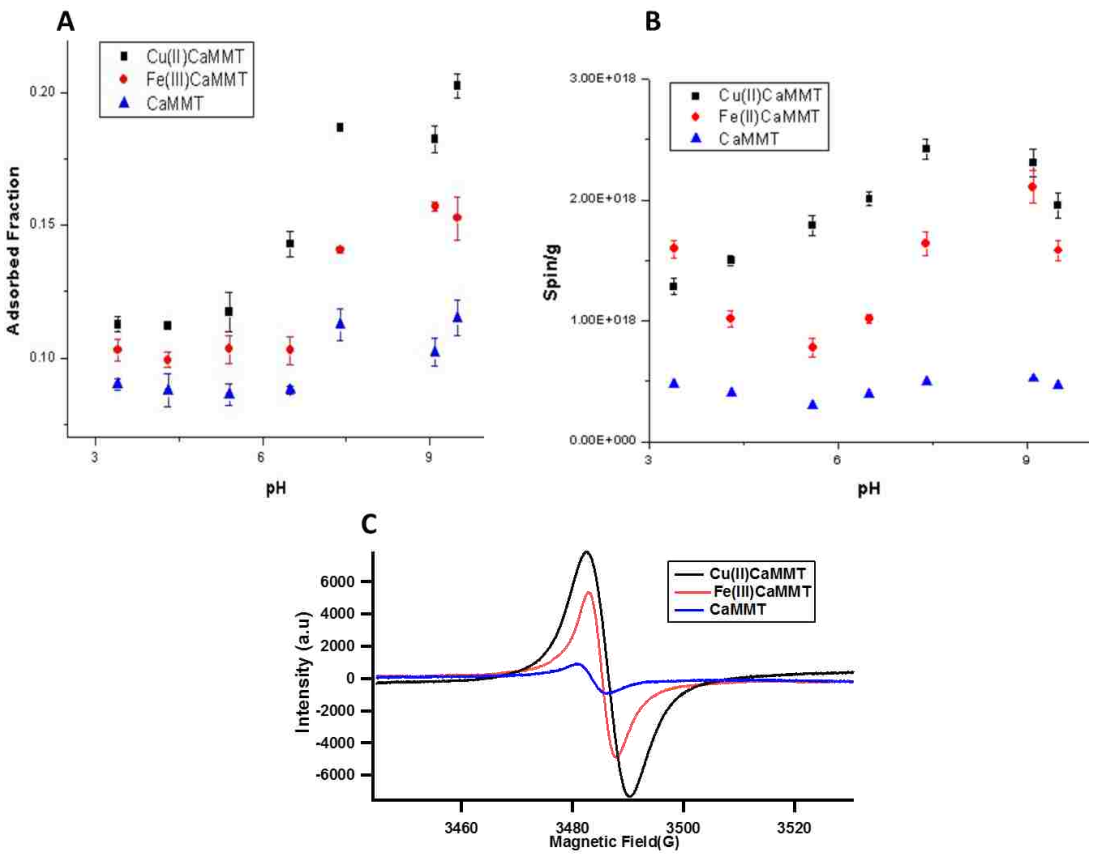

Figure 4.2 (A) Representative EPR spectra of EPFR at pH 7.4, (**B**) Fraction of catechol adsorbed on CaMMT, Fe(III)CaMMT and Cu(II)CaMMT and (**C**) Concentration of EPFR formed at pH 3.4 – pH 9.5.

Fe(III)CaMMT, and Cu(II)CaMMT with a $\Delta H_{p\text{-}p}$ peak-to-peak line width of 4.9, 5.7 and 8.2 and g-values of 2.0034, 2.0038 and 2.0041, respectively. These values are indicative of phenoxyl- and semiqunone-type radicals.3[28,30,38-39,67-69] As previously proposed, the EPFR forming mechanism at play is as follows: the physisorption of catechol to the transition metal, followed by chemisorption and a concurrent one-electron transfer from catechol to the metal redox center. [28,39,69-71] The one-electron transfer from catechol results in the reduction of Fe(III) and Cu(II) to Fe(II) and Cu(I), respectively, within the clay matrix. The presence of inherent (before any cationic exchange) Fe in CaMMT, most of which being Fe(III), could be responsible for the EPFRs formed in CaMMT. No such EPFRs were formed in CaMMT when the organic pollutant was phenol (ref), which could be indicative of the higher reactivity of catechol.

Higher EPFR concentrations were detected for Cu(II)CaMMT in comparison to Fe(III)CaMMT, at all pH conditions except at pH 3.4. This could be a result of the much higher water exchange rate of $[Cu(H_2O)_6]^{2+}$ complexes compared to $[Fe(H_2O)_6]^{3+}$, coupled with the fast self-exchange between Fe(II)-Fe(III) in $[Fe(H_2O)_6]^{3+}$ [72-78], which is almost nonexistent between Cu species. Also, the formation of EPFRs detected in Cu(II)CaMMT (*cf* Figure 4.2, B) follows the sorption trend observed in Figure 4.2, A with an increase in the EPFR concentration being seemingly proportionate to an increase in sorption as the pH increases from 3.4 to 7.4. The highest concentration of EPFRs formed in Cu(II)CaMMT was detected at pH 7.4. The trend, however, differs markedly for Fe(III)CaMMT as the highest concentrations of radicals were detected both under highly acidic (pH 3.4) and basic (pH 7.4 – pH 9.1) conditions. At acidic conditions, especially at pH 3.4 and 4.3, the high EPFR concentration encountered in Fe(III)CaMMT can be envisioned to from via the formation of a mono-coordinated catechol-Fe(III) complex formed through outer-sphere complexation involving electrostatic interactions [20,44,55-61,63] Mono-coordinated metal complexes are known to promote metal redox chemistry, this is due to less complexation of active Fe(III) centers by catechol molecules which can inhibit Fe(III) participation in electron transfer reaction.[22,44,55-57] In addition, studies have shown enhanced rates of dissolution of metal oxides at acidic (pH<5), neutral, and basic pH conditions while in the presence of catechol[20,22,44], which may also help explain the high radical concentration encountered at pH conditions: 3.4 (for Fe only), 7.4, 9.1, and 9.5. Similarly, with prolonged time, more Fe(II) and Cu(I) ions are released into the solution as a consequence of the redox reaction between catechol and active metal ions(Fe(III) and Cu(II)). The higher concentration of Fe(II) and Cu(I) in the solution could be re-oxidized by the semiquinone radical, resulting in the reintroduction of more Fe(III) and Cu(II) ions, which then can form more EPFRs over time (4-days reaction period). Typically, Fe(III) species in aqueous solutions are pH dependent and this may also play an important role in the EPFR formation since the stability and solubility of EPFRs are also affected at different pHs. For instance, up to three different Fe(III) species can exist at acidic pH

between 2.5 – 5, namely; $Fe(OH)^{2+}$, and $Fe(OH)_2^{+}$ and $Fe(OH)_3$.[36,80-86] Although $Fe(OH)^{2+}$ is the most dominant species among the three Fe(III) species, all of the above species exhibit different solubilities and rapid switches in stability as the pH changes.[36,80] This means that their interaction with catechol molecules in solution is bound to be affected. In fact, the low concentration of EPFRs encountered at pH 5.4 could be associated with the diminished concentration of $Fe(OH)^{2+}$ at pH 5. At pH >5, the precipitation and formation of polynuclear polymeric Fe(III) species begins to occur[36],[80] and, in doing so, may limit the amount of Fe(III) centers available for reduction, lowering the amount of EPFRs formed at pH 5.4.

At basic pH, both inner-sphere and outer-sphere complexations are responsible for both the sorption of catechol and EPFRs formamtion[20,23], however, for the EPFR formation, the inner-sphere complexation seems to be the dominant mechanism at play. This is due to the increasing catechol metal interaction as the pHs approaches alkalinity, which enables direct electron transfer through covalent and electrostatic bonds. Once surface saturation is achieved, inhibiting more inner-sphere interactions between catechol and the metal centers, redox activities is largely reduced. This explanation is consistent with the high radical concentrations detected from pH 7.4 to 9.1 and may also explain the gradual decrease in EPFR concentrations observed at pHs 9.1 and 9.5 for Fe(III)CaMMT and Cu(II)CaMMT systems respectively. Another plausible explanation is the saturation of active metal sites due to higher complexation rates as the pH tends towards catechol's first pK_a value[20,22,55], which in turn can induce crowding of sorbed catechol molecules, easily facilitating radical polymerization to yield other polyphenols. It is also worthwhile to note that, in alkaline solutions, catechol is susceptible to auto-oxidation, which has been shown to lead to the formation of quinones.[55] Quinones, which have lower affinity to Cu(II) and Fe(III) than catechol,[55] reduce EPFR formation.

Parameters such as the g-value and peak-to-peak line width $\Delta H_{p\text{-}p}$ were also useful in understanding the constituents of the EPFRs formed in the both Fe(III)CaMMT and Cu(II)CaMMT

systems at different pH conditions. For instance, the g-values of EPFRs formed in Fe(III)CaMMT and Cu(II)CaMMT increased from 2.0036 to 2.0046 as the pH increased from 3.4 to 9.5. This implies that phenoxyl radical and/or carbon centered radicals dominate EPFRs detected in at acidic pHs, where phenoxyl radical formation from catechol has been described to result from the decomposition of semiquinone radical.[88,89] Conversely, with increasing pH, oxygen centered semiquninone radicals become more dominant in Fe(III)CaMMT and Cu(II)CaMMT as indicated by the high g-factor. In addition to the g-factor, the peak width values ranged between ~7.0 and 9.0 for Cu(II)CaMMT and from ~5.1 to 6.4 for Fe(III)CaMMT. Indicating the presence of variable radical constituents, an effect that can lead to concentration broadening.[69] The peaks were broader at low pHs for Cu(II)CaMMT compared with Fe(III)CaMMT. Scheme 1 proposes the general mechanism for EPFRs formed for both Fe(III)CaMMT and Cu(II)CaMMT. This scheme simply shows that mono-catechol metal complexes may be responsible for the EPFRs formed at acidic pHs (below 5.4), however, the bi-complex and tris- catechol complexes are likely to be the parent complexes for EPFRs formed at pH 7.4, 9.1 and 9.5 respectively in relation to the g-factors and line widths observed.

4.3.4 Effect of Irradiation on EPFR Formation

4.3.4.1 Liquid-Solid Phase Irradiation

To understand the effects of UV irradiation on the EPFR formation in aqueous phase, Fe(III)CaMMT and Cu(II)CaMMT samples were irradiated for 6 h during EPFR formation *in situ* at four different pH values (3.4, 5.4, 7.4 and 9.5). The experiments were repeated by stirring the samples under a hot plate set at 30 °C for 6 h in the dark. For these experiments, a reduced concentration of catechol (85 mM) was utilized in order to minimize catechol photo-oxidation. As illustrated in Figure 4.3, for the Fe(III)CaMMT and Cu(II)CaMMT at both acidic pH conditions, the UV irradiated samples adsorbed less catechol compared to their non-UV irradiated counterparts, while the reverse was the case at higher pH (7.4 and 9.5). Also, similarly to the result obtained

with the non-UV catalyzed EPFR system above (*cf* Figure 4.2, A), catechol adsorption was higher for the Cu-loaded systems than for the Fe-loaded ones.

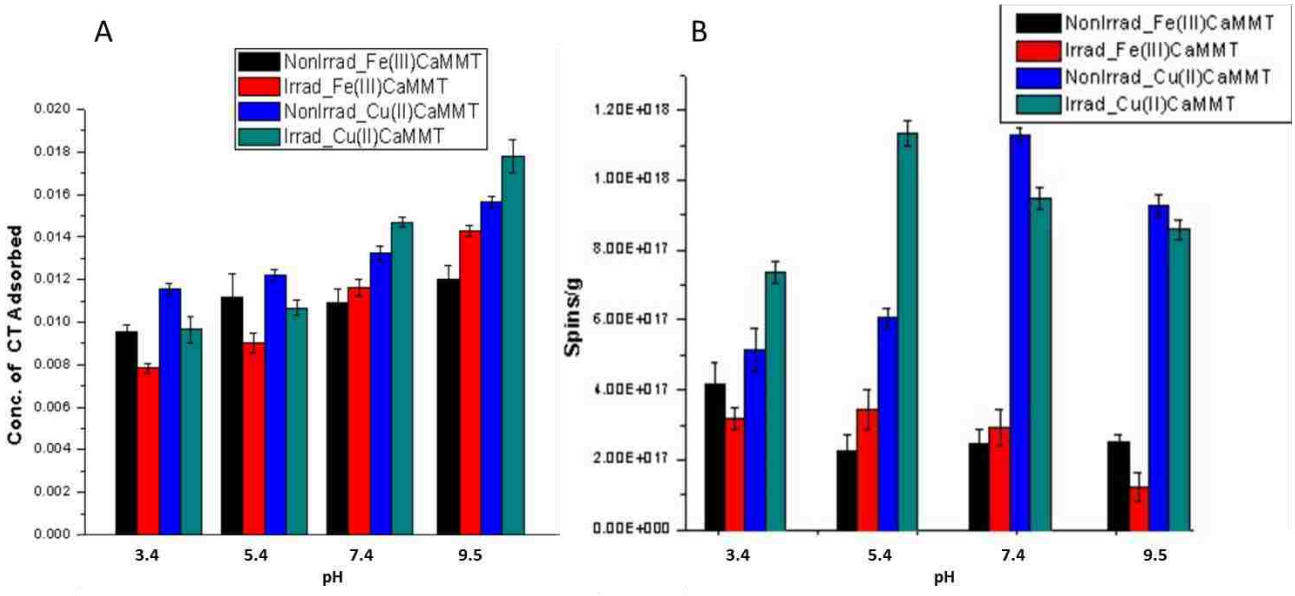

Figure 4.3 A) concentration of adsorbed catechol and B) EPFRs formed on non-UV irradiated and UV irradiated Fe(III)CaMMT and Cu(II)CaMMT samples. Reaction period for both UV Irradiation and non-UV irradiation (in the dark) was 6 h.

The reduced catechol sorption on Cu(II)CaMMT and Fe(III)CaMMT at pH 7.4 and pH 9.5 may be viewed as a result of the UV-facilitated oxidation of catechol to hydroquinone and, subsequently, to benzoquinone, and even more importantly, as a result of the formation of other polymeric products through radical-radical coupling induced by the EPFRs formed over time. Similar reaction occurs at low pH, however, due to the unstable nature of catechol-metal complex at acidic pH conditions, there is a strong probability of regeneration of catechol in the solution, which may account for the low catechol sorption witnessed at pH 3.4 and 5.4.

More importantly, photo-Fenton chemistry is known to reach optimum efficiency at acidic pH between 3.0 and 3.5 [36,81-86,90-91] by the generation of excess •OH radical through the photolysis of $Fe(OH)^{2+}$. Furthermore, the high concentrations of H^+ at acidic pH conditions facilitate the formation of more •OH radicals. [92] With high concentration of •OH radicals, catechol molecules in

solution are ultimately degraded, leading to the reduced catechol concentration in the solution and a decrease in the amount of sorbed catechol. As seen in Figure 4.3 for Fe(III)CaMMT, a reduced yield in the EPFR concentration was detected at pH values of 3.4 7.4, and 9.5. for the UV-irradiated systems. The same was encountered for Cu(II)CaMMT except that UV-irradiation caused a higher EPFR generation at pH 3.4. Remarkably, at pH 5.4 for the UV-irradiated Fe(II)CaMMT and Cu(II)CaMMT systems, higher EPFR generation was recorded compared to the non-UV irradiated. These observations can be explained in number of ways; first, the reduced EPFR formation in the UV-irradiated systems, as seen at pH 3.4, 7.4, and 9.5 for Fe(III)CaMMT, could be a result of the additional •OH radical generation through photo-Fenton reaction which may 1) degrade the available catechol in solution, therefore limiting catechol's reaction with the metal centers and/or 2) readily recombine with formed EPFRs, thus diminishing the EPFR yield. Photo-Fenton chemistry also results in the release of Fe(II) ions and other intermediate products.[33,36,81,83] The Fe(II) species released into the solution promote •OH generation at basic pH conditions, which are amenable to the formation of catechol-metal complexes that facilitate Fenton chemistry. An increased EPFR formation encountered at pH 5.4 for Fe(II)CaMMT and Cu(II)CaMMT may be attributed to the gradual disappearance of the very photo-Fenton dominant active $Fe(OH)^{2+}$ and the formation of polymeric Fe(III) species with lower photo-Fenton activity. Generally, Fenton chemistry is known to be accelerated by UV irradiation[33,36,81,83], as well as affected by pH. The generation of Fe(II) is rapidly enhanced at acidic pHs in the presence of catechol. Pignatello and co-workers reported the generation •OH radical at acidic pHs[36,83], justifying the lower EPFR concentration at pH 3.4 in the UV-irradiated system. This suggests the possible quenching of the formed EPFRs in solution over an extended reaction period. In fact, aside from the •OH radicals generated from the reduction of EPFRs, more •OH radicals can be generated through UV irradiation of Fe(III) ions in solution at acidic pH.[33,36,81-85] Similarly, with increasing pH, UV irradiation may accelerate the dissociation of catechol, the especially at high

pH conditions (7.4 and 9.5).[79,93] This may also account for the reduced amount of EPFRs encountered at those pHs.

4.3.4.2 Solid Phase UV Irradiation

The solid phase UV irradiation experiments were performed in an effort to understand the effect of ambient sunlight on EPFRs after they had been formed on Fe(III)CaMMT and Cu(II)CaMMT, in such environmental matrices as surface soils and wind-blown dust. Fe(III)CaMMT and Cu(II)CaMMT samples were chosen for being representative of the types of entities typically found in samples of the real Superfund contaminated soils. The effects of UV irradiation on dried solid clay samples were studied by exposing 25 mg of Fe(III)CaMMT and Cu(II)CaMMT containing EPFRs to UV irradiation for 30 to 360 min, the concentration of the radicals was normalized to the initial radical concentration before irradiation. As indicated in Figure 4.4, exposure of Fe(III)CaMMT and Cu(II)CaMMT to UV light caused an initial increase in radical formation at the studied pH values (3.4, 5.4, 7.4, and 9.5). The highest radical concentrations after irradiation were observed at pH 9.5 after 180 min for Fe(III)CaMMT and at pH 3.5 after 30 min for Cu(II)CaMMT, with an increase of ~16% and 11% over the non-irradiated controls, respectively.

Two distinct trends observations were made; first, the radicals formed due to UV irradiation in Fe(III)CaMMT and Cu(II)CaMMT after catechol dosing at both pH 7.4 and pH 9.5 remained relatively stable throughout the irradiation time after attaining their respective peak concentrations, whereas the radicals formed in the systems after catechol dosing pH 3.4 and pH 5.4 decreased swiftly with increasing irradiation time longer than 180 min. This observation suggests that there could be a stabilizing mechanism in place for the EPFRs formed at pH values of 7.5 and 9.5. This trend has been previously reported to be as a result of the stability afforded by the transition metal ions[30,38] in this case Fe(II) and Cu(I). Secondly, the increase in radical concentration due to UV irradiation was higher for the Fe(III)CaMMT systems than for the

Cu(II)CaMMT systems at pH 7.4 and 9.5. This later trend may suggest the presence of higher degree of unreacted catechol in Fe(III)CaMMT systems compared to Cu(II)CaMMT systems, allowing the unreacted catechol and other degraded products to be further photo-oxidized via interactions with unreacted Fe(III) and Cu(II) centers and form additional radical species.[94] No significant changes were observed in the g-factors for Fe(III)CaMMT after irradiation; however, a slight change in the g-factor (2.0038 to 2.0040) was observed for the radicals formed as a result of irradiation of the Cu(II)CaMMT system at pH 7.4. This may be as a result of the formation of more semiquinone type radical.

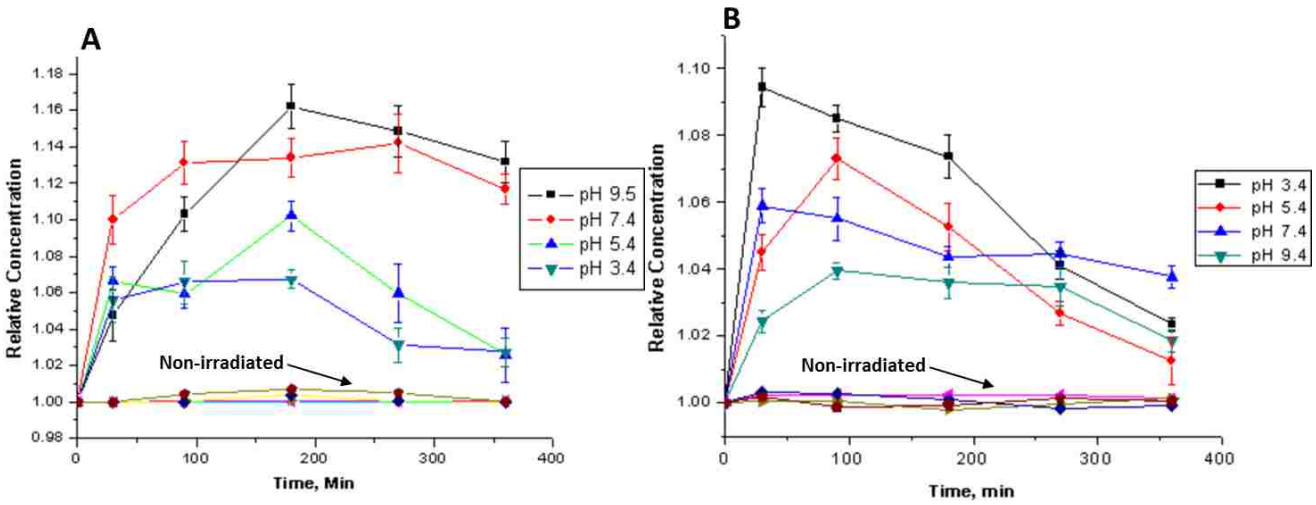

Figure 4.4 Solid-phase UV irradiated samples of A) Fe(III)CaMMT, B) and Cu(II)CaMMT EPFRs. For EPFRs formed at pH conditions of 3.4, 5.4, 7.4, and 9.5 at room temperature

It is also worthwhile to mention that radical decay was observed for Fe(III)CaMMT and Cu(II)CaMMT after prolonged UV irradiation, especially beyond 360 min which can be attributed to the radical recombination.[28,39,41] In Fe(III)CaMMT and Cu(II)CaMMT, relatively stable radicals are observed when monitored in the dark over the time period, as seen in Figure 4.4, A and B (Shown with arrows), and thus these radicals can be classified as EPFRs.

A more detailed look at the results shown in Figure 4.5, shows that the maximum radical decay is ~4% for Cu(II)CaMMT system at pH 3.4 after 12 h. After the same amount of time and

at pH 5.4, the radicals formed in Cu(II)CaMMT and Fe(III)CaMMT showed a decay amounting to ~1.5% and ~4.0%, respectively. On the other hand, UV irradiation-formed radicals at pH 7.4 and pH 9.5 in the Fe(III)CaMMT and Cu(II)CaMMT systems did not show significant decays. In fact, slight increases in radical concentrations are observed especially for the Fe(III)CaMMT systems. Overall, the results from this study illustrate that UV irradiation can increase the concentration of radicals in samples which were dosed with catechol at basic pHs and that these radicals are stable enough to be called EPFRs; however, prolonged (>6 h) UV irradiation induces radical decay, which is best illustrated by the Cu(II)CaMMT systems with acidic catechol dosing.

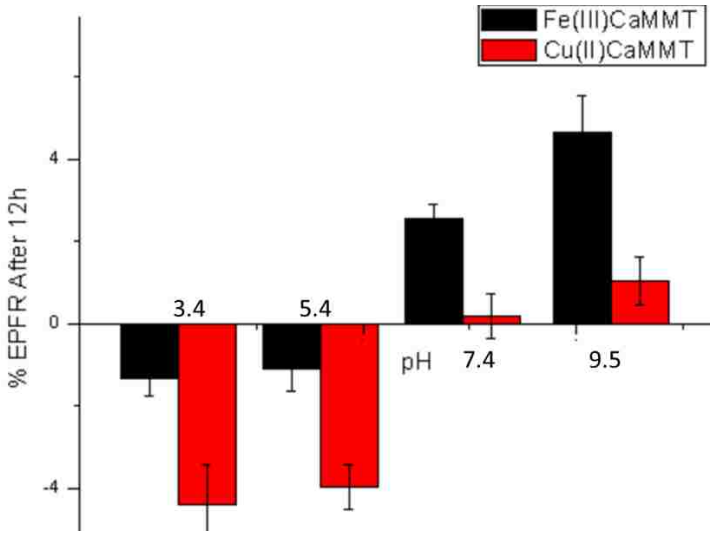

Figure 4.5 Percentage of EPFRs remaining after 12 h in the dark, following previous 6 h long UV irradiation of the Cu(II)CaMMT and Fe(III)CaMMT samples at pH values of 3.4, 5.4, 7.4, and 9.5.

4.3.5 EPFR Decay and Effects of Humidity

The stability and persistency of radicals formed in Fe(III)CaMMT and Cu(II)CaMMT at four different pHs (3.4, 5.4, 7.4, and 9.5) at different levels of humidity were studied and the results, in terms of lifetimes, are presented in Figure 4.6.

For the Cu(II)CaMMT EPFRs formed at 55 % RH, the following lifetimes were determined at 85.0, 91.6,143.2 and 128.6 days while at 78% RH the lifetimes were 3.1, 2.6, 4.8, and 6.7 days

for EPFRs formed at pH 3.4, 5.4, 7.4, and 9.5, respectively. Similarly, the decay rates for EPFRs at 55% RH at pH 3.4, 5.4, 7.4, and 9.5, were 0.000291 h^{-1}, 0.000324 h^{-1}, 0.000455 h^{-1} and 0.000490 h^{-1}, respectively. The corresponding decay rates at 78% RH were 21.3, 26.7, 32.7, and 27.4 times faster compared to those at 55% RH At both humidity conditions, the g-factor during the EPFR decay increased from ~2.0038 (mostly at acidic pHs) to 2.0044.

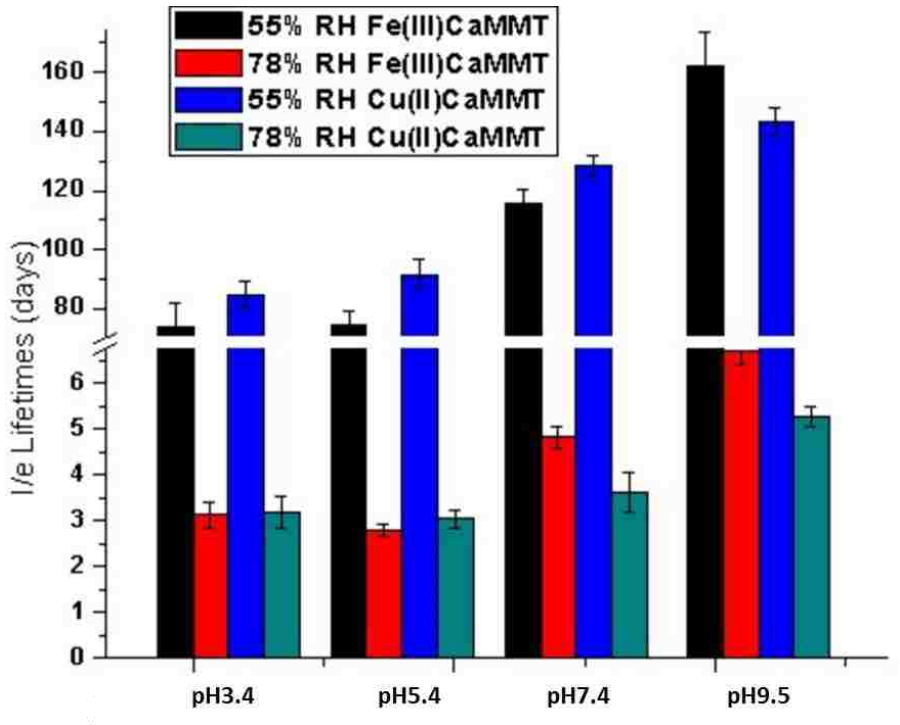

Figure 4.6 EPFR decay study for A) Fe(III)CaMMT and B) Cu(II)CaMMT, at 55% and 75 % Relative humidity (RH) at pH 3.4, 5.4, 7.4, and 9.5.

This observed increase in the g-factor has been previously attributed to the faster decay of phenoxyl-type radical.[28,39] However, as previously reported, EPFRs can decay through the desorption of organic molecules from metal surfaces aided by water molecules and/or recombination with molecular oxygen.[28,39,41] It may then be reasonable to suggest that the EPFRs formed in monodentate mononuclear catechol complexes will decay faster than those formed in monodentate binuclear, bidentate mononuclear and/or bidentate binuclear complexes. This is due to the ease with which the metal-organic molecule bond is accessed by water molecules. As a

result, the water accessible EPFR complexes may decay faster, as supported by high g-factors encountered after elongated exposure of EPFRs to humid conditions and ambient air. Also, at

both humidity conditions, higher EPFR lifetimes and lower decay rates were obtained for EPFRs formed at basic pHs (7.4 and 9.5) compared to acidic pHs (3.4 and 5.4). In addition to the metal-catechol complex structure and type, which may, in turn, dictate radical type, the π-π stacking interactions between aromatic molecules can be responsible for the EPFR stability encountered at pH 7.4 and pH 9.5, especially at 55% RH.[39,41]

For EPFRs formed in Fe(III)CaMMT, the decay rate and lifetimes showed similar behavior to those seen for Cu(II)CaMMT at both humidity conditions. At 55% RH, lifetimes of 162.3, 115.7, 74.3, and 73.8 days were observed for EPFRs formed at pHs 3.4, 5.4, 7.4, and 9.5, respectively, with the corresponding decay rates of 0.000257 h^{-1}, 0.000360 h^{-1}, 0.000561 h^{-1}, and 0.000565 h^{-1}. At 78% RH, EPFRs formed at pHs 3.4, 5.4, 7.4, and 9.5 had lifetimes of 6.7, 4.8, 2.8, and 3.1, respectively, accompanied by decay rates of 0.00622 h^{-1}, 0.00868 h^{-1}, 0.0149 h^{-1}, and 0.0134 h^{-1}, respectively. Thus, as was the case with the Cu(II)CaMMT systems, the decay rates and lifetimes of EPFRs formed at pHs 7.4 and 9.5 were higher than those formed at acidic pHs. The lifetimes of the EPFRs formed in Fe(III)CaMMT at pH 9.5 were higher at both humidity conditions in comparison to those obtained for EPFRs formed on Cu(II)CaMMT. This suggests that tris-complexes (scheme 4.1) formed by Fe species at alkaline conditions offers higher stability through π-π stacking, making them more resistant to oxidation and desorption by molecular oxygen or water molecules than EPFRs formed on Cu(II)CaMMT, which forms mostly bis-complexes.[22,55-59] The opposite explains the results for EPFRs formed at acidic conditions on both Fe(III)CaMMT and Cu(II)CaMMT, where the lower lifetimes encountered are justified by an increased molecular oxygen and water molecule accessibility. This due to the mono-catechol metal complexes that usually form at acidic pHs, hence lower degree of surface complexation.

4.4 Conclusion

In summary, ambient environmental and soil conditions play an important role in the formation and persistence of EPFRs. For the Fe(III)CaMMT systems, acidic (pH 3.4) and alkaline pHs favors the formation of EPFRs with highest concentration at 9.1, while for the Cu(II)CaMMT systems, the highest EPFRs concentration was at pH 7.4. high EPFRs concentrations with acidic pHs being the least favorable for EPFR formation. Generally, the redox activities of the transition metals and catechol are promoted through the high degree of metal-catechol complexation that occurs at neutral and alkaline pHs, which in turn favors EPFR formation.[44,93] Simulated sunlight using UV irradiation showed the effect of UV on the EPFRs forming process in Fe(III)CaMMT and Cu(II)CaMMT systems. UV irradiation caused EPFRs formation for Fe(III)CaMMT (except at pH 5.4) and Cu(II)CaMMT (at pHs 7.4 and 9.5) systems. Photo-Fenton chemistry which causes the degradation of catechol in solutions, especially at acidic pHs, and photolysis of Fe species are put forward as being responsible for the reduced EPFRs formation under UV irradiation. While accelerated sorption and photo-oxidation of catechol and catechol-metals complexes at alkaline pH may likely contribute to the reduced EPFRs formation at pHs 7.4 and 9.5.

Also, irradiated after EPFR formation—increased the EPFRs formation for both Fe(III)CaMMT and Cu(II)CaMMT systems, with the increase be higher in Fe(III)CaMMT. At neutral and alkaline pH, the irradtion formed radicals were stable through 360 minutes, and thus EPFRs, however at acid pHs irradiation formed radicals were not as stable. This can be attributed to the stability offered by the π-π stacking aromatic backbone abundant with the high metal - catechol complex at pHs 7.4 and 9.5, which stabilizes the formed EPFRs. Our results also suggest that direct UV radiation effect the redox behavior of the metal which in turn resulted in the radical decay observed after prolonged UV irradiation, especially for radicals formed at pHs 3.4 and 5.4 due to the complexation and adsorption behavior of catechol–metal complexes at those pHs. Irradiation of already formed EPFRs under dry conditions results in radical formation over the

short course but may induce radical decay over the long course, especially in Cu(II)CaMMT systems and Fe(III)CaMMT system under acidic conditions.

Finally, humidity affects the persistence of EPFRs formed on Fe(III)CaMMT and Cu(II)CaMMT. EPFRs formed at close to neutral and alkaline pHs (7.4 and 9.5) were more stable and persistent to oxidation than EPFRs formed at acidic pHs (3.4 and 5.4) at both 55 and 78% RH. This can also be attributed to a high degree of catechol complex on the metals which could block possible oxidation site by environmental oxygen and also making it difficult for desorption by water molecules in the case of 78 % RH.

The findings in this research demonstrates that in ambient environment where EPFRs are known to form in contaminated soil similar to the one previously detected at superfund sites, factors such as the ones contained in this study (UV, pH and Humidity) are bound to play a huge role in the fate of the EPFRs formed. Thus, in the contaminated soil, EPFRs are likely to form more in arid alkaline soils which are usually known with high mineral contents. However, even in low pH peat soils, with ubiquitous presence of Fe(III) in the soil high EPFRs level is inevitable. Also the results of this research shows that at periods of high precipitation, EPFRs formation is may be enormously reduced. Ultimately, EPFRs contamination arises from wind-blown dust particles of these contaminated soils which can be ingested or inhaled by humans.

4.5 References

1. Vasseur, P.; Bonnard, M.; Palais, F.; Eom, I. C.; Morel, J. L., Bioavailability of chemical pollutants in contaminated soils and pitfalls of chemical analyses in hazard assessment. *Environmental Toxicology* **2008,** *23* (5), 652-656.

2. Meijer, S. N.; Ockenden, W. A.; Sweetman, A.; Breivik, K.; Grimalt, J. O.; Jones, K. C., Global Distribution and Budget of PCBs and HCB in Background Surface Soils: Implications for Sources and Environmental Processes. *Environmental Science & Technology* **2003,** *37* (4), 667-672.

3. Meijer, S. N.; Steinnes, E.; Ockenden, W. A.; Jones, K. C., Influence of Environmental Variables on the Spatial Distribution of PCBs in Norwegian and U.K. Soils: Implications for Global Cycling. *Environmental Science & Technology* **2002,** *36* (10), 2146-2153.

4. Schuster, J. K.; Gioia, R.; Moeckel, C.; Agarwal, T.; Bucheli, T. D.; Breivik, K.; Steinnes, E.; Jones, K. C., Has the Burden and Distribution of PCBs and PBDEs Changed in European Background Soils between 1998 and 2008? Implications for Sources and Processes. *Environmental Science & Technology* **2011,** *45* (17), 7291-7297.

5. Doick, K. J.; Klingelmann, E.; Burauel, P.; Jones, K. C.; Semple, K. T., Long-Term Fate of Polychlorinated Biphenyls and Polycyclic Aromatic Hydrocarbons in an Agricultural Soil. *Environmental Science & Technology* **2005,** *39* (10), 3663-3670.

6. Gramatica, P.; Papa, E., Screening and Ranking of POPs for Global Half-Life: QSAR Approaches for Prioritization Based on Molecular Structure. *Environmental Science & Technology* **2007,** *41* (8), 2833-2839.

7. Kim, U.-J.; Yen, N. T. H.; Oh, J.-E., Hydroxylated, Methoxylated, and Parent Polybrominated Diphenyl Ethers (PBDEs) in the Inland Environment, Korea, and Potential OH- and MeO-BDE Source. *Environmental Science & Technology* **2014,** *48* (13), 7245-7253.

8 Jaligama, S.; Chen, Z.; Saravia, J.; Yadav, N.; Lomnicki, S. M.; Dugas, T. R.; Cormier, S. A., Exposure to Deepwater Horizon Crude Oil Burnoff Particulate Matter Induces Pulmonary Inflammation and Alters Adaptive Immune Response. *Environmental Science & Technology* **2015,** *49* (14), 8769-8776.

9. Truong, H.; Lomnicki, S.; Dellinger, B., Potential for Misidentification of Environmentally Persistent Free Radicals as Molecular Pollutants in Particulate Matter. *Environmental Science & Technology* **2010,** *44* (6), 1933-1939.

10. dela Cruz, A. L. N.; Cook, R. L.; Dellinger, B.; Lomnicki, S. M.; Donnelly, K. C.; Kelley, M. A.; Cosgriff, D., Assessment of environmentally persistent free radicals in soils and sediments from three Superfund sites. *Environmental Science: Processes & Impacts* **2014,** *16* (1), 44-52.

11. Dugas, T.; Lomnicki, S.; Cormier, S.; Dellinger, B.; Reams, M., Addressing Emerging Risks: Scientific and Regulatory Challenges Associated with Environmentally Persistent Free Radicals. *International Journal of Environmental Research and Public Health* **2016,** *13* (6), 573.

12. Boyd, S. A.; Mortland, M. M., Dioxin radical formation and polymerization on Cu(II)-smectite. *Nature* **1985,** *316* (6028), 532-535.

13. Gu, C.; Liu, C.; Ding, Y.; Li, H.; Teppen, B. J.; Johnston, C. T.; Boyd, S. A., Clay mediated route to natural formation of Polychlorodibenzo-p-dioxins. *Environ Sci Technol* **2011,** *45* (8), 3445-51.

14. Bronner, G.; Goss, K.-U., Sorption of Organic Chemicals to Soil Organic Matter: Influence of Soil Variability and pH Dependence. *Environmental Science & Technology* **2011,** *45* (4), 1307-1312.

15. de Boer, T. E.; Taş, N.; Braster, M.; Temminghoff, E. J. M.; Röling, W. F. M.; Roelofs, D., The Influence of Long-Term Copper Contaminated Agricultural Soil at Different pH Levels on Microbial Communities and Springtail Transcriptional Regulation. *Environmental Science & Technology* **2012,** *46* (1), 60-68.

16. Brown, M.; Sutherland, M.; Leharne, S., The effect of pH and chloride ion concentration on the mobilities of various cations in soil. *Journal of Chemical Education* **1987,** *64* (5), 448.

17. Laird, D. A.; Yen, P. Y.; Koskinen, W. C.; Steinheimer, T. R.; Dowdy, R. H., Sorption of atrazine on Soil Clay Components. *Environmental Science & Technology* **1994,** *28* (6), 1054-1061.

18. Paul, A.; Stösser, R.; Zehl, A.; Zwirnmann, E.; Vogt, R. D.; Steinberg, C. E. W., Nature and Abundance of Organic Radicals in Natural Organic Matter: Effect of pH and Irradiation. *Environmental Science & Technology* **2006,** *40* (19), 5897-5903.

19. Buerge, I. J.; Poiger, T.; Müller, M. D.; Buser, H.-R., Influence of pH on the Stereoselective Degradation of the Fungicides Epoxiconazole and Cyproconazole in Soils. *Environmental Science & Technology* **2006,** *40* (17), 5443-5450.

20. Gulley-Stahl, H.; Hogan, P. A.; Schmidt, W. L.; Wall, S. J.; Buhrlage, A.; Bullen, H. A., Surface Complexation of Catechol to Metal Oxides: An ATR-FTIR, Adsorption, and Dissolution Study. *Environmental Science & Technology* **2010,** *44* (11), 4116-4121.

21. Suresh, S.; Srivastava, V. C.; Mishra, I. M., Adsorption of catechol, resorcinol, hydroquinone, and their derivatives: a review. *International Journal of Energy and Environmental Engineering* **2012,** *3* (1), 1-19.

22. Al-Abadleh, H. A., Review of the bulk and surface chemistry of iron in atmospherically relevant systems containing humic-like substances. *RSC Advances* **2015,** *5* (57), 45785-45811.

23. Bahri, S.; Jonsson, C. M.; Jonsson, C. L.; Azzolini, D.; Sverjensky, D. A.; Hazen, R. M., Adsorption and Surface Complexation Study of L-DOPA on Rutile (α-TiO2) in NaCl Solutions. *Environmental Science & Technology* **2011,** *45* (9), 3959-3966.

24. Rodríguez, R.; Blesa, M. A.; Regazzoni, A. E., Surface Complexation at the TiO2(anatase)/Aqueous Solution Interface: Chemisorption of Catechol. *Journal of Colloid and Interface Science* **1996,** *177* (1), 122-131.

25. Price, G.; Australian Soil Fertility Manual, 3rd ed.; CSIRO Publishing, 2006; Chapter 2, pp 11.

26. Yang, W.; Holmén, B. A., Relative Effects of Surfactants and Humidity on Soil/Air Desorption of Chloroacetanilide and Dinitroaniline Herbicides. *Environmental Science & Technology* **2008,** *42* (18), 6843-6848.

27. Yang, W.; Holmén, B. A., Effects of Relative Humidity on Chloroacetanilide and Dinitroaniline Herbicide Desorption from Agricultural PM2.5 on Quartz Fiber Filters. *Environmental Science & Technology* **2007,** *41* (11), 3843-3849.

28. Nwosu, U. G.; Roy, A.; dela Cruz, A. L. N.; Dellinger, B.; Cook, R., Formation of environmentally persistent free radical (EPFR) in iron(iii) cation-exchanged smectite clay. *Environmental Science: Processes & Impacts* **2016,** *18* (1), 42-50.

29. Tao, X.; Ma, W.; Zhang, T.; Zhao, J., Efficient Photooxidative Degradation of Organic Compounds in the Presence of Iron Tetrasulfophthalocyanine under Visible Light Irradiation. *Angewandte Chemie International Edition* **2001,** *40* (16), 3014-3016.

30. Li, H.; Guo, H.; Pan, B.; Liao, S.; Zhang, D.; Yang, X.; Min, C.; Xing, B., Catechol degradation on hematite/silica-gas interface as affected by gas composition and the formation of environmentally persistent free radicals. *Scientific reports* **2016,** *6*, 24494.

31. ukushima, M.; Tatsumi, K., Degradation Pathways of Pentachlorophenol by Photo-Fenton Systems in the Presence of Iron(III), Humic Acid, and Hydrogen Peroxide. *Environmental Science & Technology* **2001,** *35* (9), 1771-1778.

32. Lan, Q.; Li, F.; Liu, C.; Li, X.-Z., Heterogeneous Photodegradation of Pentachlorophenol with Maghemite and Oxalate under UV Illumination. *Environmental Science & Technology* **2008,** *42* (21), 7918-7923.

33. Feng, H. M.; Zheng, J. C.; Lei, N. Y.; Yu, L.; Kong, K. H.; Yu, H. Q.; Lau, T. C.; Lam, M. H., Photoassisted Fenton degradation of polystyrene. *Environ Sci Technol* **2011,** *45* (2), 744-50.

34. Rajesh, J. T.; Praveen, K. S.; Ramchandra, G. K.; Raksh, V. J., Photocatalytic degradation of dyes and organic contaminants in water using nanocrystalline anatase and rutile TiO 2. *Science and Technology of Advanced Materials* **2007,** *8* (6), 455.

35. Ghiselli, G.; Jardim, W. F.; Litter, M. I.; Mansilla, H. D., Destruction of EDTA using Fenton and photo-Fenton-like reactions under UV-A irradiation. *Journal of Photochemistry and Photobiology A: Chemistry* **2004,** *167* (1), 59-67.

36. Pignatello, J. J.; Oliveros, E.; MacKay, A., Advanced Oxidation Processes for Organic Contaminant Destruction Based on the Fenton Reaction and Related Chemistry. *Critical Reviews in Environmental Science and Technology* **2006,** *36* (1), 1-84.

37. Jia, H.; Nulaji, G.; Gao, H.; Wang, F.; Zhu, Y.; Wang, C., Formation and Stabilization of Environmentally Persistent Free Radicals Induced by the Interaction of Anthracene with Fe(III)-Modified Clays. *Environ Sci Technol* **2016,** *50* (12), 6310-9.

38. Li, H.; Pan, B.; Liao, S.; Zhang, D.; Xing, B., Formation of environmentally persistent free radicals as the mechanism for reduced catechol degradation on hematite-silica surface under UV irradiation. *Environmental Pollution* **2014,** *188*, 153-158.

39. Nwosu, U. G.; Khachatryan, L.; Youm, S. G.; Roy, A.; Dela Cruz, A. L.; Nesterov, E. E.; Dellinger, B. H.; Cook, R. L., Model System Study of Environmentally Persistent Free Radicals Formation in a Semiconducting Polymer Modified Copper Clay System at Ambient Temperature. *RSC Advances* **2016**.

40. dela Cruz, A. L. N.; Gehling, W.; Lomnicki, S.; Cook, R.; Dellinger, B., Detection of Environmentally Persistent Free Radicals at a Superfund Wood Treating Site. *Environmental Science & Technology* **2011,** *45* (15), 6356-6365.

41. Cruz, A. L. N. d.; Cook, R. L.; Lomnicki, S. M.; Dellinger, B., Effect of Low Temperature Thermal Treatment on Soils Contaminated with Pentachlorophenol and Environmentally Persistent Free Radicals. *Environmental Science & Technology* **2012,** *46* (11), 5971-5978.

42. dela Cruz, A. L. N.; Cook, R. L.; Dellinger, B.; Lomnicki, S. M.; Donnelly, K. C.; Kelley, M. A.; Cosgriff, D., Assessment of environmentally persistent free radicals in soils and sediments from three Superfund sites. *Environmental Science: Processes & Impacts* **2014,** *16* (1), 44-52.

43. Kasozi, G. N.; Zimmerman, A. R.; Nkedi-Kizza, P.; Gao, B., Catechol and Humic Acid Sorption onto a Range of Laboratory-Produced Black Carbons (Biochars). *Environmental Science & Technology* **2010,** *44* (16), 6189-6195.

44. Schweigert, N.; Zehnder, A. J. B.; Eggen, R. I. L., Chemical properties of catechols and their molecular modes of toxic action in cells, from microorganisms to mammals. *Environmental Microbiology* **2001,** *3* (2), 81-91.

45. Intellicast. *http://www.intellicast.com/National/Humidity/DewPoint.aspx*(accessed (May 2016)

46. Dai, A., Recent Climatology, Variability, and Trends in Global Surface Humidity. *Journal of Climate* **2006,** *19* (15), 3589-3606.

47. Mian, S. A.; Gao, X.; Nagase, S.; Jang, J., Adsorption of catechol on a wet silica surface: density functional theory study. *Theoretical Chemistry Accounts* **2011,** *130* (2), 333-339.

48. Calzolari, A.; Ruini, A.; Catellani, A., Surface Effects on Catechol/Semiconductor Interfaces. *The Journal of Physical Chemistry C* **2012,** *116* (32), 17158-17163.

49. Yeh, I.-C.; Lenhart, J. L.; Rinderspacher, B. C., Molecular Dynamics Simulations of Adsorption of Catechol and Related Phenolic Compounds to Alumina Surfaces. *The Journal of Physical Chemistry C* **2015,** *119* (14), 7721-7731.

50. Borah, J. M.; Sarma, J.; Mahiuddin, S., Adsorption comparison at the α-alumina/water interface: 3,4-Dihydroxybenzoic acid vs. catechol. *Colloids and Surfaces A: Physicochemical and Engineering Aspects* **2011,** *387* (1–3), 50-56.

51. McBride, M. B.; Wesselink, L. G., Chemisorption of catechol on gibbsite, boehmite, and noncrystalline alumina surfaces. *Environmental Science & Technology* **1988,** *22* (6), 703-708.

52 Xu, Z., Mechanics of metal-catecholate complexes: The roles of coordination state and metal types. *Scientific reports* **2013,** *3*, 2914.

53. Ye, Q.; Zhou, F.; Liu, W., Bioinspired catecholic chemistry for surface modification. *Chemical Society Reviews* **2011,** *40* (7), 4244-4258.

54. Vasca, E.; Ferri, D.; Manfredi, C.; Torello, L.; Fontanella, C.; Caruso, T.; Orru, S., Complex formation equilibria in the binary Zn2+-oxalate and In3+-oxalate systems. *Dalton Transactions* **2003,** (13), 2698-2703.

55. Menyo, M. S.; Hawker, C. J.; Waite, J. H., Versatile tuning of supramolecular hydrogels through metal complexation of oxidation-resistant catechol-inspired ligands. *Soft Matter* **2013,** *9* (43), 10314-10323.

56. Fullenkamp, D. E.; Barrett, D. G.; Miller, D. R.; Kurutz, J. W.; Messersmith, P. B., pH-dependent cross-linking of catechols through oxidation via Fe3+ and potential implications for mussel adhesion. RSC Advances 2014, 4 (48), 25127-25134.

57. Yang, J.; Cohen Stuart, M. A.; Kamperman, M., Jack of all trades: versatile catechol crosslinking mechanisms. *Chemical Society Reviews* **2014,** *43* (24), 8271-8298.

58. Sanchez, P.; Galvez, N.; Colacio, E.; Minones, E.; Dominguez-Vera, J. M., Catechol releases iron(iii) from ferritin by direct chelation without iron(ii) production. *Dalton Transactions* **2005,** (4), 811-813.

59. Yavvari, P. S.; Srivastava, A., Robust, self-healing hydrogels synthesised from catechol rich polymers. *Journal of Materials Chemistry B* **2015,** *3* (5), 899-910.

60. Gulley-Stahl, H.; Hogan, P. A.; Schmidt, W. L.; Wall, S. J.; Buhrlage, A.; Bullen, H. A., Surface Complexation of Catechol to Metal Oxides: An ATR-FTIR, Adsorption, and Dissolution Study. *Environmental Science & Technology* **2010,** *44* (11), 4116-4121.

61. Yang, Y.; Yan, W.; Jing, C., Dynamic Adsorption of Catechol at the Goethite/Aqueous Solution Interface: A Molecular-Scale Study. *Langmuir* **2012,** *28* (41), 14588-14597.

62. Yang, Y.; Duan, J.; Jing, C., Molecular-Scale Study of Salicylate Adsorption and Competition with Catechol at Goethite/Aqueous Solution Interface. *The Journal of Physical Chemistry C* **2013,** *117* (20), 10597-10606.

63. Bao, G.; Clifton, M.; Hoette, T. M.; Mori, K.; Deng, S. X.; Qiu, A.; Viltard, M.; Williams, D.; Paragas, N.; Leete, T.; Kulkarni, R.; Li, X.; Lee, B.; Kalandadze, A.; Ratner, A. J.; Pizarro, J. C.; Schmidt-Ott, K. M.; Landry, D. W.; Raymond, K. N.; Strong, R. K.; Barasch, J., Iron traffics in circulation bound to a siderocalin (Ngal)-catechol complex. *Nature chemical biology* **2010,** *6* (8), 602-9.

64. Sahoo, S. K.; Kanungo, B. K.; Baral, M., Complexation of a tripodal amine-catechol ligand tris((2,3-dihydroxybenzylamino)ethyl)amine towards Al(III), Ga(III), and In(III). *Monatshefte für Chemie - Chemical Monthly* **2009,** *140* (2), 139-145.

65. Stumm, W., The Inner-Sphere Surface Complex. In *Aquatic Chemistry*, American Chemical Society: 1995; Vol. 244, pp 1-32.

66. Santana-Casiano, J. M.; González-Dávila, M.; González, A. G.; Millero, F. J., Fe(III) Reduction in the Presence of Catechol in Seawater. *Aquatic Geochemistry* **2010,** *16* (3), 467-482.

67. Bergmann C. P.; and Machado F. M., Carbon Nanomaterials as Adsorbents for Environmental and Biological Applications, Springer, 2015

68. Mvula, E.; Schuchmann, M. N.; von Sonntag, C., Reactions of phenol-OH-adduct radicals. Phenoxyl radical formation by water elimination vs. oxidation by dioxygen. *Journal of the Chemical Society, Perkin Transactions 2* **2001,** (3), 264-268.

69. Gehling, W.; Dellinger, B., Environmentally Persistent Free Radicals and Their Lifetimes in PM2.5. *Environmental Science & Technology* **2013,** *47* (15), 8172-8178.

70. Kiruri, L. W.; Khachatryan, L.; Dellinger, B.; Lomnicki, S., Effect of Copper Oxide Concentration on the Formation and Persistency of Environmentally Persistent Free Radicals (EPFRs) in Particulates. *Environmental Science & Technology* **2014,** *48* (4), 2212-2217.

71. Lomnicki, S.; Truong, H.; Vejerano, E.; Dellinger, B., Copper Oxide-Based Model of Persistent Free Radical Formation on Combustion-Derived Particulate Matter. *Environmental Science & Technology* **2008,** *42* (13), 4982-4988.

72. Helm, L.; Merbach, A. E., Inorganic and Bioinorganic Solvent Exchange Mechanisms. *Chemical Reviews* **2005,** *105* (6), 1923-1960.

73. Panasci, A. F.; Ohlin, C. A.; Harley, S. J.; Casey, W. H., Rates of Water Exchange on the [Fe4(OH)2(hpdta)2(H2O)4]0 Molecule and Its Implications for Geochemistry. *Inorganic Chemistry* **2012,** *51* (12), 6731-6738.

74. Reddy, T. R.; Frierdich, A. J.; Beard, B. L.; Johnson, C. M., The effect of pH on stable iron isotope exchange and fractionation between aqueous Fe(II) and goethite. *Chemical Geology* **2015,** *397*, 118-127.

75. Kozerski, G. E.; Fiorentino, M. A.; Ketterer, M. E., Determination of Aqueous FeIII/II Electron Self-Exchange Rates Using Enriched Stable Isotope Labels, Ion Chromatography, and Inductively Coupled Plasma Mass Spectrometry. *Analytical Chemistry* **1997,** *69* (4), 783-788.

76. Crosby, H. A.; Johnson, C. M.; Roden, E. E.; Beard, B. L., Coupled Fe(II)−Fe(III) Electron and Atom Exchange as a Mechanism for Fe Isotope Fractionation during Dissimilatory Iron Oxide Reduction. *Environmental Science & Technology* **2005,** *39* (17), 6698-6704.

77. Pasakarnis, T.; McCormick, M. L.; Parkin, G. F.; Thompson, A.; Scherer, M. M., FeIIaq–FeIIIoxide electron transfer and Fe exchange: effect of organic carbon. *Environmental Chemistry* **2015,** *12* (1), 52-63.

78. Neumann, A.; Wu, L.; Li, W.; Beard, B. L.; Johnson, C. M.; Rosso, K. M.; Frierdich, A. J.; Scherer, M. M., Atom Exchange between Aqueous Fe(II) and Structural Fe in Clay Minerals. *Environmental Science & Technology* **2015,** *49* (5), 2786-2795.

79. Xiao, J.; Wang, C.; Lyu, S.; Liu, H.; Jiang, C.; Lei, Y., Enhancement of Fenton degradation by catechol in a wide initial pH range. *Separation and Purification Technology* **2016,** *169*, 202-209.

80. Stefánsson, A., Iron(III) Hydrolysis and Solubility at 25 °C. *Environmental Science & Technology* **2007,** *41* (17), 6117-6123.

81. Feng, W.; Nansheng, D., Photochemistry of hydrolytic iron (III) species and photoinduced degradation of organic compounds. A minireview. *Chemosphere* **2000,** *41* (8), 1137-1147.

82. Gligorovski, S.; Strekowski, R.; Barbati, S.; Vione, D., Environmental Implications of Hydroxyl Radicals ((•) OH). *Chemical Reviews* **2015,** *115* (24), 13051-13092.

83. Sun, Y.; Pignatello, J. J., Photochemical reactions involved in the total mineralization of 2,4-D by iron(3+)/hydrogen peroxide/UV. *Environmental Science & Technology* **1993,** *27* (2), 304-310.

84. Brillas, E., A review on the degradation of organic pollutants in waters by UV photoelectro-Fenton and solar photoelectro-Fenton. *Journal of the Brazilian Chemical Society* **2014,** *25*, 393-417.

85. Mofrad, M. R.; Akbari, H.; Nezhad, M. E.; Atharizade, M.; Miranzadeh, M. B., Evaluation of Efficacy of Advanced Oxidation Processes Fenton, Fenton-like and Photo-Fenton for Removal of Phenol from Aqueous Solutions. *Journal of the Chemical Society of Pakistan* **2015,** *37* (2), 266-271.

86. Sever, M. J.; Wilker, J. J., Visible absorption spectra of metal-catecholate and metal-tironate complexes. *Dalton Transactions* **2004,** (7), 1061-1072.

87. Silva, M. R. A.; Trovó, A. G.; Nogueira, R. F. P., Degradation of the herbicide tebuthiuron using solar photo-Fenton process and ferric citrate complex at circumneutral pH. *Journal of Photochemistry and Photobiology A: Chemistry* **2007,** *191* (2–3), 187-192.

88. Dellinger, B.; Lomnicki, S.; Khachatryan, L.; Maskos, Z.; Hall, R. W.; Adounkpe, J.; McFerrin, C.; Truong, H., Formation and stabilization of persistent free radicals. *Proceedings of the Combustion Institute* **2007,** *31* (1), 521-528.

89. Lomnicki, S.; Truong, H.; Vejerano, E.; Dellinger, B., Copper Oxide-Based Model of Persistent Free Radical Formation on Combustion-Derived Particulate Matter. *Environmental Science & Technology* **2008,** *42* (13), 4982-4988.

90. Murati, M.; Oturan, N.; Aaron, J.-J.; Dirany, A.; Tassin, B.; Zdravkovski, Z.; Oturan, M. A., Degradation and mineralization of sulcotrione and mesotrione in aqueous medium by the electro-Fenton process: a kinetic study. *Environmental Science and Pollution Research* **2012,** *19* (5), 1563-1573.

91. Rozas, O.; Contreras, D.; Mondaca, M. A.; Pérez-Moya, M.; Mansilla, H. D., Experimental design of Fenton and photo-Fenton reactions for the treatment of ampicillin solutions. *Journal of Hazardous Materials* **2010,** *177* (1–3), 1025-1030.

92. Hemmati Borji, S.; Nasseri, S.; Mahvi, A. H.; Nabizadeh, R.; Javadi, A. H., Investigation of photocatalytic degradation of phenol by Fe(III)-doped TiO(2) and TiO(2) nanoparticles. *Journal of Environmental Health Science and Engineering* **2014,** *12*, 101-101.

93. Wang, Z.; Guo, Y.; Liu, Z.; Feng, X.; Chen, Y.; Tao, T., Catechin as a new improving agent for a photo-Fenton-like system at near-neutral pH for the removal of inderal. *Photochemical & Photobiological Sciences* **2015,** *14* (2), 473-480.

94. Gehling, W. M., *Environmentally persistent free radicals (EPFRs) in $PM_{2.5}$: their contribution to hydroxyl radical formation and atmospheric transformation*. [Baton Rouge, Louisiana] : [Louisiana State University], [2013]: 2013.

CHAPTER 5
A ^{13}C NUCLEAR MAGNETIC RESONANCE AND ELECTRON PARAMAGNETIC SPECTROSCOPIC COMPARISON OF HYDROPHOBIC ACID, TRANSPHILIC ACID, AND REVERSE OSMOSIS MAY 2012 ISOLATES OF ORGANIC MATTER FROM THE SUWANNEE RIVER*

5.1 Introduction

Natural organic matter is ubiquitous throughout the environment.[1] In aqueous environments it is known as dissolved organic matter (DOM). DOM plays a number or important roles, such as influencing the fate and transport, including bioavailability of both organic and inorganic pollutants, acting as a food source, inducing permeability of biomembranes, and adsorbing light.[1-9] In addition, DOM plays a major role in the carbon cycle of the planet. [10-12] These, and a number of other environmentally relevant aspects of DOM, make the study of DOM essential to our understanding of the biogeochemistry of our planet's aqueous ecosystems.[1- 2]

The chemical composition of DOM is variable depending on source materials as well as biochemistry, thus DOMs isolated from different sites across the globe are not equivalent. Even DOM isolated from the same location but at different times may be very different.[13-14] Consequently, studies based on DOM isolated from different locations are difficult to compare directly. This means that there is a need for a standard (or reference) material that is available to the research community so that different studies can be compared. The International Humic Substance Society (IHSS) has been providing such references for decades. Some of the most studied, if not the most studied, of the IHSS standards are the Suwannee River humic acid (XAD

---

*This chapter previously appeared as Ugwumsinachi G. Nwosu, Robert L. Cook "^{13}C Nuclear Magnetic Resonance and Electron Paramagnetic Spectroscopic Comparison of Hydrophobic Acid, Transphilic Acid, and Reverse Osmosis May 2012 Isolates of Organic Matter from the Suwannee River." ***Environmental Engineering Science. Jan 2015, 32(1): 14-22.***. Reproduced by permission of Mary Ann Liebert, Inc., publishers.

isolate), fulvic acid (XAD isolate), and RO (reverse osmosis) isolates. However, because the IHSS Suwannee River humic and fulvic acid versus RO samples were isolated at different times, the physicochemical properties of these different samples cannot be directly compared.

The purpose of this work was to compare the XAD (XAD-8; HPOA and XAD-4; TPIA) and RO isolates of the same source water, in this case the Suwannee River, collected in May 2012. This study compares the carbon speciation and radical content of the different isolates by solid state cross polarization magic angle spinning ^{13}C nuclear magnetic resonance (CP-MAS ^{13}C NMR) and electron paramagnetic resonance (EPR), respectively.

5.2 Experimental Protocols

The three DOM isolates (May 2012 HPOA, May 2012 TPIA, and May 2012 RO (2R101N)) investigated here were provided, as a gift, in freeze-dried form by Patricia Maurice, Department of Civil and Environmental Engineering and Earth Sciences, University of Notre Dame. The samples were collected during an IHSS-sponsored sampling trip to the Suwannee River led by E. M. Perdue (Ball State University; see Green et al., 2014 and Kuhn et al., 2014 a, b for details of sampling and isolation).[15-16] The isolates were extracted by two different protocols, namely using XAD resins [17] and reverse osmosis [18]. Two isolates were yielded by the protocol utilizing the XAD resin, namely 1) the hydrophobic acid (May 2012 HPOA) isolate, which was eluted from the XAD-8 resin with base, and 2) the transphilic acid (May 2012 TPIA) isolate, which was eluted from the XAD-4 resin with base. The HPOA isolate contains both fulvic and humic acid, as defined by the IHSS. In terms of carbon recovery and distribution, the products of the XAD isolation yield the following distribution of isolates: 60% HPOA and 15% TPIA, with hydrophilic acids, hydrophobic organic neutrals, and transphilic and hydrophilic neutrals accounting for the remaining 25%.[16] The reverse osmosis protocol yielded one isolate (May 2012 RO (2R101N)), with an overall 84.2% recovery of available carbon, designated by IHSS catalog number 2R101N, and referred to

throughout this manuscript as the RO isolate. A summary of the elemental composition, metal content, and ash content of these samples is provided in Table 5.1.[16]

5.2.1 NMR Analysis

Solid state ^{13}C NMR spectra were collected using a Bruker Avance 400 MHz spectrometer, utilizing a ramp amplitude cross polarization pulse sequence along with magic angle spinning. The following conditions were used: a contact time between the proton and carbon pools was 2 ms, the delay between scans was 1 s to allow for relaxation, and the sample was spun at 14 kHz in order to reduce possible spinning band effects.[19] Approximately 100 mg of each isolate was packed into a 4 mm rotor. Samples were packed in several 5 to 10 mg portions by applying a good amount of downward pressure using a specialized tool with an outer diameter of just under 4 mm so as to tightly fit into the rotor. The rotor was filled up to the height that allowed for a tight fitting of the rotor cap. Care was taken so as not to damage the specialized cap's blades (turbines), which are used to spin the rotor at the speed of 14 kHz. In order to monitor the spinning speed by the sensing device (built into the probe), one half of the rotor's bottom edge was then clearly marked with a continuous black line with a marker, while the other half was left unmarked, and hence, remained light (slightly off white—the inherent color of the zirconia rotor material). The rotor cap blades were then once again confirmed to be both clean and undamaged. The sample was then lowered into the NMR MAS probe, and spun up in stages (5 kHz, 8 kHz, 10 kHz, 12 kHz, and finally 14 kHz; the rotor was allowed to spin for ~2 minutes at each spinning speed). This approach allows for better spin speed stability, limiting the possibility of rotor explosion, which can be highly damaging to the probe and will certainly result in a sample loss. As the sample is spun up in stages, it continues to improve the packing of the rotor by pressing the sample against the walls of the rotor, and hence, creating a small empty cylindrical space in the middle of the rotor. If at any point during sample spin up there is an instability in the spinning (spinning speeds fluctuating up and down), the rotor should be removed and checked for any cap blade damage

and to ensure that the continuous black mark is close to half of the bottom edge of the rotor. Cap replacement or a remarking of the rotor with a black marker are the most typical *easy* fixes. Otherwise, the rotor needs to be repacked.

The NMR spectral window was subdivided into the following chemical shift regions: 0-60 ppm alkyl (~20 ppm for methyl groups of alkyl chains; ~30 ppm for methylene; ~45 ppm methine, and ~54 ppm methoxyl); 60-90 ppm O-alkyl (~72 ppm with 20 ppm spread for C2-C6 carbons of cellulose, hemi-cellulose, and similar polymeric carbohydrate structures); 90-110 ppm di-O-alkyl (anomeric carbons in carbohydrates; can also be associated with C2 carbons in guaiacyl and syringyl lignin structures as well as the C6 carbon in syringyl); 110-160 ppm aromatic (110-137 ppm C-C and C-H; 137-160 ppm C-O and C-N); 160-190 ppm carbonyl/amide; and 190-220 nm ketonic carbons.[20-28] Glycine was used as a reference for the chemical shift.

Table 5.1 Elemental Composition and Metal Content of Isolates Used in This Work (May 2012 Sampling)

Elemental composition (wt% on ash- free basis)							Metal content (in nM .mg C^{-1})			
Sample	C	H	O	N	S	Ash (wt%)	Fe	Al	Cu	Zn
HPOA	53.05	3.98	41.47	1.02	0.49	1.55	96.3	35.2	0.357	0.7
TPIA	48.02	4.01	45.45	1.82	0.79	3.47	68	40.8	26.7	6.81
RO	51.11	4.00	41.81	1.28	1.80	4.01	41.3	45.5	0.825	1.36

Data from Kuhn et al. (2014a).

5.2.2 EPR Analysis

Samples were analyzed, in the solid state, for the presence of radicals without any prior modifications. 50 mg of each sample was placed into a 4-mm ID, Suprasil EPR tube. The EPR data were acquired at room temperature using a Bruker model EMX 10/2.7 spectrometer under the following instrumental conditions: microwave frequency 9.67 GHz, microwave power of 2 mW, center field at 3452 G, sweep width of 150 G, resolution of 2048 points, receiver gain of 1×10^4, modulation frequency of 100 kHz, time constants of 1.28 ms, and sweep time of 41.94 s. 5 scans were acquired for each spectrum.

A fresh 2,2-diphenyl-1-picrylhydrazyl (DPPH) standard was used to calibrate both the field position and radical concentration. Radical concentrations in terms of spins per gram were calculated based on the integrated area of the appropriate isolates EPR signal in comparison to the integrated area of the DPPH standard.

5.3 Results and Discussion

Two different resonance methods utilizing magnetic fields to induce population difference were used in this study, namely nuclear magnetic resonance, NMR (^{13}C solid state cross polarization technique) and EPR.

5.3.1 NMR Analysis

The solid state ^{13}C NMR results for the three different Suwannee River organic matter samples are shown in Figure. 5.1, with the corresponding integration data being presented in Table 5.2. Table 5.2 also includes data for a number of IHSS isolates.[29] In order to reduce possible confusion, the following labeling will be used: 1) the current samples, i.e., samples new to this study, will be respectively referred to as May 2012 HPOA, May 2012 TPIA, and May 2012 RO (designated as 2R101N on the IHSS website), 2) the IHSS HA (1S101H) and FA (1S101F) collected in 1982-1983 and the calculated HPOA will be referred to as HA 1S101H, FA 1S101F, and HPOA 1S101C, respectively, 3) the IHSS RO (1R101N) collected in 1999 will be referred to as RO 1R101N, and 4) the IHSS HA (2S101H) and FA (2S101F) collected in 2003 and the calculated HPOA will be referred to as HA 2S101H, FA 2S101F, and HPOA 2S101C, respectively. Note that all efforts have been made to make this labeling scheme as consistent with the IHSS labeling as possible.

The Suwannee River standard fulvic and humic acids reported on the IHSS website for the both the 1982-1983 and 2003 collections were derived from the HPOA isolate. By combining the data for the HA and FA isolates reported on the IHSS website (i.e., mathematically weighing them in terms of a fraction (the percentage they accounted for of the initial HPOA sample) of the

XAD-8 (HPOA) isolate from which they were derived), it is possible to compare the IHSS XAD-8 data (1S101H and 1S101F as well as 2S101H and 2S101F) with those reported here (May 2012 HPOA). This has been done and the data are reported in Table 5.2, as HPOA 1S101C and HPOA 2S101C. The exact formulae used are reported in the footnotes of Table 5.2. The same approach was used to calculate an RO sample from the May 2012 HPOA and May 2012 TPIA NMR data, which will be referred to as May 2012 Calc. RO.

Table 5.2 Summary of Integrated 13C Nuclear Magnetic Resonance Data (Normalized to 100%)

Sample	Ketone (190-120ppm)	Carbonyl (190-110ppm)	Aromatic (160-110ppm)	Di-O-alkyl (110-90ppm)	O-alkyl (90-60ppm)	Alkyl (60-0ppm)
This work						
May 2012 HPOA	6	18	18	7	15	36
May 2012 TPIA	5	19	12	9	24	31
May 2012 RO	5	17	15	7	17	39
May 2012 Calc. RO[a]	6	18	17	7	17	35
Thorn and Cox (2009)						
Thorn and Cox TPIA	7	24	15	7	17	30
IHSS Website*						
HA 1S101H	8	19	37	9	7	21
FA 1S101F	7	20	24	5	11	33
HPOA 1S101C[b]	7	20	26	6	10	31
HA 2S101H	6	15	31	7	13	29
FA 2S101F	5	17	22	6	16	35
HPOA 2S101C[c]	5	16	25	6	15	33
RO1R101N	8	20	23	7	15	27

[a]Calculated as follows: (X·0.80)+(Y·0.20), where X and Y are the appropriate values for the May 2012 HPOA and TPIA isolates, respectively.
[b] Calculated as follows: (X·0.87)+(Y·0.13), where X and Y are the appropriate values for the FA 1S101F and HA 1S101H isolates, respectively.
[c]Calculated as follows: (X·0.71)+(Y·0.29), where X and Y are the appropriate values for the FA 2S101F and HA 2S101H isolates, respectively.
*www.humicsubstances.org/thornnmr.html (in some cases, the percentage sums to 101%), last accessed September 13, 2014.

Integration data: The integration data reveal that the May 2012 TPIA isolate is higher in O-alkyl content and lower in aromatic and alkyl content than the May 2012 HPOA isolate. In terms of carbonyl content, the May 2012 HPOA and May 2012 TPIA isolate are very similar, as is the case for ketonic and anomeric carbon content. The May 2012 RO isolate is between the

May 2012 HPOA and May 2012 TPIA fractions in terms of aromatic and O-alkyl content. Compared to the May 2012 TPIA and May 2012 HPOA isolates, the May 2012 RO isolate is higher in alkyl content and essentially equivalent in terms of carbonyl, anomeric carbon and ketonic content. If the May 2012 HPOA and May 2012 RO isolates were equivalent to the IHSS commercially available humic acid (HA 1S101H and HA 2S101H) and fulvic acid (FA 1S101F and FA 2S101F) combined (HPOA 1S101C and HPOA 2S101C) and RO 1R101N Suwannee River isolates, respectively, then the results presented here could be compared with the available liquid state ^{13}C NMR data of previous Suwannee River samples. However, due to differences between the solid and liquid state NMR techniques used, only very rough comparisons are possible. We will go forward with this comparison but, due to these points, only *grosso modo* differences will be discussed.

Carbon-13 NMR results show that the HPOA 1S101C and HPOA 2S101C isolates and the May 2012 HPOA isolate, from this study, appear to be nearly identical (±3 %) in terms of carbon speciation (Table 5.1), except for the aromatic, O-alkyl and alkyl regions (in fact, the carbon distribution data for the HPOA 1S101C and HPOA 2S101C isolates and the May 2012 HPOA isolate are within ±5%, except for the aromatic region). This closeness of the results provides some confidence when comparing the liquid ^{13}C NMR data for the isolates reported on the IHSS website [29] and in Thorn and Cox, 2009 to the solid state ^{13}C NMR data reported here, especially in the *grosso modo* fashion, as will be done here.

As the isolates reported on the IHSS website [29], in Thorn and Cox, 2009, and here were isolated in essentially the same manner, a direct comparison is possible, especially for the RO isolates (May 2012 RO and RO 1R101N) and TPIA (May 2012 TPIA and Thorn and Cox TPIA(from May 1995 sampling)) isolates. In terms of the carbon speciation, it was found that May 2012 RO isolate reported here is lower in the aromatic but higher in the aliphatic carbon content than that for the RO 1R101N isolate. Turning to the TPIA isolates, it can be seen once

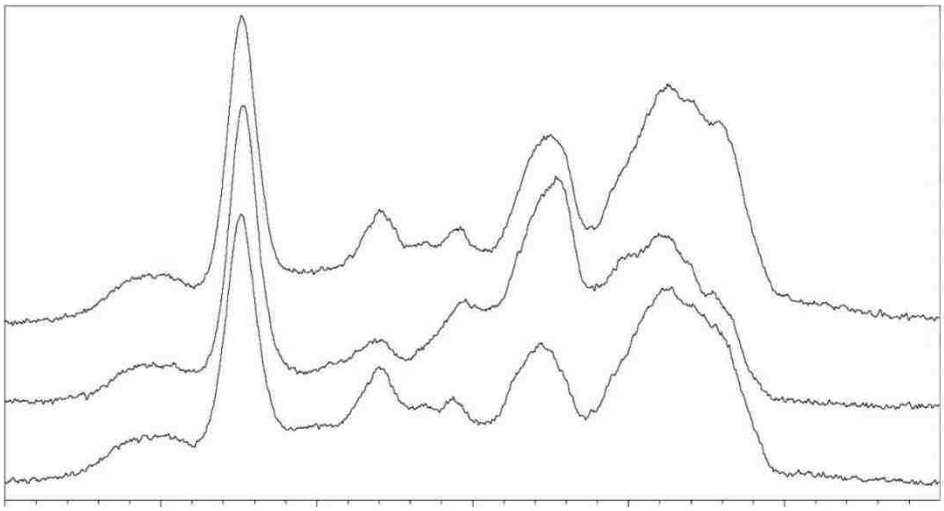

Figure 5.1 ^{13}C Ramp-CP-MAS NMR spectra of the May 2012 HPOA, May 2012 TPIA, and May 2012 RO isolates, from bottom to top, obtained with 40,960 scans.

again that the isolate reported in Thorn and Cox, 2009 [28] and the May 2012 TPIA isolate yielded similar carbon distributions. However, once again, the aromatic content is lower while the aliphatic content is higher for the more recently isolated sample (May 2012 TPIA). In addition, it can be seen that the more recent isolate has a higher O-alkyl content. If one compares the HPOA 1S101C, HPOA 2S101C, and May 2012 HPOA data, the same trends to those discussed above hold, whereby, with time, there is a decrease in aromatic content and an increase in alkyl content. The biggest change is seen between the HPOA 1S101C and the May 2012 HPOA data. Also, as with the TPIA isolates, there is an increase in O-alkyl content with time, as illustrated by HPOA 1S101C and HPOA 2S101C. Finally, HPOA 2S101C and May 2012 HPOA have essentially the same O-alkyl content.

On aggregate, the NMR data show chemical change, especially in terms of its aliphatic and aromatic nature, between Suwannee River samples collected at different times. This intriguing observation may be worthy of a future systematic and rather ambitious investigation that, ideally, utilizes the same isolation method and identical NMR techniques in order to fully determine if there is a temporal trend. Changes in inputs, mainly due to changes in flow patterns

between samplings (breaking of dams and stills) leading to differential aerobic conditions, climate change and human activities, offer other possible explanations for the observations. [15, 30-34]

A more realistic approach involves comparison of the data collected on the studied samples with those obtained for samples isolated and analyzed in the same manner, preferably in the same laboratory. Accordingly, the data presented here were compared with those reported by Lattao et al., on two HPOA and TPIA isolates isolated from two water bodies in Southern Louisiana.[27] Overall, this comparison reveals that Suwannee River samples have higher aliphatic, lower carbohydrate, lower aromatic, and almost equivalent carbonyl carbon content. However, none of these differences are very large (all fit within 10% of each other), which indicates, as does the discussion below, that Suwannee River RO isolates are good representative samples for aquatic riverine NOM.

Spectral Data: Integration of regions on a NMR spectrum can provide useful information, especially for complex heterogeneous samples, such as NOM isolates. Figure 5.1 consists of the ^{13}C ramp-CP-MAS NMR spectra for the three Suwanee River isolates under consideration in this work. These spectra are characterized by the six regions reported in Table 5.2. Below, differences in the spectra are summarized by region, in which *the reported ppm shift ranges should all be viewed only as approximate.*

Alkyl (0-60 ppm) region: All three isolates (May 2012 HPOA, May 2012 TPIA, and May 2012 RO consist of a broad peak between 5-55 ppm, with underlying peaks. These underlying peaks are most apparent in the May 2012 TPIA isolate. Closer inspection reveals four different peaks centered at approximately 20, 30, 40, and 53 ppm. These locations are only approximate due to peak overlap; however, based on previous work on HA 1S101H, HA 2S101H, FA 1S101F, and FA 2S101F [22,28,29] and other organic matter isolates[27], the carbon speciation of these peaks can be assigned to the following carbon types: methyl, methylene, methine, and methoxy (an o-alkyl originating from lignin parent materials), respectively. The RO isolate's spectrum has clear

methyl, methylene, and methine peaks, while the methoxy peak is apparent as a weak shoulder. The May 2012 HPOA isolate displays weak methyl and methylene peaks and a weak methoxy shoulder. The spectrum for the May 2012 RO, isolate is a combination of the May 2012 HPOA and May 2012 TPIA isolates.

O-alkyl (60-90 ppm) region: For all three isolates (May 2012 HPOA, May 2012 TPIA, and May 2012 RO, this region consists of a well-defined peak centered at 70 ppm with a spread of 20 ppm. This region's signature is assignable to the C2-C6 carbons of cellulose, hemi-cellulose, and other carbohydrate structures such as glucose, galactose, mannose, fructose, ribose, and xylose (as listed on the IHSS web site), as well ether and non-carbohydrate alcohol carbons. The May 2012 TPIA spectrum also has an underlying peak centered at 80 ppm illustrated by a minor shoulder spanning between 70 and 90 ppm. Once again, the May 2012 RO spectrum appears to be a hybrid of the May 2012 HPOA and May 2012 TPIA spectra.

Di-O-alkyl (90-110 ppm) region: In the May 2012 HPOA and May 2012 RO spectra in this region consist of a well-defined peak centered at 102 ppm. In the May 2012 TPIA spectrum, this feature is a less defined peak at the same location; however, this entire region is more dominant than in either the May 2012 HPOA or May 2012 RO spectra, which is also consistent with the larger O-alkyl peak in the May 2012 TPIA spectrum. The strength of the di-O-alkyl feature in the May 2012 TPIA isolate means that it significantly overlaps with the O-alkyl features, resulting in the di-O-alkyl peaks being larger but less defined compared to this same feature in either the May 2012 HPOA or the May 2012 RO spectra.

Aromatic (110-160 ppm) region: Once again, the spectra of the May 2012 HPOA and May 2012 RO isolates are closer to each other than either one is to the May 2012 TPIA isolate spectrum. In the May 2012 HPOA and May 2012 RO spectra it can be seen that this region consists of two distinct peaks centered at 115 and 130 ppm. These peaks can be assigned to protonated and non-protonated carbons, respectively. The signal assignable to the non-

protonated region is more dominant in the May 2012 HPOA isolate. Neither the May 2012 HPOA nor the May 2012 RO isolate has a distinct signal in the phenolic region (145-160 ppm); however, the May 2012 TPIA isolate has a shoulder in this spectral region.

Carbonyl/amide (160-190 ppm) and ketonic (190-220 ppm) regions: For all three samples, the carbonyl/amide peak is rather tall and featureless. There is a hint of a shoulder at a lower field for both the May 2012 HPOA and May 2012 RO isolates. In regards to the ketonic peak, it is rather broad and featureless; it is less prominent for the May 2012 TPIA isolate than for the May 2012 HPOA or May 2012 RO isolates.

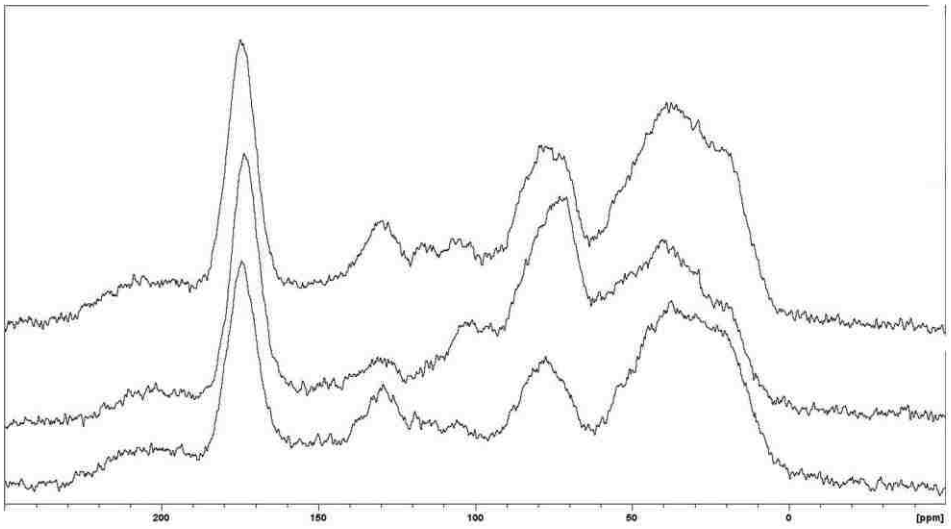

Figure 5.2 ^{13}C Ramp-CP-MAS NMR spectra of the May 2012 HPOA, May 2012 TPIA, and May 2012 RO isolates, from bottom to top, obtained with 8,192 scans.

The May 2012 HPOA isolate can be viewed as more hydrophobic than the May 2012 TPIA isolate, as it is the one that is sorbed by the XAD-8 resin, with the May 2012 TPIA isolate remaining in the aqueous phase. The NMR findings are consistent with the May 2012 HPOA isolate being more hydrophobic, as evidenced by its higher content of alkyl and aromatic moieties, and with the May 2012 TPIA isolate being more hydrophilic due to the higher content of O-alkyl moieties.

The ^{13}C NMR spectra in Figure 5.1 obtained for DOM isolates discussed in this work are rather broad and featureless compared to the ^{13}C NMR spectra one typically obtains for simple organic compounds. There are simply too many features to resolve, leading to significant overlap which blurs out the fine details. Multi-dimensional methods, both in the liquid and solid state, have been shown to resolve this issue with limited success.[27,35-36] However, the vast majority of the times when ^{13}C NMR is used to analyze DOM, fine details are not needed to obtain quantitative or semi-quantitative carbon speciation data. For example, to obtain the data reported in Table 5.1 on a modern NMR instrumentation using about 100 mg of DOM requires just over one hour of NMR time. Figure 5.2 shows ^{13}C NMR spectra for the same samples as in Figure 5.1, collected under the same conditions, but with one fifth the number of scans. In terms of time and NMR instrumental costs, these spectra are five times cheaper, with the signal-to-noise ratio decreasing by only a factor of $\sqrt{5}$ due to NMR being a signal-averaging technique. The spectra in Figures 5.1 and 5.2 offer basically the same overall bulk carbon speciation information, which is: 1) the May 2012 HPOA isolate is more dominated by alkyl and aryl aromatic moieties, 2) the May 2012 TPIA isolate is more dominated by O-alkyl moieties, 3) the May 2012 RO isolate is a hybrid of the May 2012 TPIA and May 2012 HPOA isolates, and 4) all isolates have a large amount of carbonyl carbons. If one is simply collecting a ^{13}C NMR spectrum of a NOM isolate to obtain its carbon speciation data, then it is sufficient to collect only as many scans as are needed to give a good enough signal-to-noise ratio so that clear differences in spectral features are present for each type of the major moieties, as outlined above. More scans are needed to allow for a good enough signal-to-noise ratio to tease out subtle differences, such as a shallow shoulder, to emerge in a spectrum. Due to the inherent overlapping signals that make up the spectral signal of DOM samples and their isolates, there is a limit to what extent the signal-to-noise ratio, and hence, the resolution, can be increased.

Overall, the above ^{13}C NMR results, including the determination of the structural relationship among the different isolates, are consistent with previously reported data on a range of Suwannee River organic matter isolates [22, 28] as well as those for other riverine DOM isolates.[27] Once again, this re-enforces the point that the Suwannee River RO isolate is a representative riverine DOM sample.

5.3.2 EPR Analysis

EPR data can be broken into three major types, namely the g-factor, ΔH, and spins per gram; where the g-factor gives information on the chemical make-up of the radical, ΔH provides information on how homogeneous the radicals are in terms of chemical make-up and local environment (the broader, the less homogeneous), and spins per gram is a quantitative measure of the amount of unpaired electrons (radicals) in a gram of sample.

The g-factor: Due to the chemical make-up of radicals, there is a spread of where unpaired electron signals appear. For the three May 2012 DOM isolates (May 2012 HPOA, May 2012 TPIA, May 2012 RO) reported on in Table 5.3, the spread is from 2.0041 (for the May 2012 RO isolate) to 2.0045 (for the May 2012 HPOA isolate) and are near the upper limit of those reported for other humic substances in the literature, which generally range from about 2.0030 to 2.0046 [37-39] and higher than those previously reported for Suwannee River HA 1S101H and FA 1S101F, which have g-factors of 1.9994 and 2.0040, respectively.[40] The high values for the Suwannee River samples reported here are, however, in line with organic radicals rich in oxygen groups [37], and are very close to the g-factor of a semiquinone-benzoquinone complex, H_2Q/Q.[39] All in all, the three isolate radicals appear to be fairly similar in chemical composition.

ΔH*:* Due to their complex heterogeneous nature, natural organic matter samples are known to give broad EPR spectra. As can be seen from the data presented in Table 5.3, the May 2012 TPIA isolate has the most diverse set of radicals, while the May 2012 RO isolate has the least diverse set of radicals, with the May 2012 HPOA isolate being in between. This spread of

radicals can also be seen in the EPR spectra, as presented in Figure 5.3 (note that spins per gram cannot be read directly from these spectra due to spread of the width of the signal [ΔH] and the fact that packing efficiencies for the different isolates were variable).

Spins per gram: The measurement of spins per gram quantifies the amount of radicals (unpaired electron spins) per gram of sample. Spins per gram values can be viewed as the EPR equivalent to integration in NMR; however, rather than being internally referenced to the sample, an external reference is used. This means that spins per gram is an absolute value rather than a relative value (as is usually the case for NMR integration values, and is the case for the ^{13}C NMR integration values reported here).

Table 5.3 Summary of Electron Paramagnetic Resonance Data

Sample	g-Factor	Spins per gram(10^{17})	ΔH
This work			
May 2012 HPOA	2.0043	6.38	6.24
May 2012 TPIA	2.0045	3.93	6.86
May 2012 RO	2.0041	3.59	5.26
May 2012 Calc. RO[a]	N.D.	5.89	N.D.
Saleh et al, (1994)			
HA 1S101H	1.9994	3.93	8
FA 1S101F	2.0040	5.41	9.8

[a]Calculated as follows: (X * 0.80)+(Y * 0.20), where X and Y are the appropriate values for the May 2012 HPOA and TPIA isolates, respectively.
N.D., not determined.

The spins per gram values in Table 5.3 range from 3.59×10^{17} (for the May 2012 RO isolate) to 6.38×10^{17} (for the May 2012 HPOA isolate), with the May 2012 TPIA isolate having a slightly higher value of 3.93×10^{17} value than the May 2012 RO isolate. These finding indicate that the May 2012 HPOA isolate has the highest radical concentration and the May 2012 RO isolate the lowest. Generally, NOM samples yield spins per gram on the order of magnitude of 10^{17}, thus the data for the isolates reported in this work are in line with these values. While spins per gram is an absolute quantity, there can be variations in the exact number, especially between

instruments due to geometrical arrangement, cavity couplings, microwave power, and use of standards. This means that exact comparisons can be often challenging, even more so in case of an addition of base during the isolation procedures as it may induce radicals [38] and in the presence of metal ions in the isolates, which may quench the radicals' EPR signal.[41-42]

The May 2012 HPOA isolate has 1.6 times more radicals than the May 2012 TPIA isolate. Assuming that the only radicals present are H_2Q/Q, then the May 2012 HPOA isolate is more concentrated in H_2Q/Q compared to the May 2012 TPIA isolate. This may indicate that: 1) the radicals are associated with more hydrophilic moieties, 2) the H_2Q/Q radical-forming entities are more exposed in the May 2012 HPOA isolate, and thus, are more prone to radical formation during alkaline conditions used in the isolation of the May 2012 HPOA fraction, or 3) a combination of the first two effects is in play. The concept of exposed radical forming-moieties has been previously put forward to explain the pH dependence of radical formation and the reason behind humic and fulvic acids having different radical concentrations.[38] From the spins per gram data it could be hypothesized that the more hydrophobic the isolate, the higher its concentration of radicals.

Due to the nature of the isolation method, the May 2012 RO isolate contains fewer radicals than either the May 2012 TPIA or May 2012 HPOA isolates. Since the May 2012 RO isolate is more hydrophilic than the May 2012 HPOA isolate —as shown by 13C NMR data— the above hypothesis of isolate's higher hydrophobicity correlating with the higher concentration of radicals appears to be supported. However, the spins per gram data reported by Saleh et al., for the Suwannee River HA 1S101H and FA 1S101F 40 contradict this notion as it is the FA 1S101F isolate that contains the higher radical concentration although it is more hydrophilic. This leaves two possible factors: the pH and the metal ion effects.

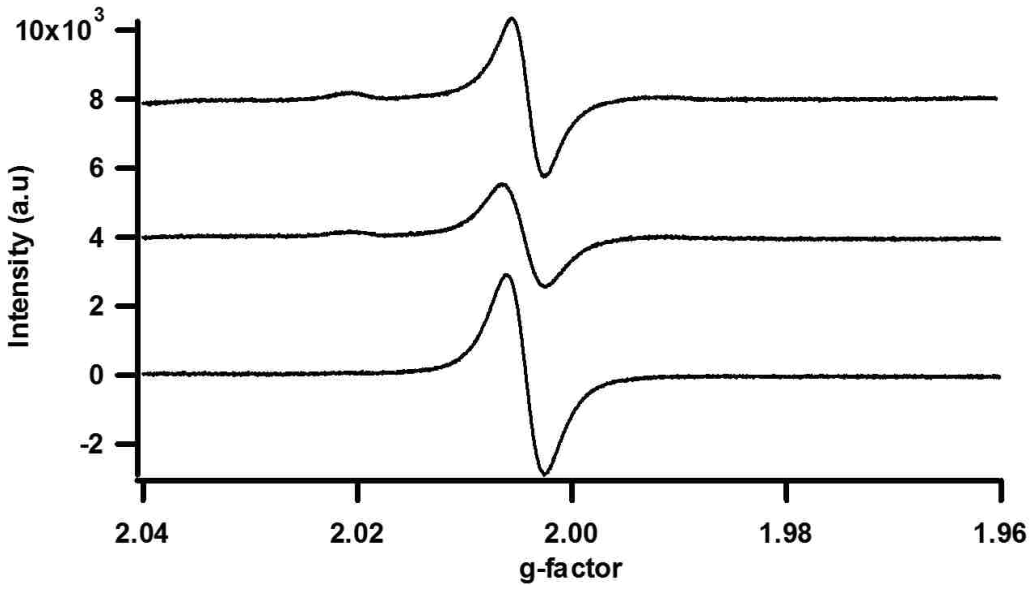

Figure 5.3 EPR spectra of the May 2012 HPOA, May 2012 TPIA, and May 2012 RO isolates, from bottom to top, obtained with 5 scans.

pH effect: Different pH conditions were used in the HPOA and TPIA isolation procedures compared to that for the RO isolate. This would mean that if the differences seen in the radical concentrations were due to the pH conditions used during the isolation procedures, namely XAD versus RO, then one would expect to see the largest difference in radical concentrations between the XAD isolates and the RO isolate. This, however, is not the case. In fact, the radical concentration of the May 2012 TPIA and May 2012 RO isolates are very close, when compared the difference in radical concentration between the May 2012 TPIA and May 2012 HPOA isolates. The weighted average of the May 2012 HPOA (80%) and May 2012 TPIA (20%) isolates (to create May 2012 Calc. RO) yields radical concentration of 5.89×10^{17} spins per gram. This is a significantly larger than the concentration of radials actually detected in the May 2012 RO isolate sample. A possible explanation for this is that, while NaOH is used in the RO isolation procedure to wash the membrane filters, this is a less severe alkaline condition compared to the one used during the XAD isolation procedure, and thus, it should produce fewer radicals. The wider ΔH values for the XAD isolates compared to the RO isolate support this and suggest, that the alkaline-

formed radicals being different in nature to the native radicals and with a wider range of g-factors. In regards to the XAD isolates, it appears that the May 2012 TPIA isolate radical concentration is chiefly due to the alkaline conditions, resulting in higher g-factor and ΔH values.

Metal ion effect: It has been shown that some metal ions quench radical signals.[41-42] The mechanism behind this quenching is thought to be due to antiferromagnetic interactions of the metal ion's *d*-subshell with the unpaired electrons of the H_2Q/Q complex. Based on the data presented in Table 5.1 from Kuhn et al., 2014a, no trend in d^n metal content and radical concentration can be found for the three isolates discussed in this work.

5.4 Summary

In rough terms (less than 50% in any area of comparison), the methods utilizing XAD resins and reverse osmosis yield DOM isolates with similar carbon speciation distribution. The ^{13}C NMR data reveal that May 2012 RO (2R101N) isolate is a hybrid of the XAD-isolated May 2012 HPOA and May 2012 TPIA isolates, with the May 2012 HPOA isolate being higher in alkyl and aromatic moieties, the May 2012 TPIA isolate being more concentrated in O-alkyl moieties, and the RO isolate being in between in regards to alkyl, O-alkyl, and aromatic moieties. This is somewhat surprising given the difference in how the two different isolation procedures work and the basic principles behind them. In very simple terms, the RO method isolates from the water sample compounds unable to cross a membrane, while the XAD-8 and XAD-4 resins, arranged in a series, isolate compounds that are "pulled out" of the water sample. The XAD method uses a large pH swing, from highly acidic (loading step) to highly alkaline (extraction step), while the RO method is gentler in terms of pH. Thus, while surprising, it is reassuring that the two methods yield similar products in terms of carbon speciation.

The XAD isolates (May 2012 HPOA and May 2012 TPIA) have higher radical concentrations than the May 2012 RO isolate, especially the May 2012 HPOA isolate. A possible hypothesis is the alkaline hydrolysis of certain functionalities, resulting in the release of catechol

moieties, which, in turn, become converted to semiquinone radicals. The difference between the May 2012 TPIA and May 2012 HPOA isolates can be postulated to be due to their hydrophobicity and the exposure of the radical-forming moieties to the alkaline aqueous phase.

The carbon speciation data reveal that the XAD method yields two distinct isolates (HPOA and TPIA) of the DOM within the original sample. Model experiments may be designed to understand how differences between these isolates influence the behavior of DOM samples. The RO isolate, on the other hand, appears to offer a more comprehensive representation of the DOM than either of the XAD isolates and is preferred when one wants to investigate the behavior of the DOM as a whole for a site. With different isolation techniques yielding samples useful for different experimental designs, it is up the experimentalist to determine which isolate best fits the experiment being carried out.

5.5 References

1. Walther, H. J., J. Buffle: Complexation Reactions in Aquatic Systems; Analytical Approach. Chichester, J. Wiley & Sons Ltd./Ellis Horwood Ltd., 1988, 692 S., 247 Abb., 126 Tab., £ 69,50, ISBN 0-470-20830-9 / 085312-557-0. *Acta hydrochimica et hydrobiologica* **1989,** *17* (2), 230-230.

2. Tipping, E. Cation Binding by Humic Substances; Cambridge University Press: Cambridge, UK, 2002.

3. Luthy, R. G.; Aiken, G. R.; Brusseau, M. L.; Cunningham, S. D.; Gschwend, P. M.; Pignatello, J. J.; Reinhard, M.; Traina, S. J.; Weber, W. J.; Westall, J. C., Sequestration of Hydrophobic Organic Contaminants by Geosorbents. *Environmental Science & Technology* **1997,** *31* (12), 3341-3347.

4. National Research Council (NRC) (2002) Bioavailability of contaminants in soils and sediments: processes, tools, and applications. National Academies Press, Washington D.C.

5. Pignatello, J. J.; Xing, B., Mechanisms of Slow Sorption of Organic Chemicals to Natural Particles. *Environmental Science & Technology* **1996,** *30* (1), 1-11.

6. Campbell, P. G. C.; Twiss, M. R.; Wilkinson, K. J., Accumulation of natural organic matter on the surfaces of living cells: implications for the interaction of toxic solutes with aquatic biota. *Canadian Journal of Fisheries and Aquatic Sciences* **1997,** *54* (11), 2543-2554.

7. Vigneault, B.; Percot, A.; Lafleur, M.; Campbell, P. G. C., Permeability Changes in Model and Phytoplankton Membranes in the Presence of Aquatic Humic Substances. *Environmental Science & Technology* **2000,** *34* (18), 3907-3913.

8. Elayan, N. M.; Treleaven, W. D.; Cook, R. L., Monitoring the Effect of Three Humic Acids on a Model Membrane System Using 31P NMR. *Environmental Science & Technology* **2008,** *42* (5), 1531-1536.

9. Ojwang', L. M.; Cook, R. L., Environmental Conditions That Influence the Ability of Humic Acids to Induce Permeability in Model Biomembranes. *Environmental Science & Technology* **2013,** *47* (15), 8280-8287.

10. Perdue, E. M.; Ritchie, J. D., 5.10 - Dissolved Organic Matter in Freshwaters A2 - Holland, Heinrich D. In *Treatise on Geochemistry*, Turekian, K. K., Ed. Pergamon: Oxford, 2003; pp 273-318.

11. Bianchi, T. S., The role of terrestrially derived organic carbon in the coastal ocean: a changing paradigm and the priming effect. *Proceedings of the National Academy of Sciences of the United States of America* **2011,** *108* (49), 19473-81.

12. Nelson, N. B.; Siegel, D. A., The global distribution and dynamics of chromophoric dissolved organic matter. *Annual review of marine science* **2013,** *5*, 447-76.

13. Bianchi, T. S.; Filley, T.; Dria, K.; Hatcher, P. G., Temporal variability in sources of dissolved organic carbon in the lower Mississippi river. *Geochimica et Cosmochimica Acta* **2004,** *68* (5), 959-967.

14. Duan, S.; Bianchi, T. S.; Sampere, T. P., Temporal variability in the composition and abundance of terrestrially-derived dissolved organic matter in the lower Mississippi and Pearl Rivers. *Marine Chemistry* **2007,** *103* (1–2), 172-184.

15. Green, N. W.; McInnis, D.; Hertkorn, N.; Maurice, P. A.; Perdue, E. M., Suwannee River Natural Organic Matter: Isolation of the 2R101N Reference Sample by Reverse Osmosis. *Environmental Engineering Science* **2014,** *32* (1), 38-44.

16. Kuhn, K. M.; Maurice, P. A.; Neubauer, E.; Hofmann, T.; von der Kammer, F., Accessibility of Humic-Associated Fe to a Microbial Siderophore: Implications for Bioavailability. *Environmental Science & Technology* **2014,** *48* (2), 1015-1022.

17. Aiken, G. R.; McKnight, D. M.; Thorn, K. A.; Thurman, E. M., Isolation of hydrophilic organic acids from water using nonionic macroporous resins. *Organic Geochemistry* **1992,** *18* (4), 567-573.

18. Sun, L.; Perdue, E. M.; and McCarthy, J. F., Using reverse osmosis to obtain organic matter from surface and ground waters. *Water Res.* ***1995,*** 29,1471-1477.

19. Mao, J. D.; Schmidt-Rohr, K., Accurate quantification of aromaticity and nonprotonated aromatic carbon fraction in natural organic matter by 13C solid-state nuclear magnetic resonance. *Environ Sci Technol* **2004,** *38* (9), 2680-4.

20. Thorn, K. A.; Folan, D. W.; MacCarthy, P. *Characterization of the International Humic Substances Society standard and reference fulvic and humic acids by solution state carbon-13 (13C) and hydrogen-1 (1H) nuclear magnetic resonance spectrometry*; 89-4196; 1989.

21. Thorn, K. A.; Arterburn, J. B.; Mikita, M. A., 15N and13C NMR investigation of hydroxylamine-derivatized humic substances. *Environmental Science and Technology* **1992,** *26* (1), 107-116.

22. Thorn, K.A., Nuclear-magnetic-resonance studies of fulvic and humic acids from the Suwannee River. In R.C. Averett, J.A. Leenheer, D.M. KcKnight, and K.A. Thorn, Eds., Humic Substances in the Suwannee River, Georgia: Interactions, Properties, and Proposed Structures. *United States Geological Suvery water-supply report 2373*, **1994**, p 141.

23. Kögel-Knabner, I., 13C and 15N NMR spectroscopy as a tool in soil organic matter studies. *Geoderma* **1997,** *80* (3–4), 243-270.

24. Almendros Martín, G.; Blanco Santos, M. J.; Dorado, J.; González-Vila, F. J.; Lankes, U., 13C NMR assessment of decomposition patterns during composting of forest and shrub biomass. *Soil Biology and Biochemistry* **2000,** *804*, 793-804.

25. Lorenz, K.; Preston, C. M.; Raspe, S.; Morrison, I. K.; Feger, K. H., Litter decomposition and humus characteristics in Canadian and German spruce ecosystems: information from tannin analysis and 13C CPMAS NMR. *Soil Biology and Biochemistry* **2000,** *32* (6), 779-792.

26. Keeler, C.; Kelly, E. F.; Maciel, G. E., Chemical–structural information from solid-state 13C NMR studies of a suite of humic materials from a lower montane forest soil, Colorado, USA. *Geoderma* **2006,** *130* (1–2), 124-140.

27. Lattao, C.; Birdwell, J.; Wang, J. J.; Cook, R. L., Studying Organic Matter Molecular Assemblage within a Whole Organic Soil by Nuclear Magnetic Resonance All rights reserved. No part of this periodical may be reproduced or transmitted in any form or by any means, electronic or mechanical, including photocopying, recording, or any information storage and retrieval system, without permission in writing from the publisher. *Journal of Environmental Quality* **2008,** *37* (4), 1501-1509.

28. Thorn, K. A.; Cox, L. G., N-15 NMR spectra of naturally abundant nitrogen in soil and aquatic natural organic matter samples of the International Humic Substances Society. *Organic Geochemistry* **2009,** *40* (4), 484-499.

29. IHSS (International Humic Substance Society). Available at: www.humicsubstances.org/thornnmr.html (accessed September 13, 2014).

30. Freeman, C.; Fenner, N.; Ostle, N. J.; Kang, H.; Dowrick, D. J.; Reynolds, B.; Lock, M. A.; Sleep, D.; Hughes, S.; Hudson, J., Export of dissolved organic carbon from peatlands under elevated carbon dioxide levels. *Nature* **2004,** *430* (6996), 195-198.

31. Fang, C.; Smith, P.; Moncrieff, J. B.; Smith, J. U., Similar response of labile and resistant soil organic matter pools to changes in temperature. *Nature* **2005,** *433* (7021), 57-59.

32. Zhang, J.; Hudson, J.; Neal, R.; Sereda, J.; Clair, T.; Turner, M.; Jeffries, D.; Dillon, P.; Molot, L.; Somers, K.; Hesslein, R., Long-term patterns of dissolved organic carbon in lakes across eastern Canada: Evidence of a pronounced climate effect. *Limnology and Oceanography* **2010,** *55* (1), 30-42.

33. Larsen, S.; Andersen, T. O. M.; Hessen, D. O., Climate change predicted to cause severe increase of organic carbon in lakes. *Global Change Biology* **2011,** *17* (2), 1186-1192.

34. Stanley, E. H.; Powers, S. M.; Lottig, N. R.; Buffam, I.; Crawford, J. T., Contemporary changes in dissolved organic carbon (DOC) in human-dominated rivers: is there a role for DOC management? *Freshwater Biology* **2012,** *57*, 26-42.

35. Cook, R. L.; McIntyre, D. D.; Langford, C. H.; Vogel, H. J., A comprehensive liquid-state heteronuclear and multidimensional NMR study of Laurentian fulvic acid. *Environ Sci Technol* **2003,** *37* (17), 3935-44.

36. Cook, R. L., Coupling NMR to NOM. *Analytical and Bioanalytical Chemistry* **2004,** *378* (6), 1484-1503.

37. Jezierski, A.; Czechowski, F.; Jerzykiewicz, M.; Chen, Y.; Drozd, J., Electron paramagnetic resonance (EPR) studies on stable and transient radicals in humic acids from compost, soil, peat and brown coal. *Spectrochimica acta. Part A, Molecular and biomolecular spectroscopy* **2000,** *56a* (2), 379-85.

38. Paul, A.; Stosser, R.; Zehl, A.; Zwirnmann, E.; Vogt, R. D.; Steinberg, C. E., Nature and abundance of organic radicals in natural organic matter: effect of pH and irradiation. *Environ Sci Technol* **2006,** *40* (19), 5897-903.

39. Ariese, F.; van Assema, S.; Gooijer, C.; Bruccoleri, A. G.; Langford, C. H., Comparison of Laurentian Fulvic Acid luminescence with that of the hydroquinone/quinone model system: Evidence from low temperature fluorescence studies and EPR spectroscopy. *Aquatic Sciences* **2004,** *66* (1), 86-94.

40. Saleh, F.Y.; Theriot, L.J.; Amani, S.K.; and Kim, I.; Electron-spin resonance of fulvic and humic acids from the Suwannee River. In R.C. Averett, J.A. Leenheer, D.M. KcKnight, and K.A. Thorn, Eds., Humic Substances in the Suwannee River, Georgia: Interactions, Properties, and Proposed Structures. *United States Geological Survey water supply report* **1994**, 2373, p 67.

41. Jerzykiewicz, M.; Jezierski, A.; Czechowski, F.; Drozd, J., Influence of metal ions binding on free radical concentration in humic acids. A quantitative electron paramagnetic resonance study. *Organic Geochemistry* **2002,** *33* (3), 265-268.

42. Giannakopoulos, E.; Stathi, P.; Dimos, K.; Gournis, D.; Sanakis, Y.; Deligiannakis, Y., Adsorption and radical stabilization of humic-Acid analogues and Pb2+ on restricted phyllomorphous clay. *Langmuir* **2006,** *22* (16), 6863-73.

CHAPTER 6
CONCLUSIONS AND FUTURE WORK

6.1 Concluding Remarks

The impetus behind this dissertation work was the detection of elevated radical signals in soils found at Superfund wood treatment sites and, subsequently, other Superfund sites that were contaminated with PCPs and other PAHs as well as transitions metals. Further investigation of the radicals at the Superfund sites revealed that they were persistent and had chemical signatures consistent with previously found environmentally persistent free radicals (EPFRs). This further investigation also revealed that the Superfund soil EPFRs were mainly associated with the clay/humin fraction of the soil. However, the complexity of real soils, including the clay/humin fraction, presents an array of analytical challenges that, collectively, make EPFR formation mechanistic studies beyond our current analytical capabilities. In order to overcome these analytical limitations, a “bottom-up” approach utilizing surrogate systems has been undertaken in this dissertation work to gain mechanistic insights into the EPFR formation at PCP-polluted Superfund sites.

Chapter 1 provided an overview of the general concept of EPFRs formation based on previously investigated systems, mainly combustion-generated particulate matter and associated surrogates, including a thorough review of available EPFR literature. Advances in the research on the effects of EPFRs on living organisms, such as humans and even plants, were also highlighted. The key analytical techniques utilized in this dissertation research such as EPR, XANES, EXAFS, XRD, XPS, FTIR and Raman spectroscopies were briefly introduced in the opening chapter. Other important aspects of this research, such as the nature of the soil systems, in particular, their inorganic/mineral, organic (SOM), and biological components as well as organic pollutant/soil interactions were also properly reviewed as they apply to this dissertation work.

As the first step to study EPFR formation, a single-component soil system composed from a Fe(III)-cation exchanged montmorillonite clay was exposed to a model pollutant precursor, here phenol. The results were discussed in chapter two and showed that the concentrations of the formed EPFRs were within the range of the EPFR concentrations detected in the real contaminated soil. Also, as evidenced by the *g*-factors in the ~2.0030 to 2.0034 range, the chemical signature of the radicals formed in the Fe-loaded clay surrogate systems was consistent with the phenoxyl radical types encountered in EPFRs in the real (Superfund) soils. In addition, the lifetimes of the EPFRs formed upon exposure to either vacuum (151.8 days), ambient air (12.4 days), or 75% humidity (2.1 days) showed the variation in the stability and persistency of EPFRs at these different environmental conditions as well as the importance of humidity on EPFR persistence. Furthermore, for the first time, evidence corroborating the mechanism involved in EPFR formation in the Fe(III)-loaded clay, as originally proposed for EPFRs formed in the real contaminated soil and the $PM_{2.5}$ systems, was provided by measuring (i) pollutant sorption by FTIR, (ii) EPFR formation by EPR, (iii) the change in oxidation states of the Fe redox center by XANES, and (iv) the number of EPFRs formed and Fe centers converted from Fe(III) to Fe(II) by the combination of EPR and XANES. The density of EPFRs was determined to be 1.5×10^{-2} spins per Fe(II) atom and was used to further justify both the mechanism of EPFRs formation and the resultant EPFR stability.

Chapter 3 of this dissertation describes the next step in the systematic study of EPFR formation, namely the role of soil organic components of the soil, specifically that of the conjugated systems. Copper-loaded montmorillonite clays were prepared to model a single component mineral soil system, while poly-*p*-phenylene (PPP) grafted on Cu(II)-loaded clays, synthesized using the Kumada catalyst-transfer chain-growth polymerization, were employed to investigate the EPFRs formed in a bi-component mineral/organic soil system. Phenol was used as the model contaminant and exposure was carried out in gas phase. The production of PPP graphed on the

copper-cation exchanged clay was confirmed by (i) the Raman vibrational bands assignable to sp^2 peaks from the aromatic backbone of the polymer and (ii) a *g*-factor of 2.0024 attributable to the PPP radicals (identified as polarons). The formation of the conjugated system provided better stability for the EPFRs formed in the bi-component soil system through π-π stacking, as indicated by a longer EPFR lifetime compared to that of a single component Cu(II)-loaded clay system (13.5 h and 56 h *vs* 20 h, respectively). The inherent radical in the poly-*p*-phenylene Cu(II)-clay system was a very good surrogate for the the quinone-quinoid type radicals found in soil organic matter. Finally, the EPFRs in the systems exposed to phenol resulted in higher ROS generation when compared to the non-phenol-exposed systems.

Chapter 4 is focused on the effects of ambient soil conditions on the formation of EPFRs. Due to the presence of higher Fe and Cu concentrations at the Superfund sites, compared to the uncontaminated neighboring soils, Fe(III) and Cu(II)-loaded montmorillonite clays, namely Fe(III)CaMMT and Cu(II)CaMMT, were used as single component soil surrogates, catechol was used as the model organic pollutant precursor, and the exposure was carried out in aqueous phase. The effects of pH, relative humidity, and UV irradiation were studied. Higher catechol sorption at near neutral and alkaline conditions (pH > 6.5) was found for both Fe(III)CaMMT and Cu(II)CaMMT. Similarly, higher amounts of EPFRs were also consistently found at high pHs**, with the exception of Fe(III)CaMMT which showed high concentrations at pH 3.4 as well. UV irradiation affected EPFR formation and •OH generation. *In situ* studies of EPFRs formed in catechol liquid exposed Fe(III)CaMMT and Cu(II)CaMMT, showed that UV irradiation could result in OH generation which ultimately dictates the fate of EPFRs eventually formed on clay surfaces. Catechol sorption was higher at alkaline pH under UV/Vis radiation, especially in the case of Cu(II)CaMMT). This trend was reversed at acidic pHs. The reduced EPFR formation at acidic pHs under UV irradiation was attributed to the photolysis of Fe species known to occur between pH 3 and 5. Since •OH radicals can be intrinsically generated from the photolysis of Fe species in this

pH range, these •OH radicals could quench EPFRs through several reaction routes, including radical recombination. Also, due to the transformation of Fe species during photolysis, the availability of Fe(III) species at acidic pHs could reduce EPFR formation. A reverse trend was observed for Cu(II)CaMMT in terms of EPFR generation in acidic media, with higher amounts of EPFRs being formed under UV irradiation compared to the non-UV-irradiated conditions. Furthermore, the results from the UV irradiation of EPFRs formed in Fe(III)CaMMT and Cu(II)CaMMT under dry and dark conditions showed that, even after the EFPR formation, some of the sorbed catechol molecules may not have completely reacted to form radicals. This was observed by the increased radical relative concentration of EPFRs formed in Fe(III)CaMMT and Cu(II)CaMMT. More EPFRs formed on Fe(III)CaMMT at pHs 7.4 and 9.5 when irradiated than at acidic pHs, while for Cu(II)CaMMT, UV irradiation caused more EPFR formation at acidic pHs than at alkaline pHs. Generally, EPFRs formed at pH 7.4 and 9.5 were more stable even with increasing irradiation time compared to the EPFRs formed at acidic pHs. Measuring EPFR concentrations after 12 h in the dark and then again after 6 h of UV irradiation also revealed that UV irradiation can cause an additional decay in the EPFR concentration, especially for EPFRs formed at acidic conditions. However, EPFRs formed at pHs 7.4 and 9.5 did not decay. These decay effects were more pronounced for EPFRs formed in Cu(II)CaMMT than in Fe(III)CaMMT. As expected, experiments conducted on the effects of humidity on EPFR lifetimes showed that humidity drastically affected EPFRs persistence and stability, resulting in shorter EPFR lifetimes in both Fe(III)CaMMT and Cu(II)CaMMT surrogate systems. The humidity-induced EPFR lifetimes were attributed to the desorption of EPFRs by water molecules. However, EPFRs formed at pHs 7.4 and 9.5 demonstrated the greatest stability when exposed to humid conditions, presumably due the higher degree of catechol-metal complexes formation at higher pHs, which stabilizes EPFRs through π-π stacking coupled with the desorption of catechol molecules from metal complexes. This stabilization mechanism is envisioned to be easier in mono-catechol-metal complexes (prevalent at low pH) compared to the bi- and tris- complexes (dominant at high pH).

In Chapter 5, two different analytical techniques, namely solid-state cross polarization magic angle spinning ^{13}C nuclear magnetic resonance (CP-MAS ^{13}C NMR) and electron paramagnetic resonance (EPR), were employed to investigate the constituents of NOM (dissolved organic matter isolates from Suwannee River), as it relates to their carbon speciation and radical contents. Specifically, the hydrophobic acid (May 2012 HPOA) and transphilic acid (May 2012 TPIA) isolates obtained from XAD-8 and XAD-4 resins, were compared with the RO (May 2012 RO) natural organic matter isolate. The CP-MAS ^{13}C NMR result showed that the TPIA and HPOA fractions were chemically unique and the RO isolate was a combination of the two. The EPR results revealed that all three isolates contained organic radicals (i.e., the EPFRs). The *g*-factors of ~2.004 measured for these radicals were indicative of the presence of a semiquinone-benzoquinone radical. In addition, the HPOA isolate was found to have the highest, and the RO isolate the lowest, radical concentration. The difference in radical concentration between the isolates was attributed to the fact that the hydroquinone-quinone (H2Q/Q) radical forming entities in May 2012 HPOA, which are associated with hydrophilic groups, may have been exposed in such a way that the alkaline extraction conditions could have promoted organic radical formation. This research reveals that EPFRs are omnipresent in the environment and that EPFRs may play an important role in carbon sequestration and transformation in the environment. Hence, EPFR formation has a boarder importance than its importance to a number of Superfund polluted sites, especially in regards to EPFR formation mechanisms in soils.

6.2 Ongoing work/Future works

The research presented in this dissertation opens a number of avenues to further explore EPFR forming mechanisms in soil using surrogate systems. The first such avenue would be to explore the bi-component system, the possibility of using a humic acid coated-magnetite Fe_3O_4, nanoparticle represent a perfect model for the humic acid - metal aggregate obtained in the real soil will be explored. Furthermore, catechol will be used as a model contaminant for this

experiment, to accommodate a wide range of behavior expected in a number of pollutants encountered at the Superfund sites.

The second part would involve investigating the role of the biological component in EPFR formation. The preliminary results have already shown that, for both Fe(III)CaMMT and Cu(II)CaMMT systems, EPFR formation increased up to 1.8 times in the presence of laccase enzymes at environmentally relevant pH and temperature conditions (see appendix 1). This means that various EPFR formation mechanism involving laccase may be involved, including: 1) laccase increasing pollutant sorption and 2) laccase oxidizing phenols and polyphenols, potentially allowing for a steady availability of catalytic redox metal cites for continuous EPFR formation in solution. These possibilities are under investigation at the moment utilizing a combination of techniques presented in this dissertation, such as EPR, XANES, and EXAFS, and well as nonlinear optical methods, such as the second harmonic generation (SHG).

Also, while the effects of SOM were investigated (chapter three), the scope of that study was limited to a conjugated aromatic surrogate of SOM. More model system designs are therefore warranted to further understand the role of SOM in EPFR formation Studies on other bi-component systems can be envisioned, such as a humic acid-coated-magnetite, Fe_3O_4, nanoparticle (HA-MNP) system, which represents a perfect model for the humic acid-metal aggregate found in real soils. Furthermore, catechol could be used as a model contaminant for this avenue of exploration to accommodate a wide range of behaviors expected from a number of pollutants encountered at the Superfund sites. This is because catechol is soluble in water, behaves differently at different pHs and can undergo a two-electron oxidation and reduction. Additionally, expecting a certain degree of success with the above mentioned surrogate systems, a tri-component system can be envisioned, consisting of an HA-MNP system in the presence of an immobilized laccase. Syntheses of other engineered soil surrogates could also be explored.

Finally, a range of different precursor pollutants, such as pesticides and other phenol-based and polyaromatic hydrocarbon compounds, both natural or anthropogenic, can be envisioned in order to study the role of EPFRs in pollutant transformation and carbon cycling and transformation in the environment. We also intend to continue our collaboration with other research cores of the LSU superfund research core.

APPENDIX A
CHAPTER 3 SUPPORTING INFORMATION

A1. Clay Modification

Preparation of substrate (Clay): A 200 mg sample of clay was dried in the vacuum oven at 70 °C overnight, and subsequently transferred to the glove box for further air-free reactions.

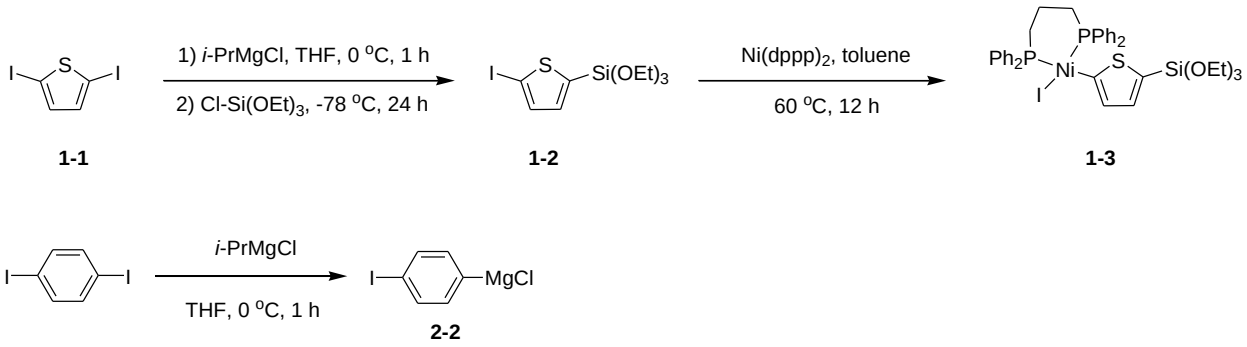

Scheme SS1-2**.** Preparation of reagents for surface-confined Kumada catalyst-transfer polymerization.

Preparation of catalytic initiator 1-3**:** The catalytic initiator **1-3** for surface-confined polymerization was prepared following the procedures described in ref. 1.

Preparation of surface-immobilized initiators on the substrate (clay): Dried clay (200 mg) was immersed into 7 mL of 2.5 mM solution of the polymerization catalytic initiator **1-3** in toluene and kept at 60 °C for 3 days with stirring. In order to remove non-chemically attached initiator, the clay samples were centrifuged at 3,000 rpm for 1 min to precipitate clay, followed by gentle rinsing with anhydrous THF. Due to air sensitive nature of compounds involved, all manipulations were carried out under a nitrogen gas flow or inside a glove box.

Grignard monomer for polymerization (compound 2-1): A solution of 0.066 g of 1,4-diiodobenzene (0.2 mmol) in 20 mL of anhydrous THF was stirred at 0 °C under a nitrogen atmosphere. A solution of isopropylmagnesium chloride (0.25 mL of 2.0 M solution, 0.205 mmol) was then added dropwise and the solution was stirred for 1 h.

Surface-confined polymerization of Grignard monomer**:** The clay modified with surface-attached catalytic initiator **1-3** was immersed into the Grignard monomer **2-2** solution prepared as described above with gentle stirring at room temperature for 12 h. The reaction mixture was then quenched with methanol, and washed successively with chloroform, acetone, methanol, and water following drying the sample in vacuum oven at 70 °C for 12 h.

A.2 EPR Spectra for DMPO-OH

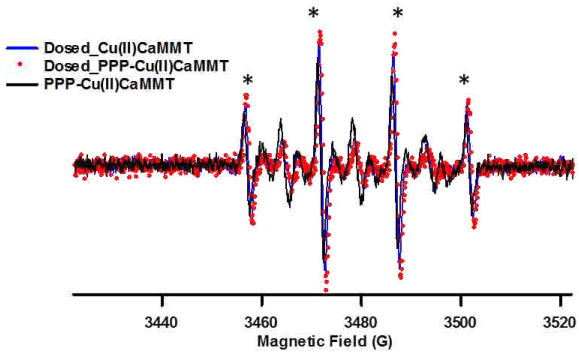

Figure S1 EPR spectra for DMPO-OH (Asterisks) after 8h incubation for Dosed_Cu(II)CaMMT (blue), phenol exposed Cu-loaded clay, Dosed _PPP-Cu(II)CaMMT (Red) and PPP-Cu(II)CaMMT(black). Spectra recorded at 100 G width.

Reference

1. C. A. Chavez, J. Choi and E. E. Nesterov, *Macromolecules*, 2014, **47**, 506-516.

APPENDIX B
LACCASES CATALYZED FORMATION OF EPFRS ON CU(II) LOADED MONTMORILLONITE CLAY

B.1 Preliminary Result

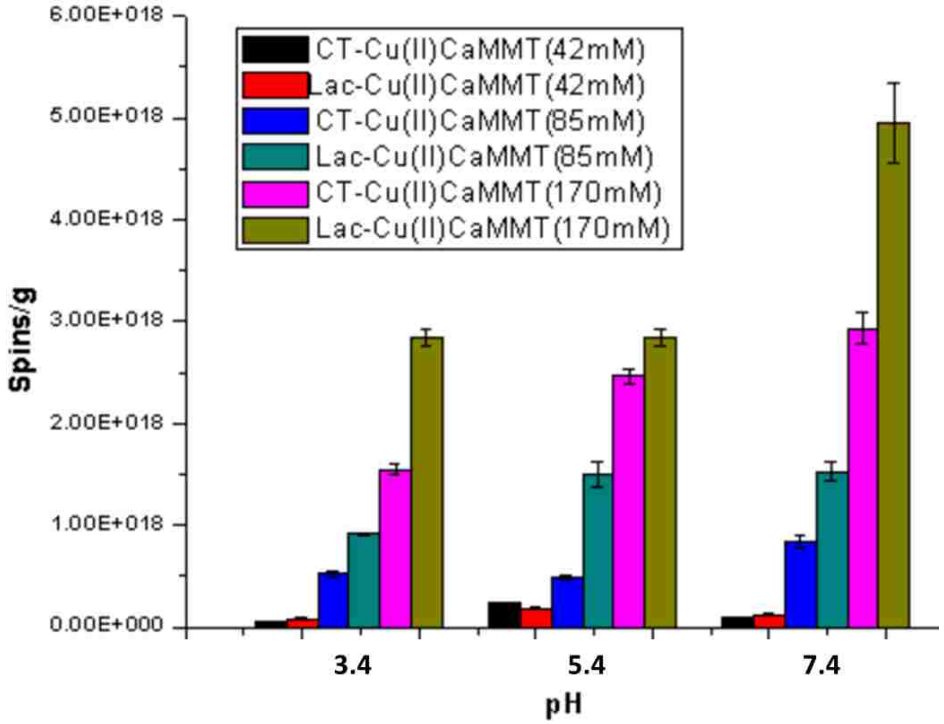

Figure S2 EPFRs formed in copper loaded montmorillonite clay after liquid phase dosing at pH 3.4, 5.5 and 7.4 No laccase catechol (CT-Cu(II)CaMMT) and sample incubated with laccase (Lac-CT-Cu(II)CaMMT) at catechol concentration of 170 *mM,* 85 *mM* and 42 *mM* respectively, with laccase concentration of 1.5 mg/mL

APPENDIX C
COPYRIGHT PERMISSION FOR CHAPTER 2 AND CHAPTER 3

RE: Copyright Permission

Gill Cockhead <CockheadG@rsc.org>

Tue 9/27/2016 1:19 AM
To:Ugwumsinachi Nwosu <unwosu2@lsu.edu>;

Dear Ugwumsinachi

The Royal Society of Chemistry (RSC) hereby grants permission for the use of your paper(s) specified below in the printed and microfilm version of your thesis. You may also make available the PDF version of your paper(s) that the RSC sent to the corresponding author(s) of your paper(s) upon publication of the paper(s) in the following ways: in your thesis via any website that your university may have for the deposition of theses, via your university's Intranet or via your own personal website. We are however unable to grant you permission to include the PDF version of the paper(s) on its own in your institutional repository. The Royal Society of Chemistry is a signatory to the STM Guidelines on Permissions (available on request).

Please note that if the material specified below or any part of it appears with credit or acknowledgement to a third party then you must also secure permission from that third party before reproducing that material.

Please ensure that the thesis states the following:

Reproduced by permission of The Royal Society of Chemistry

and include a link to the paper on the Royal Society of Chemistry's website.

Please ensure that your co-authors are aware that you are including the paper in your thesis.

Regards

Gill Cockhead
Publishing Contracts & Copyright Executive

Gill Cockhead
Publishing Contracts & Copyright Executive
Royal Society of Chemistry,
Thomas Graham House,
Science Park, Milton Road,
Cambridge, CB4 0WF, UK
Tel +44 (0) 1223 432134

Follow the Royal Society of Chemistry:
www.rsc.org/follow

Winner of The Queen's Award for Enterprise, International Trade 2013

-----Original Message-----
From: unwosu2@lsu.edu [mailto:unwosu2@lsu.edu]
Sent: 26 September 2016 19:39
To: Gill Cockhead
Subject: Copyright Permission

Name: Ugwumsinachi Nwosu
Message: I am the first author to the following publications titled "Formation of environmentally persistent free radical (EPFR) in iron(III) cation-exchanged smectite clay" published in Environmental Science: Processes & Impacts (2016,18, 42-50. DOI: 10.1039/C5EM00554J) and "Model system study of environmentally persistent free radicals formation in a semiconducting polymer modified copper clay system at ambient temperature" published in RSC Advances (2016,6, 43453-43462. DOI: 10.1039/C6RA08051K).
I would like to request for permission to use both papers as chapters in my dissertation. Thank you.

Best regards
Ugwumsinachi Godwin Nwosu

APPENDIX D
COPYRIGHT PERMISSION FOR CHAPTER 5

RE: Letter of Permission

Ballen, Karen <KBallen@liebertpub.com>

Mon 9/26/2016 2:42 PM
To:Ugwumsinachi Nwosu <unwosu2@lsu.edu>;

Dear Ugwunsinachi:

Copyright permission is granted for use of your article from ENVIRONMENTAL ENGINEERING SCIENCE in your dissertation.

Kind regards,

Karen Ballen
Manager

From: Ugwumsinachi Nwosu [mailto:unwosu2@lsu.edu]
Sent: Monday, September 26, 2016 3:33 PM
To: Ballen, Karen
Subject: Letter of Permission

To who it may concern,

I am the first author to the following publications titled "**^{13}C Nuclear Magnetic Resonance and Electron Paramagnetic Spectroscopic Comparison of Hydrophobic Acid, Transphilic Acid, and Reverse Osmosis May 2012 Isolates of Organic Matter from the Suwannee River**" published in Environmental Engineering Science. (Jan 2015, 32(1): 14-22).

I would like to request for permission to use this article in my dissertation chapter. Thank you.

Best regards
Ugwumsinachi Godwin Nwosu

VITA

Ugwumsinachi Godwin Nwosu hails from Orodo in Mbaitolu Local Government Area in Imo State, Nigeria. He was born in December of 1983 to Kodimaram Godwin Nwosu (late) and Chinyere Abigail Nwosu in Enugu, Enugu State Nigeria. He was also raised in Enugu. Godwin attended Independence Lay-out Primary School between 1988 to 1994 for his elementary school education and later enrolled in Urban Boys Secondary School from 1994 to 1997 for his Junior secondary school education. He later moved on to Uwani Secondary School from 1997-2000 for his senior secondary school education, where he obtained his O' level result after sitting for the Senior Secondary Certificate Examination (SSCE). In 2002/2003 academic year he was offered admission from the Federal University of Technology, Owerri (FUTO) in Imo State, Nigeria to study Chemistry, where he eventually graduated with a Bachelor of Science (BSc) in Chemistry, Industrial Chemistry option. Godwin carried out his one-year national youth service between March 2008 to February 2009 at the Federal Capital Territory (FCT) Abuja where he served with the Planning, Research and Statistic (PRS) Directorate of the National Agency for Food and Drug administration and Control (NAFDAC). He later proceeded to teach Chemistry and was employed as a science teacher in a High School in Enugu. Godwin was admitted into the Louisiana State University (LSU) graduate program in chemistry to pursue his doctorate in chemistry in August 2011, and in 2012, He Joined the Analytical Chemistry division in LSU under the mentorship of Dr. Robert L. Cook. Since Joining Dr. Cook's research group, his project has focused on the Investigation of Environmentally Persistent Free Radicals (EPFRs) using surrogate models, a project he has pursued with passion. During his time in LSU Chemistry department, he has taught undergraduate level chemistry classes (labs) and mentored 7 undergraduate students through bench chemistry and the use of analytical instruments. He has also authored 3 papers in peer review journals. Godwin is a candidate to receive his Doctor of Philosophy(PhD) degree in chemistry (Analytical Chemistry) in the December 2016 LSU commencement ceremony.